Using Fluctuations to Explore QCD Phase Diagram

BY

BO LING
B.A. (Nanjing University, Nanjing, China) 2009

THESIS

Submitted as partial fulfillment of the requirements
for the degree of Doctor of Philosophy in Physics
in the Graduate College of the
University of Illinois at Chicago, 2016

Chicago, Illinois

Defense Committee:

Professor Mikhail Stephanov, Chair and Advisor
Professor Olga Evdokimov
Visiting Assistant Professor G. Todd Springer, Colgate University
Professor Zhenyu Ye
Professor Ho-Ung Yee

To my family,

and all other people I love.

ACKNOWLEDGMENTS

I want to thank my committee, especially my advisor-Mikhail Stephanov, for their wonderful help during my thesis completion.

TABLE OF CONTENTS

TABLE OF CONTENTS (Continued)

CHAPTER **PAGE**

LIST OF FIGURES

LIST OF ABBREVIATIONS

UIC	University of Illinois at Chicago
QCD	Quantum Chromodynamics
QGP	Quark Gloun Plasma
RHIC	Relativistic Heavy Ion Collider — BNL
LHC	The Large Hadron Collider — CERN
EOS	Equation of State

SUMMARY

Quantum Chromodynamics is one of the most remarkable theories of nature. Its mathematical foundations are concise, yet the phenomenology which the theory describes is broad and diverse. QCD phenomenology at finite temperature and baryon number density is one of the least explored regimes of the theory(1). Thermodynamic properties of QCD theory are most readily expressed in terms of a phase diagram in the space of thermodynamic parameters as T and μ_B. In other hand, the event-by-event fluctuations of suitably chosen observables in heavy ion collisions can tell us about the thermodynamic properties of the hadronic system at freeze-out, as well as the thermodynamic properties at early time such as initial state. In this thesis, we are going to use fluctuations to study QCD phase structure.

CHAPTER 1

INTRODUCTION

1.1 QCD Phase Diagram

QCD at finite temperature and chemical potential is a rich topic in modern physics, and understanding its phase structure and other related properties has a great importance. Asymptotic freedom (2; 3) allows QCD to be consistent down to arbitrary short distance scale, allowing us to define QCD theory in terms of some fundamental microscopic degrees of freedom: quarks and gluons(1; 4). Thus, all the phase information could be well understood through studying the QCD thermal partition function (See §8.3 of (5))

$$\mathbb{Z}(T,\mu) = \int \mathcal{D}\bar{\Psi}\mathcal{D}\Psi\mathcal{D}A e^{-\mathcal{S}_E} \tag{1.1}$$

with

$$\mathcal{S}_E = \int_0^{\frac{1}{T}} dx_0 \int d^3x \left(\frac{1}{2g^2} tr(F^{\mu\nu}F_{\mu\nu}) - \sum_{f=1}^{N_f} \bar{\Psi}_f \left[\not{\partial} + \not{A} + m_f + \frac{\mu_B}{N_c}\gamma_0 \right] \Psi_f \right), \tag{1.2}$$

However, QCD theory has no numerically small fundamental parameters other than quark masses, therefore full analytical treatment of QCD theory in Equation 1.2 and Equation 1.1 is very difficult. The only independent intrinsic scale in this theory is the dynamically generated confinement scale $\Lambda_{\mathrm{QCD}} \sim 1$ fm. In certain limits, in particular, for large values of the ex-

ternal thermodynamic parameters temperature T and/or baryon-chemical potential $\mu_{_B}$, when thermodynamics is dominated by short-distance QCD dynamics, the theory can be studied analytically, due to the asymptotic freedom(1; 4). For example, QCD perturbation theory shows that, color confinement and chiral symmetry breaking arises at low temperature $T \ll \Lambda_{QCD}$ and high baryon chemical potential $\mu_B \sim m_{_N}$, $m_{_P} \sim 1$GeV (6; 7). At zero baryon chemical potential $\mu_{_B} = 0$ but intermediate temperature $T \sim \Lambda_{QCD}$, the Lattice QCD calculations, which do not rely on small parameter expansions but rely on small baryon chemical potential, show there is a smooth crossover connected the high temperature and low temperature phases (8; 9; 10; 11). Even though the sign problem of QCD limits the applicability of Lattic QCD at finite chemical potential (12; 13), nevertheless, a multitude of effective models have been used to investigate the QCD phase diagram, which all indicate a first order phase transition at large μ_B (14; 15; 16; 17; 18). Figure 1 shows a sketch of QCD phase diagram (4). The ending point of first order line, known as QCD critical point, is distinct in the phase diagram, and locate it in $(T, \mu_{_B})$ plane is important for both theory and experiments, and we will discuss more in the following of this chapter.

1.2 Thermal Fluctuations and Event-By-Event Fluctuations

Let's first review how event-by-event measurements related to thermal dynamic fluctuations. As pointed by L. D. Landau (19), the statistical average of thermal function X is equal to the time average in equilibrium

$$\bar{X} = \int X(p,q)\,\rho(p,q)\,dpdq = \lim_{T_t\to\infty} \frac{1}{T_t}\int_0^{T_t} X(t)dt, \tag{1.3}$$

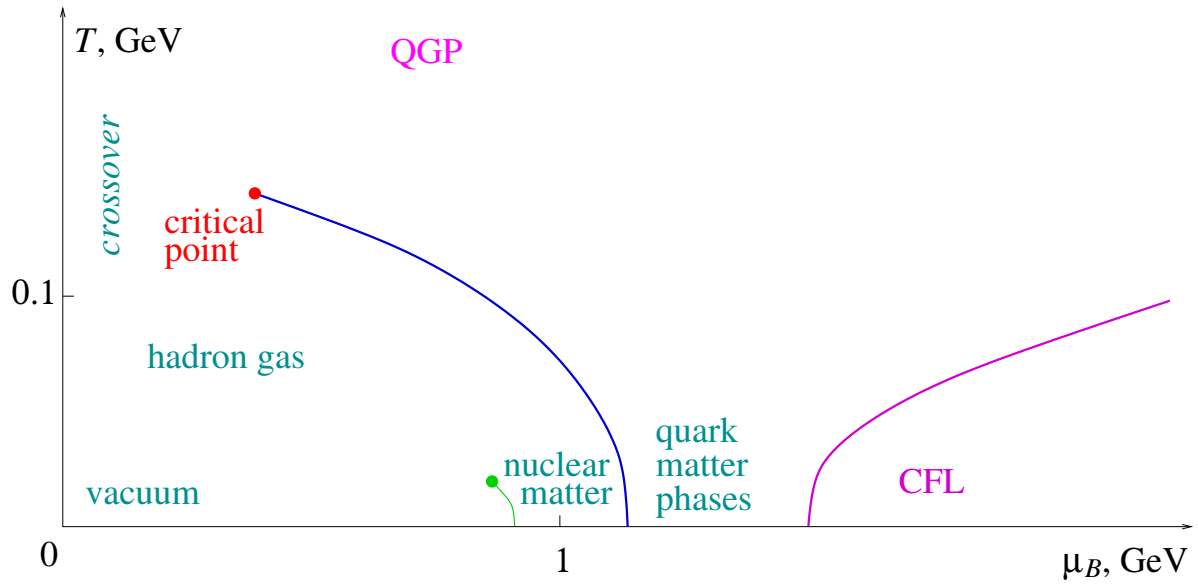

Figure 1. Sketch of QCD Diagram.

where $dpdq$ are the differential phase volume, $\rho(p,q)$ is the phase density, and T_t is the total measuring time. The fluctuation is defined as the thermal function departing from the average $\delta X(t) = X(t) - \bar{X}$, then the probability of obtaining such a fluctuating value is given by

$$d\mathbb{P}(\delta X) = \lim_{T_t \to \infty} \frac{\sum_t \delta_{t,t_i}}{T_t} = \rho(p,q)\,\Delta p \Delta q, \tag{1.4}$$

where t_i is the time when $X(t_i) = \delta X + \bar{X}$ for specific value of δX, and $\Delta p \Delta q$ is the small phase volume where the system occupies during $\Delta t \equiv \sum_t \delta_{t,t_i}$. The first equality in Equation 1.4 is related to the experiment measuring, while the second equality tells us how to calculate the probability of the fluctuation from statistical physics. Nevertheless, since the QCD matter

created in Heavy Ion Collisions is not in global equilibrium, one can not measure any quantity for a long time. Instead, people can only measure the final state of each event with the same initial conditions, and can only find the event average and event-by event fluctuations with the pool of events those have the same initial conditions. This procedure is equivalent to the long time average, so the event by event average and event by event fluctuations are the same as them in Equation 1.3 and Equation 1.4. This basic observation allows us to connect event-by-event measurements with thermal fluctuations in ensemble theory perfectly.

1.3 Evolutions of Hot QCD Matter Created in Heavy Ion Collisions

To create hot dense QCD matter near crossover region or critical region, powerful accelerators make head-on collisions between two highly Lorentz contracted heavy ions, such as gold or lead nuclei. In these heavy-ion collisions, the hundreds of protons and neutrons meshed into a hot dense QCD plasma within proper time of $1fm/c$ and volume of order fm^3. This fireball made of QCD plasma instantly cools, and the strong interacting quarks and gluons recombine into a blizzard of ordinary matter that speeds away in all directions. The debris contains particles such as pions, kaons, protons and neutrons. The charged particle spectrum observed in RHIC and LHC both have a plateau at central rapidity region, so people make the assumption that this fireball is boost invariant. The boost invariant initial condition is first introduced by j.D. Bjorken (20) to explain the particle spectrum of proton-proton collisions and now is applied in the hot dense matter created in heavy ion collisions.

The collision starts with two incoming nuclei traveling at nearly the speed of light. During the very short time τ_0 within 1 fm/c after the collision (21; 22; 23; 24; 25; 26; 27; 28), the system

is dominated by hard processes like quark pair production, jet production and fragmentation. With the evolution of interactions among partons, the system reaches (local) equilibrium and forms a strongly interacting Quark Gloun Plasma: QGP (29; 30). Due to the strong internal pressure, the QGP expands and cools isentropically with slowing increasing total entropy due to small viscosities (31; 32; 33). Once the media temperature drops within the crossover region or first order phase boundary, the phase transition from QGP to hadronic matter occurs: Hadronization (34). As the system cools further, the inelastic scattering stops and the yields of hadron species are fixed: Chemical Freeze-out (35). Finally elastic interactions between particles stop and the system comes to the state of free streaming: Kinetic Freeze-out at time $\tau_f \sim 10fm/c$ (36; 31; 37; 38; 33; 29; 30; 39). The final state particles then stream out and are detected experimentally, and the full evolution history is depicted in Figure 2.

QCD Equation of State (EOS) or susceptibility do change when the phase transition (either crossover or first order) happen during hydrodynamic evolution of hot QCD matter, but it is hard to test from the single charged particle spectrum, because its determining factors such as the final flow , freeze-out temperature, freeze-out time and system size are not so sensitive to E.O.S or susceptibility, but more rely on the boundary and initial conditions (37; 38; 33). Therefore, in order to find a signature of crossover or a QCD critical point, we need measure the variance or even higher moments of event-by-event particle spectrum, which is related to the thermal fluctuations in statistical ensemble theory (40; 41).

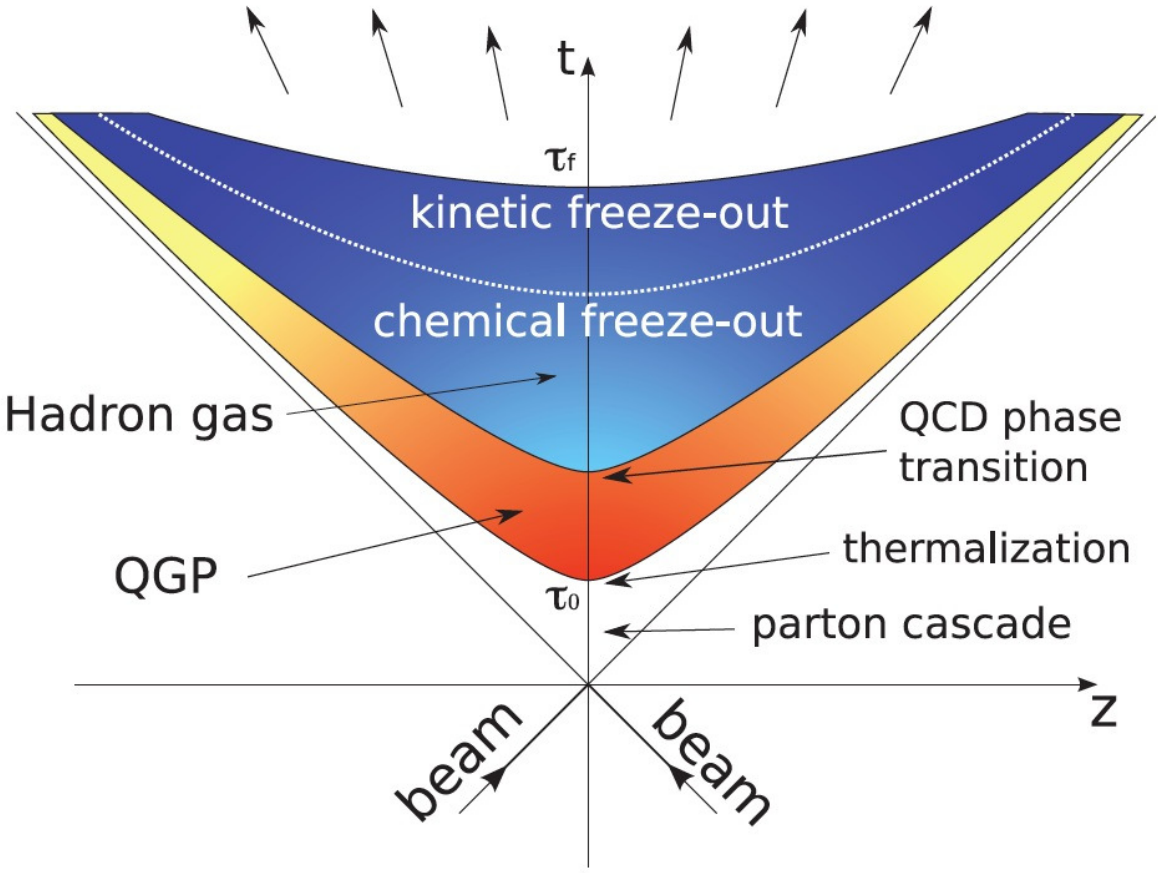

Figure 2. Sketch of Time Evolution of QGP

1.4 Measurements of Fluctuations in Heavy Ion Collisions

1.4.1 Experimental signals of QGP

It has a great importance that we have a clear signal of the quark-gluon plasma (QGP), not only for the experiments at RHIC but also for our fundamental understanding of strong interactions as well as understanding of the state of matter in the very early universe(42). The

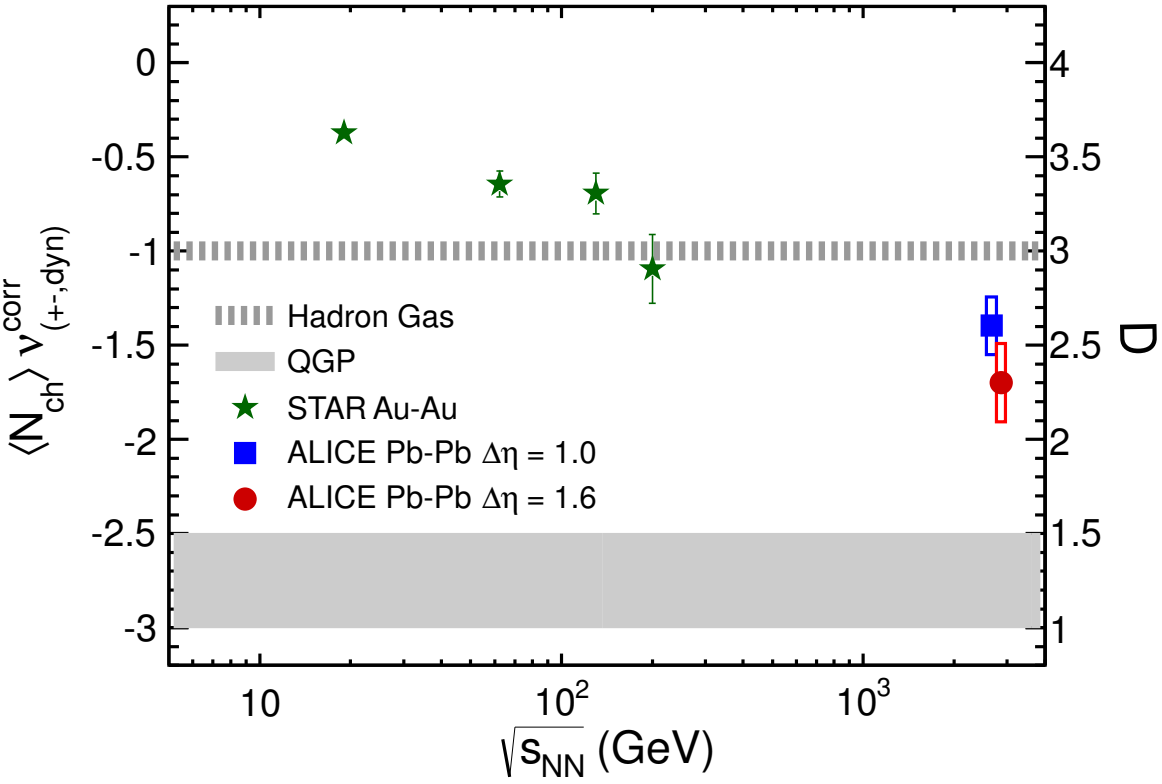

Figure 3. Energy dependence of the netcharge fluctuations D_m

magnitude of the fluctuations of net baryon number or electric charge in a finite volume of QCD matter differs widely between the confined and deconfined phases and these differences may be exploited as indicators of the formation of a quark-gluon plasma in RHIC and LHC experiments, because fluctuations created in the initial state and in the process of medium expansion survive until freeze-out, due to the rapid expansion of the hot fireball and the memory

effects for conserved quantity (43; 42; 44; 45). One main quantity, which is a signal of total charge fluctuations, called D-measure is defined as

$$D_m \equiv 4\frac{\langle \delta Q^2 \rangle}{\langle N_{ch} \rangle} \tag{1.5}$$

where

$$Q \equiv N_+ - N_-,\ N_{ch} \equiv N_+ + N_-,\ \delta Q = Q - \langle Q \rangle \tag{1.6}$$

with N_+, N_- are the numbers of positive and negative charged particles in one event. The symbol $\langle\rangle$ is the average over all the events with the same collision conditions. It has been shown that $D_m^{pion} \simeq 4$ for an uncorrelated free pion gas, and after taking resonance yields into account, this value decreases to $D_m^{Hadron} \simeq 3$. While for QGP matter, D_m is significantly lower and has been calculated to be $D_m^{QGP} \simeq 1.0-1.5$ (42; 46; 47). This difference between the hadron gas and QGP is very distinct to see from data collecting at RHIC as well as LHC as shown in Figure 3 (46; 47; 48). For the top RHIC energy of $\sqrt{s_{NN}} = 200GeV$, the value of D-measure is closed to the value of Hadron gas, whereas for collisions happening at lower energy , the value is above the value of Hadron Gas, while at $\sqrt{s_{NN}} = 2.76TeV$, we observe significantly lower fluctuations comparing to those in lower energy collisions. This monotonic decreasing behavior of D-measure when increasing collision energy, indicates that the matter created in LHC and the top energy collisions of RHIC, is in the deeper region of QGP phase. The value of D-measure away from non-interacting limit 4 is also a signal of phase transition as we will show later in Chapter.3.

1.4.2 Experimental signals of QCD critical point

QCD critical point is a distinct singular feature of the phase diagram, and locate this point in (μ_B, T) plane is an important and well defined task. Even though the exact location of the critical point is not known to us yet, the available theoretical estimates strongly indicate that the point is within the region of the phase diagram probed by the heavy-ion collision experiments(1; 41). The key feature of QCD critical point is the divergence of the correlation length ξ and the divergence of the magnitude of the fluctuations, thus by scanning on the phase diagram, some non-monotonous behaviors of the magnitude of the thermal fluctuations, such variance of multiplicity and transverse momentum, could be catched by Event-by-Event fluctuations in RHIC experiments (49; 50; 41).

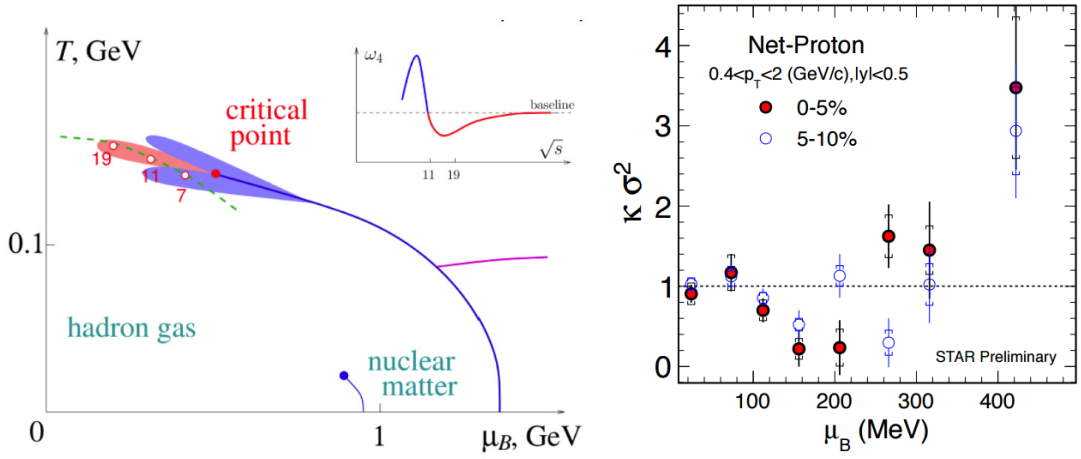

Figure 4. Sign of kutosis in theory and experiments

Nevertheless, the magnitude of ξ is limited by the system size, and most stringently by the finite-time effects due to critical slowing down (49; 51; 40; 41), which makes the correlation length may reach at most the value of $2 \sim 3$ fm (51). Compared to its natural value of 1 fm, this relative small divergence may make discovering the critical non-monotonous behavior be challenging task, if the measures depend on ξ too weakly. Recently, higher, non-Gaussian, moments of the fluctuations which depend much more sensitively on ξ, are suggested for searching QCD critical point (40; 52; 41). The 4-th moment (or kurtosis) of the charge fluctuations are predicted to change the sign (41) when scanning on the phase diagram from crossover region to the first order transition region. The theoretical prediction and experiment measures of this sign change are depicted in Figure 4 which are reported in (41; 53; 54). For $0-5\%$ most-central collisions, within the statistical and systematic errors of the data, the values of the normalized kurtosis $\kappa\sigma_2$ shows a non-monotonic behavior as a function of collision energy $\sqrt{s}$ varying from 7.7 GeV to 39 GeV, for which the chemical freeze-out temperatures are found to be ranging from 135 to 150 MeV and the chemical freeze-out chemical potential $\mu_{_B}$ are found to be range from 420 to 200 MeV (39; 54). This is the region where QCD critical point is probably located.

Lots of theoretical efforts have been done to study the fluctuations near QCD criitcal point as well as their experimental consequences, but most of the calculations are limited on the system in global equilibrium without longitudinal or radial flow. Until recently, some efforts are made to study the impact of longitudinal expansion on two particle correlations (55; 56; 57; 58; 59), and on the signature of higher moments at freeze-out, and we will show some of our related work here. This thesis is organized as the following: In Chapter.2, we will

develop relativistic hydrodynamics with stochastic noise from Boltzamann equation, and study the general properties of its boost invariant solution. In Chapter.3, we will use the theory developed in Chapter.2 to study the charge fluctuation as well as its relation to "Balance Function". In Chapter.4, we will study the acceptance dependence of the cumulants of protons near critical point.

CHAPTER 2

RELATIVISTIC HYDRODYNAMICS WITH STOCHASTIC NOISE

Hydrodynamics is an effective theory that describes the long wavelength and low frequency space-time evolution of the densities of the conserved quantities such as energy, momentum, electric charge and baryon number(55). In this chapter, we will focus on relativistic hydrodynamics, which describe the evolution of fluids whose microscopic constituents are constrained by Lorentz symmetry, such as fireball created in Relativistic Heavy-Ion Collisions(60). Relativistic hydrodynamics have obtained a great success in explaining lots of discoveries such as Bjorken-like plateau(61; 62; 63; 64), elliptic flow as well as higher order harmonics(65; 31; 66; 38; 67; 68) and the long rapidity "Ridge" correlations (69; 70), in which only initial state fluctuations are considered. Until recently, relativistic theory of hydrodynamic fluctuations with applications to Heavy Ion Collisions are explored (55; 56; 57). In this chapter, we will study the formal theory of relativistic hydrodynamics with stochastic noise.

2.1 Relativistic Hydrodynamic Fluctuations From Kinetic Theory

In this section, we will develop the theory of relativistic stochastic hydrodynamics using kinetic theory. It could describe the evolution of non-equilibrium thermal fluctuations, in particular, the evolution of the stochastic fluctuations in fast expanding systems such as fireball created in Heavy Ion Collisions. An alternative derivation using Entropy Current can be found

in (55), and the interpretation of stochastic hydrodynamics as a field theory can be found in (71).

2.1.1 Setup

Using kinetic theory to study non-relativistic and relativistic viscous hydrodynamics has a long history(72; 73; 74; 75; 76; 77; 78), and using non-relativistic kinetic theory with random force to study viscous hydrodynamics with stochastic noise has also been done many years ago (79; 80), while the corresponding version of relativistic case has not been well discussed. In this section, we will derive relativistic viscous hydrodynamics with stochastic noise. Following (81; 79; 80; 82; 83; 45), we write down the Relativistic Stochastic Boltzmann Equation as

$$p^\mu \partial_\mu \left[f_0(1+h)\right] = -u{\cdot}p\, f_0(x,p) \int d\chi'\, K(x,p,p')\, f_0(x,p')\, h(x,p')\, u{\cdot}p' + \boldsymbol{\zeta_F}(p,x), \tag{2.1}$$

where we have defined the collision kernel $K(p,p')$ that is symmetric under $p \leftrightarrow p'$, the random force $\boldsymbol{\zeta_F}(p,x)$ that is associated with collisions, the equilibrium distribution function $f_0(x,p) = e^{\mu(x)/T(x) - u(x)\cdot p/T(x)}$, the non-equilibrium distribution

$$f(x,p) = f_0(x,p)\left[1 + h(x,p)\right]. \tag{2.2}$$

The Lorentz invariant phase integral is

$$\int d\chi \equiv \int \frac{d^4p}{(2\pi)^4}\, 2\Theta(p^0)\, 2\pi\, \delta(p^2 - m^2) = \frac{1}{(2\pi)^3} \int \frac{d^3\boldsymbol{p}}{E_{\boldsymbol{p}}} \tag{2.3}$$

where the mass of the particle is m, $\boldsymbol{p}$ and $E_{\boldsymbol{p}}$ are the particle momentum and energy in boost frame defined by four velocity u^μ, and $\Theta(p^0)$ is Heaviside function. The normal conversed current is define as

$$J^\mu \equiv \int d\chi \, p^\mu \, f \tag{2.4}$$

and the normal energy momentum tensor is defined as

$$T^{\mu\nu} \equiv \int d\chi \, p^\mu \, p^\nu \, f \tag{2.5}$$

The charge conservation

$$\partial_\nu J^\nu = \partial_\nu \int d\chi p^\nu \left[f_0 (1 + h) \right] = 0 \tag{2.6}$$

requires the collision kernel has a zero mode 1

$$\int d\chi \, (u{\cdot}p) \; f_0(x,p) \; \left[\int d\chi' \, K\left(x, p, p'\right) \; f_0(x,p') \, h(p') \; \left(u{\cdot}p'\right) \right] = 0, \tag{2.7}$$

$$\int d\chi \, \boldsymbol{\zeta_F}(x,p) = 0. \tag{2.8}$$

The energy momentum conservation

$$\partial_\nu T^{\mu\nu} = \partial_\nu \int d\chi \, p^\nu \, p^\mu \; \left[f_0 (1 + h) \right] = 0 \tag{2.9}$$

requires the collision kernel has another four zero modes p^μ

$$\int d\chi p^\mu \ (u\cdot p) \ f_0(x,p) \ \left[\int d\chi' \, K(p,p') \, f_0(x,p') \, h(x,p') \ \left(u\cdot p'\right)\right] = 0, \tag{2.10}$$

$$\int d\chi p^\mu \, \boldsymbol{\zeta_F}(p,x) = 0. \tag{2.11}$$

As it was argued by Fox (79; 80) using "H-Theorem", the thermal average of the random force vanishes

$$\langle \boldsymbol{\zeta_F}(x,p) \rangle = 0, \tag{2.12}$$

where $\langle \ \rangle$ is the average over all thermal ensembles; while the correlation of the random force is related to the collision kernel

$$\left\langle \boldsymbol{\zeta_F}(p,x) \boldsymbol{\zeta_F}(p',x') \right\rangle = 2 f_0(x,p) \, f_0(x,p') \ (u\cdot p) \ \left(u\cdot p'\right) \ K\left(x,p,p'\right) \ \delta(x^\mu - x'^\mu). \tag{2.13}$$

Following (79; 80), we can expand the collision kernel as the summation of all "eigen-modes" $\Phi_i(p)$ which depend on the space time through their dependence on the local temperature and flow velocity

$$K(x,p,p') = \sum_{i=5}^{\infty} \lambda_i(x) \, \Phi_i(p) \Phi_i(p'), \tag{2.14}$$

so does the random force

$$\boldsymbol{\zeta_F}(x,p) = \sum_{i=5}^{\infty} f_0(x,p) \ (u\cdot p) \ \boldsymbol{F}_i(x) \, \Phi_i(p). \tag{2.15}$$

The eigen-modes $\Phi_i(p)$ form a complete orthogonal basis, which means

$$\sum_{i=0} \Phi_i(p)\, \Phi_i(p') = f_0^{-1/2}(x,p)\ f_0{}^{-1/2}(x,p')\ (u{\cdot}p)^{\frac{1}{2}}\ \left(u{\cdot}p'\right)^{\frac{1}{2}}\ \delta^4\left(p-p'\right), \tag{2.16}$$

and

$$\int d\chi\, u{\cdot}p\, f_0(x,p)\, \Phi_i(p)\Phi_j(p) = \delta_{i,j}. \tag{2.17}$$

It is interesting to note that, Equation 2.17 , Equation 2.14 and Equation 2.15 guarantee that Equation 2.8 and Equation 2.11 are satisfied because zero modes are all orthogonal to the fast modes, thus Equation 2.17 is essential for linearized Blotzmman equation Equation 2.1 to be consistent with hydrodynamics. Another important thing to mention that the zero modes 1 and p^μ are not all orthogonal to each other, but their certain combinations do. For example,

$$\Phi_0 \propto 1,\ \Phi_{i=1,2,3} \propto p^i,\ \Phi_4 \propto u{\cdot}p - \frac{\int d\chi\, f_0(x,p)\ (u{\cdot}p)^2}{\int d\chi\, f_0(x,p)\, u{\cdot}p} \tag{2.18}$$

Using Equation 2.13, Equation 2.14 and Equation 2.15 we find

$$\left\langle \boldsymbol{F}_l(x)\boldsymbol{F}_k(x')\right\rangle = 2\lambda_l\, \delta_{lk}\, \delta(x^\mu - x'^\mu). \tag{2.19}$$

We can solve Equation 2.1 order by order using Chapman-Enskog expansion. Up to first order in the gradients of temperature and flow, it yields

$$p^\mu \partial_\mu f_0 = -u{\cdot}p\, f_0(x,p) \int d\chi'\, K\left(x,p,p'\right)\ f_0(x,p')\, h_1(x,p')\, u{\cdot}p' + \boldsymbol{\zeta}_{\boldsymbol{F}}(p,x). \tag{2.20}$$

2.1.2 Distribution function in non-equilibrium

To find the first order gradient correction of the distribution function, we can expand h_1 in Equation 2.20 as a linear combination of eigen-modes of collision kernel

$$h_1(x,p) = \sum_{i=5}^{\infty} a_i(x)\Phi_i(p). \tag{2.21}$$

The summation are only over fast modes because all zero modes can be absorbed into the equilibrium distribution f_0 through a re-definition of flow velocity and local temperature (84). Also, for simplicity, we will work in Landau frame, and the Landau-Lifshitz condition is read as

$$u_\mu J^\mu = n \tag{2.22}$$

$$u_\mu T^{\mu\nu} = u_\mu T_0^{\mu\nu} \tag{2.23}$$

where

$$T_0^{\mu\nu} \equiv \int d\chi\, p^\mu\, p^\nu\, f_0 \tag{2.24}$$

The Landau-Lifshitz condition written in terms of the condition on the non-equilibrium correction $h(x,p)$ to distribution function $f(x,p)$ are

$$\int d\chi\ (u{\cdot}p)\ f_0(x,p)\, h(x,p) = 0, \tag{2.25}$$

$$\int d\chi \ (u\cdot p) \ p^{\mu} \, f_0(x,p) \, h(x,p) = 0. \tag{2.26}$$

The above is true up to all orders in gradient expansion, and it also means the non-equilibrium correction $h(x,p)$ is a linear combination of fast modes(excluding zero modes) only in Landau frame, which is consistent with Equation 2.21.

Substitute Equation 2.14 and Equation 2.21 into Equation 2.20 and use the orthogonal relation in Equation 2.17, we get:

$$p^{\mu}\partial_{\mu} f_0 = -u\cdot p \, f_0 \sum_{i=5}^{\infty} \lambda_i \, a_i \, \Phi_i(p) + \boldsymbol{\zeta_F}(x,p) \tag{2.27}$$

Using orthogonality to project the coefficient of every fast mode in Equation 2.21, we get

$$a_i = \frac{1}{\lambda_i} \left(F_i - \int \Phi_i(p) \, p^{\mu} \partial_{\mu} f_0 \right). \tag{2.28}$$

Thus

$$h_1 = \sum_{i=5}^{\infty} \left[\frac{1}{\lambda_i} \left(\boldsymbol{F}_i - \int d\chi' \, \Phi_i(p') \, p'^{\mu} \, \partial_{\mu} f_0(x,p') \right) \right] \Phi_i(p). \tag{2.29}$$

Since the energy momentum tensor

$$T^{\mu\nu} = \int d\chi \, p^{\mu} \, p^{\nu} \, f_0(1+h), \tag{2.30}$$

we find it can be separated into three parts

$$T^{\mu\nu} = T_0^{\mu\nu} + T_{\rm vis}^{\mu\nu} + S^{\mu\nu}. \tag{2.31}$$

The ideal non-viscous part has been defined before

$$T_0^{\mu\nu} = \int d\chi\, p^\mu\, p^\nu\, f_0(x,p) = \varepsilon u^\mu u^\nu + p h^{\mu\nu}, \tag{2.32}$$

where we have defined

$$h^{\mu\nu} \equiv u^\mu u^\nu - g^{\mu\nu} \tag{2.33}$$

and ε and p are the local energy density and pressure in Landau Frame. The viscous part is

$$T_{\rm vis}^{\mu\nu} \equiv -\int d\chi\, p^\mu\, p^\nu\, f_0(x,p) \sum_{i=5}^{\infty} \left[\frac{1}{\lambda_i} \int d\chi'\, \Phi_i\left(p'\right)\, p'^\rho\, \partial_\rho\, f_0(x,p') \right] \Phi_i(p), \tag{2.34}$$

and the stochastic part is

$$S^{\mu\nu} \equiv \int d\chi\, p^\mu\, p^\nu\, f_0(x,p) \sum_{i=5}^{\infty} \frac{1}{\lambda_i}\, \boldsymbol{F}_i\, \Phi_i(p). \tag{2.35}$$

The correlations of the stochastic part $S^{\mu\nu}$ is read as

$$\begin{aligned}\left\langle S^{\mu\nu}(x)S^{\rho\sigma}(x')\right\rangle &= \int d\chi d\chi'\, p^\mu\, p^\nu\, p'^\rho\, p'^\sigma\, f_0(x,p)\, f_0(x,p') \sum_{i=5}^{\infty} \frac{1}{\lambda_i} \sum_{j=5}^{\infty} \frac{1}{\lambda_j} \left\langle \boldsymbol{F}_i' \boldsymbol{F}_j \right\rangle\, \Phi_i(p)\, \Phi_j(p') \\ &= \int d\chi d\chi'\, p^\mu\, p^\nu\, p'^\rho\, p'^\sigma\, f_0(x,p)\, f_0(x',p') \sum_{i=5}^{\infty} \frac{2}{\lambda_i}\, \Phi_i(p)\, \Phi_i(p')\, \delta(x^\mu - x'^\mu).\end{aligned} \tag{2.36}$$

Similarly, the current

$$J^\mu = \int d\chi\, p^\mu\, f_0(1+h_1), \tag{2.37}$$

can also be written as three parts

$$J^\mu = J_0^\mu + \Delta J^\mu + I^\mu. \tag{2.38}$$

The ideal part is

$$J_0^\mu \equiv \int d\chi\, p^\mu\, f_0 = n u^\mu, \tag{2.39a}$$

the diffusive part is

$$\Delta J^\mu \equiv -\int d\chi\, p^\mu\, f_0 \sum_{i=5}^{\infty} \left[\frac{1}{\lambda_i} \int d\chi'\, \Phi_i(p')\, p'^\rho\, \partial_\rho f_0' \right] \Phi_i(p), \tag{2.39b}$$

and the stochastic noise is

$$I^{\mu} \equiv \int d\chi\, p^{\mu}\, f_0 \sum_{i=5}^{\infty} \frac{1}{\lambda_i}\, \boldsymbol{F}_i\, \Phi_i(p). \tag{2.39c}$$

The correlations of stochastic current is read as

$$\begin{aligned} \langle I^{\mu}(x) I^{\nu}(x') \rangle &= \int d\chi d\chi'\, p^{\mu}\, p'^{\nu}\, f_0\, f'_0 \sum_{i=5}^{\infty} \frac{1}{\lambda_i} \sum_{j=5}^{\infty} \frac{1}{\lambda_j} \left\langle \boldsymbol{F}'_i \boldsymbol{F}_j \right\rangle\, \Phi_i(p)\, \Phi_j(p') \\ &= \int d\chi d\chi'\, p^{\mu}\, p'^{\nu}\, f_0\, f'_0 \sum_{i=5}^{\infty} \frac{2}{\lambda_i}\, \Phi_i(p)\, \Phi_i(p')\, \delta(x^{\mu} - x'^{\mu}). \end{aligned} \tag{2.40}$$

2.1.3 Fluctuation dissipation theorem

Now let's consider a general system with massive particles and finite chemical potential. First we note

$$p^{\mu} \partial_{\mu} f_0 = \left[p^{\mu} \partial_{\mu} \left(\frac{\mu}{T} \right) - p^{\mu} p^{\nu} \partial_{\mu} \left(\frac{u_{\nu}}{T} \right) \right]\, f_0, \tag{2.41}$$

and substitute this into Equation 2.34, then we find the viscous energy momentum tensor is

$$\begin{aligned} T^{\alpha\beta}_{\text{vis}} &= \sum_{i=5}^{\infty} \frac{1}{\lambda_i} \left(\int d\chi\, p^{\alpha}\, p^{\beta}\, f_0\; \Phi_i(p) \right) \Big[\; \frac{\partial_{\rho} u_{\sigma}}{T} \left(\int d\chi'\, \Phi_i(p')\, p'^{\rho}\, p'^{\sigma}\, f'_0 \right) \\ &+ \partial_{\rho} \left(\frac{1}{T} \right) \left(\int d\chi'\, \Phi_i(p')\, p'^{\rho}\; (u \cdot p')\; f'_0 \right) - \partial_{\rho} \left(\frac{\mu}{T} \right) \left(\int d\chi'\, \Phi_i(p')\, p'^{\rho}\, f'_0 \right) \;\Big] \end{aligned} \tag{2.42}$$

From the orthogonal relation in Equation 2.17, it is easy to see that

$$\int d\chi' \, \Phi_i(p') \, p'^{\rho} \, \left(u \cdot p'\right) \, f_0' = 0 \tag{2.43}$$

because p^μ is one of the zero mode. Since

$$\int d\chi' \, \Phi_i(p') \, p'^{\rho} \, f_0' \propto u^\rho \tag{2.44}$$

I claim

$$\int d\chi' \, \Phi_i(p') \, p'^{\rho} \, f_0' = 0 \tag{2.45}$$

because 1 is also a zero mode. Thus

$$T^{\alpha\beta}_{\rm vis} = \frac{\partial_\rho u_\sigma \cdot}{T} \sum_{i=5}^{\infty} \frac{1}{\lambda_i} \left(\int d\chi \, p^\alpha \, p^\beta \, f_0 \; \Phi_i(p) \right) \left(\int d\chi' \, \Phi_i(p') \, p'^{\rho} \, p'^{\sigma} \, f_0' \right) \tag{2.46}$$

The shear stress tensor can be found to be

$$\begin{aligned} & \pi^{\mu\nu} \equiv \frac{1}{2} P^{\mu\nu}_{\alpha\beta} \, T^{\alpha\beta}_{\rm vis} \\ = \; & \frac{1}{2} P^{\mu\nu}_{\alpha\beta} \, \partial_\rho u_\sigma \cdot \sum_{i=5}^{\infty} \frac{1}{T \, \lambda_i} \left(\int d\chi \, p^\alpha \, p^\beta \, f_0 \; \Phi_i(p) \right) \left(\int d\chi' \, \Phi_i(p') \, p'^{\rho} \, p'^{\sigma} \, f_0' \right) \\ \equiv \; & \eta_{\rm shear} \, \sigma^{\mu\nu}. \end{aligned} \tag{2.47}$$

where we have defined the traceless space projection tensor $P^{\mu\nu}_{\alpha\beta}$

$$P^{\mu\nu,\alpha\beta} \equiv h^{\mu\alpha}h^{\nu\beta} + h^{\nu\alpha}h^{\mu\beta} - \frac{2}{3}h^{\mu\nu}h^{\alpha\beta}, \tag{2.48}$$

and the traceless shear tensor

$$\sigma^{\mu\nu} \equiv P^{\mu\nu}_{\alpha\beta}\,\partial_\alpha u_\beta. \tag{2.49}$$

Now let's write

$$\begin{aligned}
&\sum_{i=5}^{\infty} \frac{1}{T\,\lambda_i} \left(\int d\chi p^\alpha p^\beta f_0(x,p)\,\Phi_i(p)\right)\left(\int d\chi' \Phi_i(p') p'^\rho p'^\sigma f_0(x,p')\right) \\
= \;& a\,h^{\alpha\beta}\,h^{\rho\sigma} + b\,\left(h^{\alpha\rho}\,h^{\beta\sigma} + h^{\alpha\sigma}\,h^{\rho\beta}\right) + c\left(u^\alpha u^\beta h^{\rho\sigma} + u^\rho u^\sigma h^{\alpha\beta}\right) \\
&+ d\left(u^\alpha u^\rho h^{\beta\sigma} + u^\alpha u^\sigma h^{\beta\rho} + u^\beta u^\rho h^{\alpha\sigma} + u^\beta u^\sigma h^{\alpha\rho}\right) + e\,u^\alpha u^\beta u^\rho u^\sigma,
\end{aligned} \tag{2.50}$$

Using the orthogonal relation between zero modes p^μ and the fast modes $\Phi_{i\geq 5}(p)$, we find

$$c = d = e = 0.$$

Substitute Equation 2.50 into Equation 2.47, then we find

$$b = \eta_{\text{shear}}. \tag{2.51}$$

The bulk viscous stress tensor is

$$\Pi \equiv -\frac{1}{3}\cdot h_{\alpha\beta}\, T^{\alpha\beta}_{vis} \tag{2.52}$$

$$\equiv \zeta\, \partial{\cdot}u. \tag{2.53}$$

Using Equation 2.50, we can find the bulk viscosity

$$\zeta = \left(a + \frac{2}{3}b\right). \tag{2.54}$$

Meanwhile, using Equation 2.50, we find Equation 2.36 becomes

$$\begin{aligned}\left\langle S^{\alpha\beta}(x)\, S^{\rho\sigma}(x')\right\rangle &= 2T\left[a\, h^{\alpha\beta}\, h^{\rho\sigma} + b\left(h^{\alpha\rho}\, h^{\beta\sigma} + h^{\alpha\sigma} h^{\rho\beta}\right)\right] \\ &= 2T\left[\left(\zeta - \frac{2}{3}\eta_{\text{shear}}\right) h^{\alpha\beta}\, h^{\rho\sigma} + \eta_{\text{shear}}\left(h^{\alpha\rho}\, h^{\beta\sigma} + h^{\alpha\sigma}\, h^{\rho\beta}\right)\right]\delta(x^{\mu} - x'^{\mu})\end{aligned} \tag{2.55}$$

This is the fluctuations and the dissipation theorem for relativistic fluid.

Now let's look at the diffusive current. After some calculation, we find

$$\begin{aligned}\Delta J^{\mu} &= \sum_{i=5}^{\infty} \frac{1}{\lambda_i}\left(\int d\chi\, p^{\mu}\, f_0(p)\, \Phi_i(p)\right)\Big[-\partial_{\rho}\left(\frac{\mu}{T}\right)\int d\chi'\, \Phi_i(p')\, p'^{\rho}\, f_0(p') \\ &\quad + \partial_{\rho}\left(\frac{u_{\sigma}}{T}\right)\int d\chi'\, \Phi_i(p')\, p'^{\rho}\, p'^{\sigma}\, f_0(p')\Big],\end{aligned} \tag{2.56}$$

Using the orthogonal relation Equation 2.17, we find the last term which evolve gradient of velocity vanishes. Thus

$$\Delta J^{\mu} = -\partial_{\rho}\left(\frac{\mu}{T}\right)\sum_{i=5}^{\infty}\frac{1}{\lambda_i}\left(\int d\chi\, p^{\mu}\, f_0(p)\,\Phi_i(p)\right)\left(\int d\chi'\,\Phi_i(p')\,p'^{\rho}\, f_0(p')\right) \tag{2.57}$$

The correlations of the stochastic current

$$\langle I^{\mu} I^{\nu}\rangle = \int d\chi d\chi'\, p^{\mu}\, p'^{\nu}\, f_0\, f_0'\sum_{i=5}^{\infty}\frac{2}{\lambda_i}\,\Phi_i(p)\,\Phi_i(p')\,\delta(x^{\mu}-x'^{\mu}). \tag{2.58}$$

Again, we write

$$\int d\chi d\chi'\, p^{\mu}\, p'^{\nu}\, f_0\, f_0'\sum_{i=5}^{\infty}\frac{2}{\lambda_i}\,\Phi_i(p)\,\Phi_i(p') = c\, u^{\mu}u^{\nu} + d\, h^{\mu\nu} \tag{2.59}$$

It is easy to see $c = 0$ because of the orthogonal relations between the zero mode and the fast modes. Finally, we find

$$\Delta J^{\mu} = \sigma T\,\Delta^{\mu}(\frac{\mu}{T}), \tag{2.60}$$

where we have defined the space gradient

$$\Delta^{\mu} \equiv -h^{\mu\nu}\,\partial_{\nu} \tag{2.61}$$

and the conductivity

$$\sigma = \frac{1}{3\,T} \int \sum_{i=5}^{\infty} d\chi d\chi'\, f_0\, f_0'\, \frac{1}{\lambda_i}\, \Phi_i(p)\, \Phi_i(p')\, p_\mu \cdot h^{\mu\nu} p'_\nu. \tag{2.62}$$

The correlations of the stochastic current then is

$$\left\langle I^\mu(x)\, I^\nu(x') \right\rangle = 2\sigma T\, h^{\mu\nu} \delta(x^\mu - x'^\mu). \tag{2.63}$$

2.1.4 Summary

Now let's summarize the results we have got so far, which we will use in next section and Chapter.3. The energy momentum tensor could be written as

$$T^{\mu\nu} = T_0^{\mu\nu} + T_{\rm vis}^{\mu\nu} + S^{\mu\nu} \tag{2.64}$$

The idea part is

$$T_0^{\mu\nu} = \varepsilon\, u^\mu u^\nu + p\, h^{\mu\nu} \tag{2.65}$$

where ε is the energy density, p is the pressure, u^μ is fluid four velocity, $h^{\mu\nu} = u^\mu u^\nu - g^{\mu\nu}$. The viscous part is

$$T_{\rm vis}^{\mu\nu} = \eta_{\rm shear}\, \sigma^{\mu\nu} - \zeta\, h^{\mu\nu}\, \partial \cdot u \tag{2.66}$$

and the shear tensor is

$$\sigma^{\mu\nu} \equiv P_{\alpha\beta}^{\mu\nu}\, \partial_\alpha u_\beta \tag{2.67}$$

The stochastic part $S^{\mu\nu}$ satisfies

$$\langle S^{\mu\nu} \rangle = 0 \ , \tag{2.68}$$

and

$$\left\langle S^{\alpha\beta} S^{\rho\sigma} \right\rangle = 2T \left[\left(\zeta - \frac{2}{3} \eta_{\text{shear}} \right) h^{\alpha\beta} \, h^{\rho\sigma} + \eta_{\text{shear}} \left(h^{\alpha\rho} \, h^{\beta\sigma} + h^{\alpha\sigma} \, h^{\rho\beta} \right) \right] \delta(x^{\mu} - x'^{\mu}) \ . \tag{2.69}$$

The energy momentum conservation is just

$$\partial_{\mu} \, T^{\mu\nu} = 0. \tag{2.70}$$

Similarly, the current can also written as three parts

$$J^{\mu} = J^{\mu}_{0} + \Delta J^{\mu} + I^{\mu} \tag{2.71}$$

The ideal part is

$$J^{\mu}_{0} = n \, u^{\mu} \tag{2.72}$$

where n is the charge density. The diffusive part is

$$\Delta J^{\mu} = \sigma T \, \Delta^{\mu}(\frac{\mu}{T}) \tag{2.73}$$

where the conductivity is

$$\sigma = \sum_{i=5}^{\infty} \frac{1}{3\,\lambda_i\,T} \int d\chi d\chi'\, f_{_0}\, f'_{_0}\; \Phi_i(p)\, \Phi_i(p')\, p_\mu \cdot h^{\mu\nu} \cdot p'_\nu, \tag{2.74}$$

and the space gradient is

$$\Delta^\mu = -h^{\mu\nu}\, \partial_\nu. \tag{2.75}$$

The stochastic part I^μ satisfies

$$\langle I^\mu \rangle = 0, \tag{2.76}$$

and

$$\langle I^\mu I^\nu \rangle = 2\sigma T\, h^{\mu\nu} \delta(x^\mu - x'^\mu). \tag{2.77}$$

The charge conservation is just

$$\partial_\mu\, J^\mu = 0. \tag{2.78}$$

2.2 Boost Invariant Solutions of Relativistic Hydrodynamics with Stochastic Noise

In this section, we consider, as an example, the application of the stochastic hydrodynamic equations derived in the previous section, on the hydrodynamic fluctuations around Bjorken's boost-invariant solution of relativistic hydrodynamics (61; 55; 56). For highly relativistic heavy ion collisions at LHC and the top range of RHIC energies, the fluctuations of energy and momentum density decouple from the fluctuations of the charge density (55; 57); while near the critical point, all of these fluctuations couple with each other and all have manifest effects on

final experimental observables (56). For simplicity and illustration purpose, we shall focus on longitudinal flow fluctuations by integrating all densities over the coordinates x and y perpendicular to the beam direction or z axis, which effectively reduces the dimensionality of the problem to $(1+1)$, and study the dynamics in the limit of zero baryon chemical potential $\mu_{_B} = 0$. Here we only study the general structure of the equal time correlations induced by stochastic noise which are not well discussed in previous literatures, and the more quantitative and concrete results could be found in (55; 56; 57).

2.2.1 Background solution and hydro equations of linear fluctuations

It is convenient to view the Bjorken boost-invariant flow in Bjorken coordinates: proper time τ and spatial rapidity η defined as

$$\begin{aligned} \tau &= \sqrt{t^2 - z^2} \\ \eta &= \tanh^{-1}(z/t) \\ t &= \tau \cosh\eta \\ z &= \tau \sinh\eta \end{aligned} \tag{2.79}$$

where (t, x, y, z) is the space time coordinate. The average values of hydrodynamic quantities depend only on proper time τ. While the fluctuations after integrating out the transverse dependence, depend on both τ and η. The flow velocity is given by $u^\mu = x^\mu/\tau + \delta u^\mu$, where

the last term denotes the fluctuations. We express the fluctuations of the longitudinal flow in terms of the rapidity variable ω which we define as

$$\begin{aligned} u^0 &= \cosh(\eta + \omega(\eta, \tau)) \\ u^3 &= \sinh(\eta + \omega(\eta, \tau)) \,. \end{aligned} \tag{2.80}$$

The local pressure depends on the temperature which in turn depends on both coordinates. The average value of temperature T depends only on the proper time, but fluctuations of T depend on both coordinates. Therefore

$$\begin{aligned} T &= \bar{T}(\tau) + \delta T(\eta, \tau) \\ \mu &= \bar{\mu}(\tau) + \delta\mu(\eta, \tau) \\ P &= \bar{P}(\tau) + \delta P(\eta, \tau) \\ \epsilon &= \bar{\epsilon}(\tau) + \delta\epsilon(\eta, \tau) \,, \end{aligned} \tag{2.81}$$

where the $\bar{X}$ refers to the average value of the function X. Due to the reduced (1+1) dimensionality of this model this condition allows us to express the stochastic noise discussed in last section in terms of two single scalar functions f_n and f_s as

$$S^{\mu\nu} = w(\tau)\, f_s(\eta, \tau)\, h^{\mu\nu}, \quad I^\eta = \frac{s(\tau)}{\tau}\, f_n(\eta, \tau) \tag{2.82}$$

which leads

$$\langle f_s(\eta_1,\tau_1)f_s(\eta_2,\tau_2)\rangle = \frac{2T(\tau_1)}{A\tau_1 w^2(\tau_1)}\left[\frac{4}{3}\eta_{\rm shear}(\tau_1)+\zeta(\tau_1)\right]\delta\left(\tau_1-\tau_2\right)\delta\left(\eta_1-\eta_2\right) \tag{2.83}$$

$$\langle f_n(\eta_1,\tau_1)f_n(\eta_2,\tau_2)\rangle = \frac{2\sigma\, T(\tau_1)}{A\tau_1 s^2(\tau_1)}\,\delta\left(\tau_1-\tau_2\right)\delta\left(\eta_1-\eta_2\right) \tag{2.84}$$

where we have defined A be the transverse area of Bjorken system. The hydrodynamic evolution of these fluctuations can be studied using stochastic relativistic hydrodynamics developed in last section.

The boost invariant background solutions, when dissipation is neglected, is simply the entropy conservation

$$\frac{d(\tau s)}{d\tau} = 0 \tag{2.85}$$

which has the solution $s(\tau) = s(\tau_0)\tau_0/\tau$. Here τ_0 is the initial proper time (when thermalization first is achieved). Including the viscous correction

$$\Delta T^{\mu\nu}_{vis} = -h^{\mu\nu}\left(\frac{4}{3}\eta_{\rm shear}+\zeta\right)\nabla\cdot u, \quad \Delta J^{\mu}_{B} = 0 \tag{2.86}$$

Defining

$$\nu \equiv (4\eta_{\rm shear}/3+\zeta)/s, \tag{2.87}$$

the back ground equation becomes

$$\frac{d(\tau s)}{d\tau} = \frac{\nu s}{\tau T}. \tag{2.88}$$

Then Equation 2.88 means that the entropy per unit rapidity interval, $\tau s A$, increases due to dissipation. The explicit solution requires knowing the relationship between s and T, in other words the equation of state, plus the temperature dependence of ν.

Now we account for fluctuations by adding noise. At this point, we make no assumption about the form of the equation of state or the temperature dependence of ν. Up to linear order in small fluctuation, the energy, momentum and charge conservation give three independent equations (55)

$$\tau\frac{\partial\delta\epsilon}{\partial\tau}+\delta w(1-h)-w\delta h+\tau^2 S^{\eta\eta}+w\,(1-2h)\,\frac{\partial\omega}{\partial\eta}=0\ , \tag{2.89}$$

$$\tau\frac{\partial\delta n}{\partial\tau}+\delta n+n\frac{\partial\omega}{\partial\eta}+\tau\frac{\partial I^{\eta}}{\partial\eta}+\frac{\sigma T}{\tau}\cdot\tau\partial_{\tau}\left(\frac{\mu}{T}\right)\partial_{\eta}\omega-\frac{\sigma T}{\tau}\cdot\frac{\partial^2}{\partial\eta^2}\left(\frac{\mu}{T}\right)=0\ , \tag{2.90}$$

$$\tau\frac{\partial\left[w(1-h)\omega\right]}{\partial\tau}+2w\omega(1-h)+\frac{\partial}{\partial\eta}(\delta p+\tau^2 S^{\eta\eta}-hw)-hw\frac{\partial^2\omega}{\partial\eta}=0\ . \tag{2.91}$$

Here n and $w\equiv\varepsilon+p$ are the smooth background solutions which depend only on τ, and $h\equiv\frac{\frac{4\eta_{\rm shear}}{3}+\zeta}{\tau\,w}$. For simplicity, we shall only consider relativistic heavy ion collisions at LHC and the top range of RHIC energies where $n=0$ approximately, then $w=T\,s$, $\delta\varepsilon=T\,\delta s$, $\delta\,p=s\delta\,T$, $h=\frac{\nu}{T\tau}$ and Equation 2.90 decouples with Equation 2.89 and Equation 2.91. The fluctuations δp, δs, $\delta\varepsilon$, and δw can all be expressed in terms of a new dimensionless variable

$$\rho\equiv\delta s/s, \tag{2.92}$$

then $\delta\varepsilon = w\rho$ and $\delta p = v_q^2 w\rho$ where we have defined the speed of sound

$$v_q^2 \equiv \left(\frac{\partial p}{\partial \varepsilon}\right)_{\frac{n}{s}} = \frac{s\,\delta T}{T\,\delta s}. \tag{2.93}$$

with a new dimensionless quantity being defined as

$$\mathbf{q} \equiv \frac{n}{s}. \tag{2.94}$$

We find $\delta q = \frac{\delta n}{s}$ when $n = 0$, then Equation 2.89, Equation 2.90 and Equation 2.91 becomes (55; 57)

$$\tau\frac{\partial \rho}{\partial \tau} + h v_q^2 \rho + f_s + (1-h)\,\frac{\partial \omega}{\partial \eta} = 0\ , \tag{2.95}$$

$$\tau\frac{\partial \omega}{\partial \tau} + \omega\left(1 - v_q^2 + h(1+v_q^2)\right) + \left(v_q^2 - h\right)\frac{\partial \rho}{\partial \eta} + \partial_\eta f_s - h\frac{\partial^2 \omega}{\partial \eta^2} = 0\ . \tag{2.96}$$

$$\tau\frac{\partial \delta q}{\partial \tau} + h\delta q + \partial_\eta f_n - \frac{\sigma}{\chi\tau}\cdot\frac{\partial^2 \delta q}{\partial \eta^2} = 0\ , \tag{2.97}$$

where we have used Equation 2.82, rescale the fluctuation of the flow $\omega \to (1-h)\omega$ and neglect the temperature dependence of ν.

Since the unperturbed solution is boost-invariant and independent of η, it is advantageous to use the Fourier transformation

$$\tilde{X}(k,\tau) = \int_{-\infty}^{\infty} d\eta e^{-ik\eta} X(\eta,\tau) \tag{2.98}$$

where X stands for ρ, ω or q, then Equation 2.95,Equation 2.96 and Equation 2.97 can be written as the Langevin Equation

$$\tau \frac{\partial \tilde{\boldsymbol{\Psi}}}{\partial \tau} + \boldsymbol{D}\, \tilde{\boldsymbol{\Psi}} + \tilde{\boldsymbol{f}} = 0, \tag{2.99}$$

where we have defined the hydrodynamic variable

$$\tilde{\boldsymbol{\Psi}} = \begin{pmatrix} \tilde{\rho} \\ \tilde{\omega} \\ \tilde{q}, \end{pmatrix} \tag{2.100}$$

the drift matrix as

$$\boldsymbol{D} \equiv \begin{pmatrix} h v_q^2 & ik(1-h) & 0 \\ ik\left(v_q^2 - h\right) & (1-v_q^2) + h(1+v_q^2) + hk^2 & 0 \\ 0 & 0 & \frac{\sigma}{\chi^\tau} k^2 + h \end{pmatrix} \tag{2.101}$$

and the stochastic noise as

$$\tilde{\boldsymbol{f}} = \begin{pmatrix} f_s \\ ikf_s \\ ikf_n \end{pmatrix}. \tag{2.102}$$

so that

$$\left\langle \tilde{\boldsymbol{f}}(\tau_1,k_1)\,\tilde{\boldsymbol{f}}(\tau_2,k_2)\right\rangle \;=\; 2\pi\delta(k_1+k_2)\,\delta(\tau_1-\tau_2)\cdot\frac{2\,h}{s\,A}\begin{pmatrix}1 & -ik_1 & 0\\ ik_1 & k_1^2 & 0\\ 0 & 0 & 0\end{pmatrix} +2\pi\delta(k_1+k_2)\,\delta(\tau_1-\tau_2)\cdot\frac{2\,\sigma T}{s^2\,\tau A}\begin{pmatrix}0 & 0 & 0\\ 0 & 0 & 0\\ 0 & 0 & k_1^2\end{pmatrix}. \tag{2.103}$$

In k-space the correlators of any pair of hydro variables X and Y are

$$\left\langle\,\tilde{X}(k_1,\tau_1)\,\tilde{Y}(k_2,\tau_2)\,\right\rangle \;=\; \frac{2\pi}{A}\delta(k_1+k_2)\int_{\tau_0}^{\min(\tau_1,\tau_2)}\frac{d\tau}{\tau^2}\frac{2\,T(\tau)\,h(\tau)}{w(\tau)}\,\tilde{G}_{Xs}(k_1;\tau_1,\tau)\tilde{G}_{Ys}(k_2;\tau_2,\tau) +\frac{2\pi}{A}\delta(k_1+k_2)\int_{\tau_0}^{\min(\tau_1,\tau_2)}\frac{d\tau}{\tau^2}\frac{2\,T(\tau)\,\sigma(\tau)}{s^2(\tau)\,\tau}\,\tilde{G}_{Xn}(k_1;\tau_1,\tau)\tilde{G}_{Yn}(k_2;\tau_2,\tau) \tag{2.104}$$

Here have used Equation 2.83 and Equation 2.84 and defined $\tilde{G}_{Xs}$ and $\tilde{G}_{Xn}$ to be the Green functions of Equation 2.99 which are going to be found later. For the most part we shall be interested in the equal-(proper)time correlation function at the freeze-out time τ_f, which can be written as

$$\tilde{\boldsymbol{C}}_{XY}\,(k,\tau_f)\equiv\langle\tilde{X}(k_1,\tau_f)\tilde{Y}(k_2,\tau_f)\rangle, \tag{2.105}$$

and the real space thermal correlations can be found

$$\boldsymbol{C}_{XY}(\eta_1 - \eta_2; \tau_f) \equiv \int dk_1 dk_2 e^{ik_1\eta_1 + ik_2\eta_2} \left\langle \tilde{X}(k_1, \tau_f)\, \tilde{Y}(k_2, \tau_f) \right\rangle \tag{2.106}$$

Equation 2.104 and Equation 2.105 show directly that a fluctuation at point η at time τ induces a correlation between points η_1 and η_2 at later time τ_f via a hydrodynamically propagating response.

2.2.2 Formal solutions of linear fluctuations

The solution to Equation 2.99 for arbitrary noise and drift, with the given initial conditions, can be written as

$$\tilde{\boldsymbol{\Psi}}(k, \tau) = -\int_{\tau_0}^{\tau} \frac{d\tau'}{\tau'} \tilde{\boldsymbol{U}}(k; \tau, \tau') \tilde{\boldsymbol{f}}(k, \tau') \tag{2.107}$$

which is equivalent to say that the matrix elements of $\tilde{\boldsymbol{U}}(k; \tau_f, \tau)$ are the Green functions $\tilde{G}_{Xs}$ and $\tilde{G}_{Xn}$. Substitute Equation 2.107 into Equation 2.99, we find $\tilde{\boldsymbol{U}}$ satisfies

$$\tau \frac{\partial \tilde{\boldsymbol{U}}(k; \tau, \tau')}{\partial \tau} + \boldsymbol{D}(k, \tau) \tilde{\boldsymbol{U}}(k; \tau, \tau') = 0 \tag{2.108}$$

subject to the condition $\tilde{\boldsymbol{U}}(k; \tau, \tau) = 1$. Explicitly

$$\tilde{\boldsymbol{U}}(k; \tau, \tau') = \mathcal{T} \exp\left\{ -\int_{\tau'}^{\tau} \frac{d\tau''}{\tau''} \boldsymbol{D}(k, \tau'') \right\} \tag{2.109}$$

In order to simplify Equation 2.109 we first write

$$\tilde{\boldsymbol{U}}(\tau,\tau') = \tilde{\boldsymbol{U}}(\tau,\tau_n)\tilde{\boldsymbol{U}}(\tau_{n-1},\tau_{n-2})\cdots\tilde{\boldsymbol{U}}(\tau_2,\tau_1)\tilde{\boldsymbol{U}}(\tau_1,\tau') \tag{2.110}$$

where the time difference between τ_n and τ_{n-1} is so small that we can partly neglect the time dependence of the drift matrix $\boldsymbol{D}$. (Neglect the time evolution of its eigen-vectors, but keep the time dependence of its eigen-values.) Then we define the eigen-value and eigen-vector of the drift matrix $\boldsymbol{D}$ to be $\tilde{\lambda}_i$ and φ_i, and ϕ_i to be the dual vector such that $\phi_i \cdot \varphi_j = \delta_{ij}$, which means the drift matrix can be written as

$$\boldsymbol{D}(\tau) = \sum_i \tilde{\lambda}_i(\tau)\varphi_i(\tau) \otimes \phi_i(\tau) \tag{2.111}$$

then

$$\tilde{\boldsymbol{U}}(\tau_n,\tau_{n-1}) = \sum_i \exp\left[-\int_{\tau_n}^{\tau_{n+1}} \tilde{\lambda}_i \frac{d\tau}{\tau}\right] \varphi_i(\tau_{n-1}) \otimes \phi_i(\tau_n) \tag{2.112}$$

if $\tau_n - \tau_{n-1} \ll \tau_n$. Then Equation 2.110 yields

$$\tilde{\boldsymbol{U}}(\tau_f,\tau) = \sum_i \exp\left[-\int_{\tau}^{\tau_f} \frac{d\tau'}{\tau'} \tilde{\lambda}_i(\tau')\right] \varphi_i(\tau) \otimes \phi_i(\tau_f), \tag{2.113}$$

which is much simpler than Equation 2.109.

After we find $\tilde{\boldsymbol{U}}$ from Equation 2.113, we can find the correlation matrix C defined in Equation 2.105

$$\tilde{\boldsymbol{C}}(k_1, k_2; \tau_f) = \int_{\tau_0}^{\tau_f} \frac{d\tau_1 d\tau_2}{\tau_1} \tilde{\boldsymbol{U}}(\tau_f, \tau_1) \cdot 2\tilde{\boldsymbol{Q}}(\tau_1, \tau_2, k_1, k_2)\delta(\tau_1 - \tau_2) \cdot \tilde{\boldsymbol{U}}^{\dagger}(\tau_f, \tau_2) \tag{2.114}$$

where we have defined

$$2\tilde{\boldsymbol{Q}}(\tau_1, \tau_2, k_1, k_2)\delta(\tau_1 - \tau_2) \equiv \frac{1}{\tau_2}\langle \tilde{\boldsymbol{f}}(\tau_1, k_1)\tilde{\boldsymbol{f}}^{\dagger}(\tau_2, k_2)\rangle \tag{2.115}$$

It is not hard to find that the correlation matrix in Equation 2.114 satisfies

$$\tau_f \frac{\partial \tilde{\boldsymbol{C}}}{\partial \tau_f} + \mathbf{D}\,\tilde{\boldsymbol{C}} + \left(\mathbf{D}\,\tilde{\boldsymbol{C}}\right)^{\dagger} = 2\tilde{\boldsymbol{Q}}, \tag{2.116}$$

where we have used that

$$\tau_f \frac{\partial \tilde{\boldsymbol{U}}(k, \tau_f, \tau)}{\partial \tau_f} + \mathbf{D}\,(k, \tau_f)\,\tilde{\boldsymbol{U}}(k, \tau_f, \tau) = 0 \tag{2.117}$$

Let's define the equilibrium solution of $\tilde{\boldsymbol{C}}$ as $\tilde{\boldsymbol{E}}$ (General Susceptibility) which satisfies

$$\mathbf{D}\,\tilde{\boldsymbol{E}} + \left(\mathbf{D}\,\tilde{\boldsymbol{E}}\right)^{\dagger} = 2Q, \tag{2.118}$$

and define the residue $\tilde{\boldsymbol{C}}' = \tilde{\boldsymbol{C}} - \tilde{\boldsymbol{E}}$ as non-equilibrium contribution, then we find the following

$$\tilde{\boldsymbol{C}}'(\tau_f) = \tilde{\boldsymbol{U}}(\tau_f, \tau_0)\tilde{\boldsymbol{C}}'(\tau_0)\tilde{\boldsymbol{U}}^\dagger(\tau_f, \tau_0) - \int_{\tau_0}^{\tau_f} d\tau\, \tilde{\boldsymbol{U}}(\tau_f, \tau_0) \cdot \frac{d\tilde{\boldsymbol{E}}}{d\tau} \cdot \tilde{\boldsymbol{U}}^\dagger(\tau_f, \tau_0). \tag{2.119}$$

Finally we find the solution

$$\tilde{\boldsymbol{C}}(\tau_f) \quad = \quad \boldsymbol{E}(\tau_f) + \tilde{\boldsymbol{U}}(\tau_f, \tau_0)\tilde{\boldsymbol{C}}'(\tau_0)\tilde{\boldsymbol{U}}^\dagger(\tau_f, \tau_0) - \int_{\tau_0}^{\tau_f} d\tau\, \tilde{\boldsymbol{U}}(\tau_f, \tau) \cdot \frac{d\tilde{\boldsymbol{E}}}{d\tau} \cdot \tilde{\boldsymbol{U}}^\dagger(\tau_f, \tau). \tag{2.120}$$

Equation 2.120 is the main result in this section, and it says the equal time correlations contain three parts:

- Contribution from final time thermal equilibrium correlations, and this piece is a delta function in space. This part is the result of fluctuations-dissipation theorem Equation 2.103, and it contains two parts: (a) a trivial manifestation of statistical fluctuations in the gas, a reflection of the fact that particles are trivially correlated with themselves (See §116 of (19)). We denote this piece as "**Self Correlations**"; (b)the correlations due to internal interactions between particles.
- Contribution from the initial state fluctuations. Here "initial state fluctuations" $\boldsymbol{C}'(\tau_0) = \boldsymbol{C}(\tau_0) - \boldsymbol{E}(\tau_0)$ is the difference between the complete correlations $\boldsymbol{C}(\tau_0)$ and the thermal equilibrium correlations $\boldsymbol{E}(\tau_0)$ that is completely determined by Equation 2.118[1]. The value of $\boldsymbol{C}(\tau_0)$ is usually too hard to find from first principle, due to the quantum fluc-

[1] $\boldsymbol{E}$ is more or less like the heat capacity or charge susceptibilities.

tuations in the densities of the two colliding nuclei and the fluctuations of the energy deposition mechanism. Nevertheless, the fact that the initial state of the matter created in the ultra-relativistic heavy-ion collisions such as Pb-Pb collisions at LHC or the top energy collisions of Au-Au at RHIC is dominated by saturated glue carrying no electric and baryon charge, might suppress the contribution of initial state fluctuations to the charge correlations at freeze-out time. This makes charge-charge correlations be more promising quantities to test the consequence of stochastic noises, by comparing to the event-by-event fluctuations measured at LHC and at top energy collisions of RHIC. We will discuss more details in Chapter.3.

- Contribution from the time change rate of $\mathbf{E}(\tau)$ in expanding media, which could be charge susceptibility or entropy in the whole volume. This is the most interesting part in Equation 2.120 and a novel discovery we found in (57). If the system undergoes a crossover or a first order phase transition, one would expect $\mathbf{E}(\tau)$ changes dramatically, so that this piece of contribution dominates; otherwise, this piece vanishes. We will see more details in Chapter.3.

Surprisingly, though the fluctuation-dissipation theorem tells us the magnitude of the stochastic noises are proportional to the transport coefficients such as charge conductivity σ, shear viscosity $\eta_{\rm shear}$ and bulk viscosity ζ, the overall magnitude of final pair correlations, which is due to the stochastic noises, are determined by $\mathbf{E}$, which are only directly related to the susceptibilities and heat capacity.

CHAPTER 3

FIRST APPLICATION: BALANCE FUNCTION AND CHARGE FLUCTUATIONS

In this chapter, we will apply the theory developed in Chapter.2 to study the electric charge fluctuations as well as its experimental signal-"Balance Function" at LHC and top energy of RHIC. This chapter is following (57).

3.1 A review of balance functions

For completeness we review here definitions and properties of the balance functions (85; 86).

To define the balance function we divide the phase space occupied by particles produced in a heavy-ion collision into (infinitesimally) small cells. For the purpose of this paper we consider cells in rapidity y and azimuthal angle ϕ (but integrated over transverse momentum) and denote the coordinates of the cell $\Gamma = (\phi, y)$ and the volume of the cell $d\Gamma = d\phi\, dy$. We denote the number of particles of charge $a = +, -$ in a cell as $dN^a(\Gamma)$ and its event average $\langle dN^a(\Gamma)\rangle$. Since $\langle dN^a(\Gamma)\rangle \sim d\Gamma$ is infinitesimally small, the probability of finding more than one particle in a cell is negligible ($\mathcal{O}(d\Gamma^2)$ for two or more particles) and the average $\langle dN^a(\Gamma)\rangle \ll 1$ is also the probability to find a particle of charge a in the cell.

The conditional probability of finding a particle of charge b in another cell Γ_2 given a particle of charge a in the cell Γ_1 can be found as $\langle dN^b(\Gamma_2)\, dN^a(\Gamma_1)\rangle / \langle dN^a(\Gamma_1)\rangle$ which is easy

to understand keeping in mind that $dN^a(\Gamma)$ is either 0 or (rarely) 1. The balance function as a function of a pair of cells is given by:

$$B(\Gamma_2,\Gamma_1)=\frac{1}{2}\sum_{a=+,-}\frac{\langle dN_2^{-a}dN_1^a\rangle-\langle dN_2^a dN_1^a\rangle}{d\Gamma_2\langle dN_1^a\rangle}=\frac{\langle n_2^{-a}n_1^a\rangle-\langle n_2^a n_1^a\rangle}{\langle n_1^a\rangle} \tag{3.1}$$

where we used a shorthand $dN_i^a \equiv dN^a(\Gamma_i)$ and introduced density per phase space volume $n \equiv dN/d\Gamma$. The balance function measures a difference in conditional probabilities of finding a particle of the opposite charge $-a$ vs the same charge a in the cell Γ_2 given a particle of the charge a in cell Γ_1. This probability is proportional to the volume $d\Gamma_2$ of the cell and is infinitesimally small, while its ratio to $d\Gamma_2$, as in Equation 3.1, is finite.

Since we are considering a case when $\mu = 0$, we can use $\langle n_1^-\rangle = \langle n_1^+\rangle$ to simplify Equation 3.1:

$$B(\Gamma_2,\Gamma_1)=-\frac{\left\langle (n_2^+-n_2^-)(n_1^+-n_1^-)\right\rangle}{2\langle n_1^+\rangle}=-\frac{\left\langle n_2^{net}\, n_1^{net}\right\rangle}{\langle n_1^{ch}\rangle}, \tag{3.2}$$

Since $n^{net} = dN_{net}/dyd\phi$ and $N_{net} = \delta N_{net}$ ($\langle N_{net}\rangle = 0$), this gives us Equation 3.72 used in the text.

One also defines the balance function as a function of the phase space displacement $\Delta\Gamma \equiv \Gamma_2 - \Gamma_1 = (y_2 - y_1, \phi_2 - \phi_1)$ by summing in Equation 3.1 over all cells Γ_1 and Γ_2 separated by $\Delta\Gamma$. To obtain a finite result for infinitely many infinitesimally small cells ($d\Gamma_i \to 0$) we multiply by $d\Gamma_1 d\Gamma_2$. We can then write this summation as an integral:

$$B(\Delta\Gamma)=\left(\int d\Gamma\right)^{-1}\int d\Gamma_2\int d\Gamma_1\;\delta(\Gamma_2-\Gamma_1-\Delta\Gamma)\,B(\Gamma_2,\Gamma_1)\,. \tag{3.3}$$

The normalization factor is chosen in such a way that the result tends to a finite limit with increasing total phase-space volume ($\int d\Gamma$). The expression in Equation 3.3 simplifies in the case of azimuthal and boost ($\Gamma \to \Gamma + \Delta\Gamma$) invariance. Since in this case the balance function $B(\Gamma_2, \Gamma_1)$ can only depend on $\Delta\Gamma$ we find from Equation 3.3, simply,

$$B(\Delta\Gamma) = B(\Gamma + \Delta\Gamma, \Gamma), \tag{3.4}$$

for any Γ.

The derivation above assumes that the rapidity acceptance window is infinite: $y \in (-\infty, \infty)$, or more precisely, is much larger than the rapidity range of the balance function $B(\Delta y, \Delta\psi)$. In practice, the rapidity interval has a finite width Y. Still assuming boost invariance, but integrating in Equation 3.3 over the finite rapidity window of width Y we find the balance function in a finite rapidity acceptance:

$$B(\Delta\Gamma; Y) = B(\Delta\Gamma; \infty)\, \frac{Y - \Delta y}{Y} \tag{3.5}$$

where we used $\int dy = Y$ and $\int dy_2 \int dy_1\ \delta(y_2 - y_1 - \Delta y) = Y - \Delta y$.

To express the D-measure D_m (42) in terms of the balance function we substitute $N_{net} = \int d\Gamma\, n^{net}(\Gamma)$ and $N_{ch} = \int d\Gamma\, n^{ch}(\Gamma)$ into the definition

$$D_m \equiv 4\frac{\langle(\delta N_{net})^2\rangle}{\langle N_{ch}\rangle} = 4\left(\int d\Gamma\right)^{-1} \int d\Gamma_1 \int d\Gamma_2\ \frac{\left\langle n_2^{net}\, n_1^{net}\right\rangle}{\langle n^{ch}\rangle} \tag{3.6}$$

The integrand is $-B(\Gamma_2, \Gamma_1)$ as given by Equation 3.3, except for $\Gamma_1 = \Gamma_2$, when Equation 3.3 does not apply (we have only defined $B(\Gamma_2, \Gamma_1)$ for $\Gamma_1 \neq \Gamma_2$). We can calculate the contribution from the cells $\Gamma_1 = \Gamma_2$ to Equation 3.6 separately. We note that since dN^a takes (most of the time) values 0 or 1, $(dN^a)^2 = dN^a$ and thus $\langle (dN^+ - dN^-)^2 \rangle = \langle dN^+ + dN^- \rangle$, or $\langle \delta N_{net}^2 \rangle = \langle \delta N_{ch} \rangle$, up to terms of order $\mathcal{O}(d\Gamma)^2$. Therefore, since $n = dN/d\Gamma$, the integrand in Equation 3.6 for $\Gamma_1 = \Gamma_2$ is $\langle (n^{net})^2 \rangle / \langle n^{ch} \rangle = 1/d\Gamma$. Summation over all cells with $\Gamma_1 = \Gamma_2$ gives therefore a contribution to D_m equal to (up to infinitesimally small terms $\mathcal{O}(d\Gamma)$), $4 \left(\int d\Gamma \right)^{-1} \int d\Gamma d\Gamma \cdot 1/d\Gamma = 4$. This is the value of D_m for completely uncorrelated particles. Adding the contributions from $\Gamma_1 \neq \Gamma_2$ we find therefore

$$D_m = 4 \left(1 - \left(\int d\Gamma \right)^{-1} \int d\Gamma_1 \int d\Gamma_2 \, B(\Gamma_2, \Gamma_1) \right) = 4 \left(1 - \int d(\Delta\Gamma) \, B(\Delta\Gamma) \right), \qquad (3.7)$$

where we used Equation 3.3 for the last equality. Thus the magnitude of the balance function indicates how deep the fireball created in heavy ion collisions is in QGP region.

3.2 Electric Charge Fluctuation in 3+1 Bjorken Expanding System

3.2.1 Hydrodynamics and noise

Hydrodynamics describes the slow evolution of conserved quantities such as energy, momentum, and conserved charges. In the case of QCD the charge could be the baryon number, electric charge, or strangeness. At top energies at RHIC and at LHC most particles in the final state are pions, which carry only electric charge. Therefore in this work we shall focus on electric charge fluctuations. The extension to other conserved charges such as baryon number

or strangeness should be straightforward. The five hydrodynamic equations of motion are the conservation equations for energy-momentum and charge

$$\begin{aligned} \nabla_\mu(T^{\mu\nu}) &= 0, \\ \partial_\mu(\sqrt{-g}J^\mu) &= 0. \end{aligned} \tag{3.8}$$

Here ∇_μ denotes the covariant derivative with respect to the background metric $g_{\mu\nu}$ and $g \equiv \det[g_{\mu\nu}]$ – we shall only consider flat space-time, but use curvilinear (Bjorken) coordinates. Fluctuations are described by adding stochastic noise terms $S^{\mu\nu}$ and I^μ, as explained in (19) or, in relativistic context, in (55):

$$\begin{aligned} T^{\mu\nu} &= T^{\mu\nu}_{\text{ideal}} + \Delta T^{\mu\nu} + S^{\mu\nu}, \\ J^\mu &= nu^\mu + \Delta J^\mu + I^\mu. \end{aligned} \tag{3.9}$$

Here, n and u^μ are the charge density and fluid velocity, $T^{\mu\nu}_{\text{ideal}}$ is the stress-energy tensor for an ideal fluid, and $\Delta T^{\mu\nu}$ and ΔJ^μ are dissipative (gradient) corrections to stress and current. The dissipative correction to the current to the first order in gradients is given by

$$\Delta J^\mu = \sigma T \Delta^\mu \left(\frac{\mu}{T}\right), \tag{3.10}$$

where σ is the charge conductivity, μ is the chemical potential, and $\Delta^\mu \equiv -h^{\mu\nu}\partial_\nu$ ($h^{\mu\nu} \equiv u^\mu u^\nu - g^{\mu\nu}$) is the spatial derivative in the local rest frame of the fluid (whose 4-velocity is u^μ). The diffusion coefficient D is related to the conductivity by Einstein relation

$$D = \frac{\sigma}{\chi}, \tag{3.11}$$

where χ is the electric charge susceptibility

$$\chi \equiv \left(\frac{\partial n}{\partial \mu}\right)_T. \tag{3.12}$$

The hydrodynamic equations Equation 3.8 are non-linear. However, in the domain of applicability of hydrodynamics these equations can be linearized (82) in the perturbations around a given solution of the (non-linear) deterministic equations of motion, i.e., Equation 3.8 without noise. Such linearized approach is sufficient to study two-point correlations which are the subject of this paper.

To find two-point correlation functions of hydrodynamic variables we need to know the two-point correlation functions of the noise. One-point functions vanish by definition of the noise. The fluctuation-dissipation theorem determines the magnitude of the two-point correlator:

$$\langle I^\mu(x)\rangle = 0, \tag{3.13}$$

$$\langle I^\mu(x) I^\nu(y)\rangle = 2\sigma T h^{\mu\nu}\delta(x-y), \tag{3.14}$$

where σ and T are functions of space and time given by the solution of the deterministic (without noise) hydrodynamic Equation 3.8. The correlators of $S^{\mu\nu}$ are written down in (55), but we will not need them in this work.

Generalization to non-linear treatment of fluctuations is an interesting problem, potentially relevant for the study of higher-point correlations or fluctuations near a critical point. Although linearized treatment is sufficient for the purposes of this paper, it is worth keeping in mind the issues involved in the non-linear generalization. The most obvious issue is that the noise would become multiplicative since the magnitude of its correlator in Equation 3.14 would be a function of the fluctuating hydrodynamic variables. The formal definition in Equation 3.14 would have to be supplemented by a prescription (e.g., Ito or Stratonovich) to resolve the well-known equal-time product ambiguity (see, e.g., Ref. (87)). The non-linearities also give rise to short-distance singularities (88) reminiscent of the ultraviolet divergences in quantum field theories. Such issues do not arise in the linearized treatment and we leave them outside of the scope of this paper.

3.2.2 Bjorken expansion and linear perturbations

We shall use the well-known boost-invariant Bjorken solution (61) of the deterministic hydrodynamics Equation 3.8 as the background for the linearized fluctuation analysis. It is most convenient to describe the Bjorken flow in the coordinates $(\tau, \vec{x}_\perp, \eta)$ defined as

$$\tau \equiv \sqrt{t^2 - z^2}, \tag{3.15}$$

$$\eta \equiv \tanh^{-1}\left(\frac{z}{t}\right). \tag{3.16}$$

Bjorken time τ is invariant under boosts along the z axis while Bjorken rapidity η shifts by a constant (the boost rapidity). The liquid undergoing boost-invariant expansion is locally at rest in these coordinates

$$\bar{u}^{\mu}(x) = \{1, \vec{0}, 0\}. \tag{3.17}$$

while the energy (or entropy) density is a function of τ, which can be found by solving an ordinary differential equation.

We denote the background quantities with an overbar, and consider small perturbations to entropy density, flow velocity and charge density expressed as $\rho \equiv \delta s/\bar{s}$, δu^x, δu^y, δu^η, and δn:

$$\begin{aligned} \varepsilon(\tau, \vec{x}_\perp, \eta) &= \bar{\varepsilon}(\tau) + \bar{T}(\tau)\bar{s}(\tau)\, \rho(\tau, \vec{x_\perp}, \eta) \\ &\quad + \bar{\mu}(\tau)\, \delta n(\tau, \vec{x_\perp}, \eta); \end{aligned} \tag{3.18}$$

$$u^{\mu}(\tau, \vec{x}_\perp, \eta) = \{1, \delta\vec{u}_\perp(\tau, \vec{x}_\perp, \eta), \delta u^\eta(\tau, \vec{x}_\perp, \eta)\}\,; \tag{3.19}$$

$$n(\tau, \vec{x}_\perp, \eta) = \bar{n}(\tau) + \delta n(\tau, \vec{x}_\perp, \eta); \tag{3.20}$$

where, as in Equation 3.17, we are working in the Bjorken coordinates. The quantity δu^τ vanishes at linear order due to the unit norm constraint $u_\mu u^\mu = 1$.

In general, the fluctuations of the charge and the energy density mix in Equation 3.8. However, in the special case of zero background net charge density ($\bar{n} = 0$) or, equivalently, zero chemical potential ($\bar{\mu} = 0$) the fluctuations of the charge density δn separate, at linear order considered here, from the fluctuations of entropy density and flow velocity. Since we are going to study only fluctuations of charge density, this simplifies our task considerably.

For top-energy RHIC collisions and at LHC the chemical potential is very small compared to relevant microscopic (QCD) scale and the approximation $\bar{\mu} = 0$ is useful. Since, as far as charge correlations are concerned, we can ignore entropy and flow velocity fluctuations, we shall no longer distinguish between quantities such as $\bar{s}$ and s, or $\bar{T}$ and T.

The stochastic charge diffusion equation in Equation 3.8 becomes

$$\partial_\tau J^\tau + \frac{J^\tau}{\tau} + \partial_\eta J^\eta + \vec{\nabla}_\perp \cdot \vec{J}_\perp = 0 \tag{3.21}$$

Since for the fluid locally at rest Equation 3.17 the only derivatives in $\Delta^\mu(\mu/T)$ are spatial and since T depends on τ only, we can simplify Equation 3.10 for ΔJ^μ:

$$\Delta J^\mu = \sigma \Delta^\mu \mu = D \Delta^\mu n, \tag{3.22}$$

which is Fick's law of diffusion. Substituting this into Equation 3.21, we find

$$\frac{1}{\tau}\partial_\tau \left(\tau \delta n\right) - D\left[\nabla_\perp^2 + \frac{1}{\tau^2}\partial_\eta^2\right]\delta n = -\nabla_i I^i - \nabla_\eta I^\eta. \tag{3.23}$$

We use Latin indices $i, j, ...$ to denote the two transverse directions.

To facilitate the analysis of azimuthal correlations it is useful to decompose the noise current in the transverse plane as [1]

$$I^i = \tau \nabla_j \left[g^{ij} I_S - \epsilon^{ij} I_V \right]. \tag{3.24}$$

Only I_S will contribute to Equation 3.23. In order to solve Equation 3.23, we express $\vec{x}_\perp$ in polar coordinates r and ψ, and use a Fourier-Bessel transformation for δn, I^η and I_S, which we define, for any function X, as

$$\begin{aligned} X(\tau, r, \psi, \eta) &= \sum_n \frac{e^{in\psi}}{2\pi} \int_{-\infty}^{\infty} \frac{dk_\eta}{2\pi} e^{ik_\eta \cdot \eta} \int_0^\infty dk_\perp k_\perp \\ &\times \quad J_n(k_\perp r) \tilde{X}_n(\tau, k_\perp, k_\eta), \end{aligned} \tag{3.25}$$

$$\begin{aligned} \tilde{X}_n(\tau, q_\perp, q_\eta) &= \int_0^{2\pi} e^{-in\psi} d\phi \int_{-\infty}^{\infty} e^{-iq_\eta \eta} d\eta \int_0^\infty r dr \\ &\times \quad J_n(q_\perp r) X(\tau, r, \psi, \eta). \end{aligned} \tag{3.26}$$

Inverting the transformation requires the closure relation,

$$\int_0^\infty r dr J_n(k_\perp r) J_n(q_\perp r) = \frac{\delta(k_\perp - q_\perp)}{k_\perp}. \tag{3.27}$$

---

[1] We are splitting a two-component vector into the gradient of a scalar, I_S, and a divergenceless two-vector, which, in two dimensions can also be written in terms of a scalar I_V.

3.2.3 Solution and correlations

The charge density fluctuation at a time τ_f sourced by the hydrodynamic noise I is given by (upon Fourier-Bessel transform)

$$\delta\tilde{n}_n(\tau_f, k_\perp, k_\eta) = \frac{1}{\tau}\int_{\tau_0}^{\tau_f} d\tau \left[(\tau k_\perp)^2 \tilde{I}_{S,n} - i\tau k_\eta \tilde{I}_n^\eta\right] e^{-H(\tau_f,\tau,k_\perp,k_\eta)} \tag{3.28}$$

where we defined

$$H(\tau_f, \tau, k_\perp, k_\eta) \equiv \int_\tau^{\tau_f} d\tau' D\left(\tau'\right)\left(\frac{k_\eta^2}{\tau'^2} + k_\perp^2\right). \tag{3.29}$$

The coefficients of $k_\perp^2$ and k_η^2 in Equation 3.29 are the squared diffusion distances in the $x_\perp$ and η directions. It is easy to see that by considering the equation $dl^2 = Ddt$ for the diffusion (random walk) distance dl in time dt in locally comoving frame. The length element in Bjorken coordinates is $dl^2 = \tau^2 d\eta^2 + dx_\perp^2$ and the time element is $dt = d\tau$. Thus the diffusion distance squared in the rapidity direction is given by $(\Delta\eta)^2 = \int d\tau D/\tau^2$ and in the transverse direction by $(\Delta x_\perp)^2 = \int d\tau D$.

To determine the charge density correlations, one needs Fourier-Bessel transform of the noise correlators in Equation 2.63:

$$\left\langle \tilde{I}_n^\eta(\tau, k_\perp, k_\eta)\tilde{I}_m^{*\eta}(\tau', q_\perp, q_\eta)\right\rangle = \frac{2\sigma T}{\tau^3}\delta(\tau - \tau')\hat{\delta}_{nm}(k, q), \tag{3.30}$$

$$\left\langle \tilde{I}_{S,n}(\tau, k_\perp, k_\eta)\tilde{I}_{S,m}^{*}(\tau', q_\perp, q_\eta)\right\rangle = \frac{2\sigma T}{\tau^3 k_\perp^2}\delta(\tau - \tau')\hat{\delta}_{nm}(k, q). \tag{3.31}$$

Here we introduced a shorthand

$$\hat{\delta}_{nm}(k,q) \equiv (2\pi)^2 \delta_{n,m} \delta(k_\eta - q_\eta) \frac{\delta(k_\perp - q_\perp)}{k_\perp}. \tag{3.32}$$

Using Equation 3.28,Equation 3.30 and Equation 3.31 we find for the charge density correlations (at equal time τ_f)

$$\begin{aligned} & \langle \delta\tilde{n}_n(\tau_f, k_\perp, k_\eta) \delta\tilde{n}^*_m(\tau_f, q_\perp, q_\eta) \rangle \\ = \quad & \hat{\delta}_{nm}(k,q) \frac{1}{{\tau_f}^2} \int_{\tau_0}^{\tau_f} \frac{2\sigma(\tau')T(\tau')}{\tau'} \left[(\tau')^2 k_\perp^2 + k_\eta^2 \right] e^{-2H(\tau_f, \tau', k_\perp, k_\eta)} d\tau' \end{aligned} \tag{3.33}$$

With the aid of Einstein Relation Equation 3.11, Equation 3.33 can be written as

$$\langle \delta\tilde{n}_n(\tau_f, k_\perp, k_\eta) \delta\tilde{n}^*_m(\tau_f, q_\perp, q_\eta) \rangle = \hat{\delta}_{nm}(k,q) \frac{1}{{\tau_f}^2} \int_{\tau_0}^{\tau_f} \chi(\tau') T(\tau') \tau' \frac{d}{d\tau'} e^{-2H(\tau_f, \tau', k_\perp, k_\eta)} d\tau'. \tag{3.34}$$

Finally, performing an integration by parts, we find

$$\left\langle \delta\tilde{n}_n(\tau_f, k_\perp, k_\eta) \delta\tilde{n}^*_m(\tau_f, q_\perp, q_\eta) \right\rangle = \hat{\delta}_{mn}(k,q) \cdot \frac{1}{\tau_f} \left[\chi_f T_f - s_f \tilde{A}(\tau_f, k_\perp, k_\eta) \right] \tag{3.35}$$

where we defined a dimensionless function in Fourier-Bessel space as

$$\tilde{A}(\tau_f, k_\perp, k_\eta) \equiv \frac{1}{s_f \tau_f} \left(\chi_0 T_0 \tau_0 e^{-2H(\tau_f, \tau_0, k_\perp, k_\eta)} + \int_{\tau_0}^{\tau_f} d\tau' e^{-2H(\tau_f, \tau', k_\perp, k_\eta)} \frac{d(\chi T \tau')}{d\tau'} \right). \tag{3.36}$$

Note that

$$\tilde{A}(\tau_f, k_\perp = 0, k_\eta = 0) = \frac{\chi_f T_f}{s_f}\,. \tag{3.37}$$

This, according to Equation 3.35, implies vanishing of $\langle \delta n(x)\delta n(y)\rangle$ integrated over all space (this is trivially seen also in Equation 3.33), which is a consequence of charge conservation.

It is useful to rewrite the integral over τ' in Equation 3.36 in terms of an integral over temperature T', which is straightforward. It is also useful to rewrite the integral in the definition of H in Equation 3.29 in the same way. For that we need to know $dT'/d\tau'$. We shall neglect viscous corrections and use the ideal hydro equation $\tau s = constant$, or

$$\frac{dT}{d\tau} + \frac{T v_s^2(T)}{\tau} = 0, \tag{3.38}$$

where we have used

$$v_q^2 \equiv (\partial p/\partial \varepsilon)_q = \frac{s dT}{T ds} \tag{3.39}$$

at zero charge density. Then,

$$H(T_f, T, k_\perp, k_\eta) = \int_{T_f}^{T} \left(\frac{D(T')s(T')}{\tau_f s_f}\, k_\eta^2 + \frac{s_f \tau_f D(T')}{s(T')}\, k_\perp^2 \right) \frac{dT'}{v_s^2 T'} \tag{3.40}$$

For later use, we define dimensionless quantities $\hat{D}(T) \equiv DT$, and $\hat{s}(T) \equiv s(T)/T^3$. Then $H(T_f, T, k_\perp, k_\eta)$ can be written as

$$H(T_f, T, k_\perp, k_\eta) = \frac{k_\eta^2}{\tau_f s_f} \int_{T_f}^{T} \frac{\hat{D}(T')\hat{s}(T')T'}{v_s^2(T')} dT' + s_f \tau_f k_\perp^2 \int_{T_f}^{T} \frac{\hat{D}(T')}{v_s^2(T')\hat{s}(T')(T')^5} dT', \quad (3.41)$$

where the function $\hat{s}$ can be taken directly from lattice data (see Section 3.2.5). The speed of sound can also be found from $\hat{s}$:

$$v_s^2(T) = \left(3 + \frac{d\ln\hat{s}}{d\ln T}\right)^{-1}. \quad (3.42)$$

Combining Equation 3.36 and Equation 3.41, we find

$$\tilde{A}(\tau_f, k_\perp, k_\eta) = \left[\frac{\chi_0 T_0}{s_0} e^{-2H(T_f, T_0, k_\perp, k_\eta)} - \int_{T_f}^{T_0} dT \frac{d}{dT}\left(\frac{\chi T}{s}\right) e^{-2H(T_f, T, k_\perp, k_\eta)}.\right]. \quad (3.43)$$

3.2.4 Discussion and Interpretation

Equation 3.35 describes the charge density correlation due to stochastic noise and is the main result of this section, along with the definitions Equation 3.41, Equation 3.43.

The correlator in the square brackets in Equation 3.35 naturally separates into a singular part – the first term, which is independent of k and is thus a δ-function in coordinate space, and the regular part – the second term, which vanishes at large k.

For a Boltzmann gas (which is a good approximation at freezeout) we can identify the singular term with the equilibrium self-correlation, which exists even in a non-interacting gas.

On general grounds, the correlation function of a gas of particles in equilibrium is expected to have such a delta-function term

$$\langle \delta n(\vec{x}_1) \delta n(\vec{x}_2) \rangle = \bar{n}\, \delta^3(\vec{x}_1 - \vec{x}_2) + ... \tag{3.44}$$

where "..." denotes the correlations from interactions (see §116 of (19)). This delta function is not due to a correlation between *two* particles, as it is present even in a free gas. It is a trivial manifestation of statistical *fluctuations* in the gas, a reflection of the fact that particles are trivially correlated with themselves. In a free Boltzmann gas $\bar{n} = \chi T$ which is exactly the factor appearing in Equation 3.35. The factor of ${\tau_f}^{-1}$ in Equation 3.35 is the volume Jacobian factor, $1/\sqrt{-g}$, for the delta-function in Bjorken coordinates. Because experimental measures count only *two*-particle correlations it is necessary to separate the self-correlation term before comparing with the data. The separation of such a self-correlation term has been also discussed in (89), but not in (55; 56).

We now turn to the non-singular contribution to the correlator in Equation 3.43. We note that the dimensionless quantity $\chi T/s$ (charge susceptibility per entropy) and its T-dependence plays an important role. The first term in $\tilde{A}$ is a three-dimensional negative Gaussian with width (in position space) given by the diffusion distance over the entire expansion history (since τ_0), and a magnitude controlled by the initial value of $\chi_0 T_0/s_0$. If $\chi T/s$ were constant, which would be the case in a conformal theory, and is approximately the case in high temperature QGP,

all non-trivial correlations resulting from the diffusion history of hydrodynamical fluctuations would be contained in this negative Gaussian.

The second term in Equation 3.36 is due to the change of $\chi T/s$. This term is a superposition of many Gaussians with different widths and amplitudes. Because this contribution clearly requires the (charge-carrying) constituents of the plasma to change, its main contribution comes from the QCD crossover region. We also find that this term gives the dominant contribution to the charge correlations in heavy-ion collisions. It is, therefore, essential for our calculation to know $\chi T/s$ throughout the history of a heavy-ion collision, especially in the crossover region, which is the subject of the next section.

3.2.5 The Temperature Dependence of Susceptibility per Entropy

The behavior of entropy density s and charge susceptibility χ as a function of temperature is easy to understand qualitatively and semi quantitatively. In the crossover region the QCD matter undergoes a smooth transition from the hadron gas to the QGP state. This leads to a significant increase in the number of degrees of freedom (liberation of color), i.e., growth of s/T^3. Although the number of charged degrees of freedom also increases, their average charge is smaller in QGP, and as a result the growth of χ/T^2 is only moderate. The growth of s/T^3 is much more significant (due to the gluons) and as a result the dimensionless ratio $\chi T/s$ decreases with temperature in the crossover region.

In this section, we compute the charge susceptibility and entropy density for a free gas. This should be a decent approximation to the system created in a heavy ion collision provided the temperature is much greater than or much less than the crossover temperature.

In the low temperature region, a Hadron Resonance Gas (HRG) of noninteracting resonances is typically assumed. Rather than including all resonances, we will assume only free pions and kaons. We assume Boltzmann statistics because the analytical results are available in closed form. The entropy density is

$$(Ts)_{HRG} = \varepsilon + P = \frac{3m_K^3 T}{2\pi^2} K_3\left(\frac{m_K}{T}\right) + \frac{3m_\pi^3 T}{2\pi^2} K_3\left(\frac{m_\pi}{T}\right), \tag{3.45}$$

and the electric charge susceptibility is

$$(\chi T)_{HRG} = \frac{2m_\pi^2 T}{2\pi^2} K_2\left(\frac{m_\pi}{T}\right) + \frac{2m_K^2 T}{2\pi^2} K_2\left(\frac{m_K}{T}\right). \tag{3.46}$$

Then we find

$$\left(\frac{\chi T}{s}\right)_{HRG} = \frac{2T}{3}\left[\frac{m_\pi^2 K_2\left(\frac{m_\pi}{T}\right) + m_K^2 K_2\left(\frac{m_K}{T}\right)}{m_\pi^3 K_3\left(\frac{m_\pi}{T}\right) + m_K^3 K_3\left(\frac{m_K}{T}\right)}\right] \tag{3.47}$$

If we use Bose-Einstein statistics instead of Boltzmann statistics, there is about a 4% enhancement for entropy, and an 18% enhancement for charge susceptibility at $T = 150$ MeV.

In the very high temperature region, we assume Boltzmann statistics, two massless quarks, a massive strange quark, and gluons (SB limit). We have

$$(Ts)_{QGP} = \frac{160T^4}{\pi^2} + \frac{6m_s^3 T}{\pi^2} K_3\left(\frac{m_s}{T}\right), \tag{3.48}$$

and,

$$(\chi T)_{QGP} = \frac{2T^3}{3\pi^2}\left[10 + \frac{m_s^2}{T^2}K_2\left(\frac{m_s}{T}\right)\right]. \tag{3.49}$$

Thus, in free QGP Phase

$$\left(\frac{\chi T}{s}\right)_{QGP} = \frac{1}{3}\left[\frac{10 + (\frac{m_s}{T})^2 K_2\left(\frac{m_s}{T}\right)}{80 + 3(\frac{m_s}{T})^3 K_3\left(\frac{m_s}{T}\right)}\right]. \tag{3.50}$$

If we use Fermi-Dirac statistics instead of Boltzmann statistics, there is 17% decrease in the charge susceptibility and a 1% decrease in the entropy at $T = 150$ MeV. We see that around 16-fold increase of s/T^3 in QGP relative to the pion gas overwhelms the only 2-fold increase of χ/T^2 leading to a significant decrease of $\chi T/s$.

These simple estimates are in qualitative and semi quantitative agreement with lattice QCD calculations (8; 9; 10; 11; 90) which show that both entropy density and electric charge susceptibility change significantly in the crossover region. Figure Figure 5 shows our attempt to extract the ratio $\chi T/s$ from these lattice results. In our exploratory analysis we shall ignore statistical or systematic errors on these data and use equation of state shown in Figure 5 in our computations.

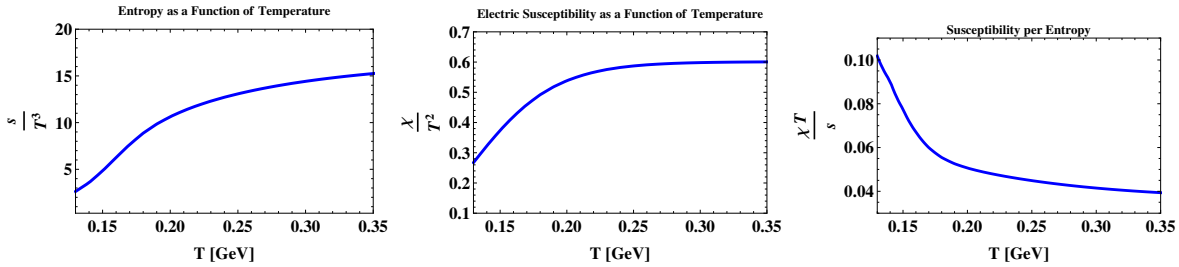

Figure 5. EOS and electric susceptibility from lattice QCD

3.3 Towards comparison with experiment

With the lattice data on electric susceptibility χ, the entropy density s and the charge diffusion coefficient[1] D, one can use the results of Equation 3.35, Equation 3.41 and Equation 3.43 to determine the spatial correlations of the net charge due to hydrodynamic fluctuations. These position space correlations need to be translated into particle momentum space correlations which are measured experimentally in a heavy-ion collision. To achieve this goal we need to address several important issues.

3.3.1 Partial chemical equilibrium

The lattice equation of state, discussed in Sec. 3.2.5, describes QCD matter in full thermal and chemical equilibrium. Although this is a reasonable approximation during much of the expansion history, it breaks down after chemical freezeout. The rate of reactions responsible for chemical equilibration (inelastic collisions) is too slow in the hadronic phase to maintain

[1]Lattice data on the charge conductivity or the diffusion coefficient D is subject to more uncertainties due to the analytic continuation from imaginary to real time and will be discussed at the end of this section and in Section 3.3.7.

chemical equilibrium. However, the thermal (kinetic) equilibrium is maintained until later times. In the intermediate region between the chemical and kinetic freezeout the matter can be described using the so-called partial chemical equilibrium (PCE) equation of state (91).

Rather than using the PCE equation of state we shall use a simpler approach, based on the observation in Ref. (92) that the PCE equation of state expressed as pressure vs energy density is very similar to the full equilibrium (FE) equation of state. Since hydrodynamic equations involve the equation of state $p(\varepsilon)$, their solution under PCE should be similar to their solution under FE. [1] The difference is manifested when we ask what the temperature is, given a value of the energy density, i.e., at a given point in time in the expansion history. Thus the actual kinetic freezeout temperature T_{kf}, which determines the final (observed) momentum spectra of the particles, is different from the temperature, T_{hf} which would correspond to the final energy density in full equilibrium equation of state. The results of Ref. (92) suggest that for the kinetic freezeout temperature $T_{kf} \approx 100$ MeV the reasonable choice of the corresponding temperature at which the FE equation of state gives the same energy density is around $T_h \approx 130$ MeV. In this approach one ends hydrodynamic evolution at a final temperature (hydrodynamic freezeout) T_h and implements the freezeout procedure with the momentum spectra of particles determined by T_{kf} (92).

---

[1] To maintain simplicity and transparency of our results we make an assumption that the same is true for the charge susceptibility χT. The charge susceptibility was not discussed in Ref. (92), and it would be interesting to test this natural assumption by applying the same methods to calculate χT. Deviations from this assumption can be included in our approach if necessary.

Additional conservation laws emerging under PCE are reflected in the appearance of corresponding chemical potentials. For our study we will need to use a chemical potential for the total pion number (the sum of the numbers of π^+ and π^-), μ_π. The value of this chemical potential has also been estimated in Ref. (92) in the range of $\mu_\pi \sim 80$ MeV. We shall use the above values for T_{kf}, T_{hf} and μ_π in our calculations of the balance functions below.

3.3.2 Transverse expansion

Since significant contribution to the balance function comes from the crossover region, we must also take into account the fact that, due to finite transverse size of the colliding nuclei, the expansion does not remain purely Bjorken. Radial flow becomes significant at times τ of order the initial radius of the nucleus R_0 and the expansion approaches isotropic 3D expansion at later times. As a result the entropy density drops much faster, approximately as τ^{-3} during this later period, as opposed to τ^{-1} during the 1D Bjorken period (38; 93).

Since analytical treatment of the full 3D expansion is beyond our reach, we consider a simple idealized approximation by assuming that the 3D stage of the expansion is short enough (due to fast drop in entropy, and thus, temperature) that the diffusion during this period can be neglected. We shall refer to this picture as the sudden transverse expansion approximation. In this idealized picture of the collision the expansion follows the 1D Bjorken solution until a point in time which we denote τ_{1D}, upon which it undergoes sudden transverse expansion and freezes out shortly thereafter at time τ_f with a pattern of flow given by the blast-wave ansatz.

We determine the charge correlator at time τ_{1D} (instead of τ_f) using Equation 3.35 and Equation 3.43 derived under conditions of the $1D$ Bjorken expansion

$$\langle \delta\tilde{n}_n(\tau_{1D}, k_\perp, k_\eta)\, \delta\tilde{n}^*_m(\tau_{1D}, q_\perp, q_\eta)\rangle \quad = \quad \frac{s_{1D}}{\tau_{1D}} \quad \cdot \quad \left[\left(\frac{\chi T}{s}\right)_{1D} - \tilde{A}(\tau_{1D}, k_\perp, k_\eta)\right], \quad (3.51)$$

where $\tilde{A}(\tau_{1D}, k_\perp, k_\eta)$ is given by Equation 3.43 with τ_f replaced with τ_{1D}. We then should treat Equation 3.51 as the initial condition for the period of the "sudden" 3D expansion. This fast expansion is essentially adiabatic and thus the ratio n/s is conserved. Since the entropy density drops from s_{1D} to s_f during this period, the charge density must also drop by the same factor. This means the charge correlator at time τ_f obeys

$$\left\langle \delta\tilde{n}_n\, \delta\tilde{n}^*_m \right\rangle_f = \frac{s_f^2}{s_{1D}^2} \left\langle \delta\tilde{n}_n\, \delta\tilde{n}^*_m \right\rangle_{1D}, \quad (3.52)$$

where $\langle \delta\tilde{n}_n\, \delta\tilde{n}^*_m \rangle_{1D}$ is given by Equation 3.51. Thus

$$\left\langle \delta\tilde{n}_n\, \delta\tilde{n}^*_m \right\rangle_f = \cdot \frac{s_f}{\tau_f} \cdot \frac{s_f \tau_f}{s_{1D}\tau_{1D}} \cdot \left[\left(\frac{\chi T}{s}\right)_{1D} - \tilde{A}(\tau_{1D}, k_\perp, k_\eta) \right]. \quad (3.53)$$

The first (local in position space) term in Equation 3.53 contains the contribution of the self-correlation which we need to subtract. As discussed in Section 3.2.4, this self-correlation term is given by $\hat{\delta}_{mn}(k,q)(\chi T/\tau)_f$. Thus we write the charge density correlations at freezeout as

$$\left\langle \delta\tilde{n}_n\, \delta\tilde{n}^*_m \right\rangle_f \equiv \hat{\delta}_{mn}(k,q) \left(\frac{\chi_f T_f}{\tau_f} - \frac{s_f}{\tau_f} \tilde{A}_f(k_\perp, k_\eta) \right), \quad (3.54)$$

which defines two-particle hydrodynamic correlator $\tilde{A}_f(k_\perp, k_\eta)$ at freezeout. Comparing Equation 3.53 and Equation 3.54, we find

$$\tilde{A}_f(k_\perp, k_\eta) = \frac{s_f \tau_f}{s_{1D}\tau_{1D}} \cdot \tilde{A}(\tau_{1D}, k_\perp, k_\eta) + \left(\frac{\chi T}{s}\right)_f - \frac{s_f \tau_f}{s_{1D}\tau_{1D}} \cdot \left(\frac{\chi T}{s}\right)_{1D} \tag{3.55}$$

and use it to calculate the balance function later in this section.

From Equation 3.55 we see that the density-density correlations built during the 1D Bjorken expansion period are diluted due to the transverse expansion by a factor $(s_f \tau_f)/(s_{1D}\tau_{1D})$ which would be equal to 1 if the system continued pure 1D expansion until freeze-out. Furthermore, the correlator $\tilde{A}_f$ contains a local term, independent of k, because the last two terms in Equation 3.55 do not cancel. This is the contribution of the noise from the period of the sudden transverse expansion. It is represented by a delta function in position space because the noise is local and we neglected diffusion during this short time, which would otherwise broaden the delta function.

3.3.3 Cooper-Frye freezeout

In order to compare our results with experimental measurements, we need to translate the hydrodynamic correlations in position space into correlations in the kinematic (momentum) space of the observed particles. For this purpose we use the standard Cooper-Frye prescription for pions:

$$\frac{dN_Q}{dyd\phi} = \frac{1}{(2\pi)^3} \int p_\perp dp_\perp \int d\sigma_\mu p^\mu \, f_Q(\vec{x}, \vec{p}) \,, \tag{3.56}$$

where $f_Q = \exp\{Q\mu/T_{hf} + \mu_\pi/T_{kf} - p_\mu u^\mu/T_{kf}\}$ is the equilibrium distribution function for pions carrying charge Q (equal to ± 1) in the Boltzmann approximation [1].

We have also defined kinematic rapidity as $y \equiv \tanh^{-1}(p^z/E)$, kinematic azimuthal angle as $\phi \equiv \tan^{-1}(p^y/p^x)$, and denoted the freezeout hypersurface normal 4-vector as $d\sigma_\mu$. The $p_\perp$ integration range is determined by experimental $p_\perp$ cuts. We choose an isochronous freeze-out condition [2] at $\tau = \tau_f$, thus

$$d\sigma_\mu p^\mu = \tau_f m_\perp d^2x_\perp d\eta \cosh(y-\eta), \tag{3.57}$$

where $m_\perp \equiv \sqrt{p_\perp^2 + m^2}$, with m being the rest mass of the pion.

Since we are interested in the effect of the hydrodynamic fluctuations, we expand the distribution function to linear order in fluctuations of temperature, chemical potential, and fluid velocity. If the average of the net chemical potential $\bar{\mu}$ is 0, then only the chemical potential fluctuation survives in the difference between particles and antiparticles:

$$\delta\frac{dN_{net}}{dyd\phi} = \frac{2\tau_f}{(2\pi)^3 T_{hf}} \cdot \int m_\perp^2 dm_\perp \int d^2x_\perp \int d\eta \cdot \delta\mu(\tau_f, \vec{x}_\perp, \eta)\, \cosh(y-\eta) f_0(\vec{x}, \vec{p}), \tag{3.58}$$

---

[1] The factors $1/T$ accompanying μ and μ_π in f_Q reflect the definitions of these chemical potentials. While μ is defined in terms of the FE equation of state used in hydrodynamics, the potential μ_π accounts for the pion excess at kinetic freezeout due to PCE.

[2] For net charge correlations at zero chemical potential this is equivalent to isothermal freeze-out because fluctuations of temperature do not mix with charge fluctuations.

where f_0 is the Boltzmann distribution function at $\mu = 0$ and

$$N_{net} \equiv N_+ - N_-. \tag{3.59}$$

Fluctuations of chemical potential are related to those of the charge density by $\delta n = \chi\, \delta\mu$.

3.3.4 Blast Wave

As we already discussed in Section 3.3.2, finiteness of the transverse size of the system leads to transverse expansion. We shall describe the transverse flow velocity profile $v_r(r)$ using transverse rapidity $\kappa(r)$

$$v_r(r) = \frac{u^r}{u^\tau} \equiv \tanh\kappa(r). \tag{3.60}$$

The distribution function f_0 can be then written as (94)

$$f_0(\vec{x},\vec{p}) = \exp\left\{\hat{\mu}_\pi + \hat{p}_\perp \cos(\phi-\psi)\sinh\kappa_f(r) - \hat{m}_\perp \cosh(y-\eta)\cosh\kappa_f(r)\right\} \tag{3.61}$$

where $\kappa_f(r)$ describes the radial flow profile at kinetic freeze-out, ψ is the position space azimuthal angle characterizing the direction of the radius-vector $\vec{x}$, and we introduced convenient dimensionless variables:

$$\hat{\mu}_\pi = \mu_\pi/T_{kf} \quad \hat{m}_\perp = m_\perp/T_{kf}, \quad \hat{p}_\perp = p_\perp/T_{kf}. \tag{3.62}$$

We apply the standard blast-wave approach, i.e., we specify the radial flow profile $\kappa(r)$ at freezeout by hand (as a linear function of r) and limit the transverse size of the system: $r < R$.

Such an approach is known to provide a reasonable approximation to single particle observables computed using a full hydrodynamic solution which includes transverse expansion (95).

Finally, we have

$$\delta\frac{dN_{net}}{dyd\phi} = \frac{\tau_f T_{kf}^3 R^2}{\chi_{hf} T_{hf}} \int d^2\vec{x}_\perp \int_{-\infty}^{\infty} d\eta \cdot \delta n(\tau_f, \vec{x}_\perp, \eta)\, F(\vec{x}, \vec{p}), \tag{3.63}$$

where we introduced the function

$$F(\vec{x}, \vec{p}) \equiv \frac{1}{4\pi^3 R^2} \int \hat{m}_\perp^2 d\hat{m}_\perp \cosh(y-\eta) \cdot f_0(\vec{x}, \vec{p}) \Theta(R-r). \tag{3.64}$$

which acts as a kernel of the transformation from the position variables $\vec{x}$ to kinematic variables $\vec{p}$. We normalized F in such a way that its Fourier-Bessel transform is dimensionless (see below).

To proceed, we introduce Fourier-Bessel expansions for both δn and F in Equation 3.63. Due to azimuthal and boost invariance (and integration over $m_\perp$ in Equation 3.64) the function $F(\vec{x}, \vec{p})$ depends only on three arguments: r and the differences $\phi - \psi$, and $y - \eta$. We define the Fourier-Bessel transform with respect to these three variables as $\tilde{F}_n(k_\perp, k_y)$ in terms of which we find, substituting Equation 3.25 and using the closure relation Equation 3.27

$$\delta\frac{dN_{net}}{dyd\phi} = \frac{\tau_f T_{kf}^3 R^2}{\chi_{hf} T_{hf}} \int_{-\infty}^{\infty} \frac{dk_y e^{ik_y y}}{2\pi} \sum_n \frac{e^{in\phi}}{2\pi} \int_0^{\infty} k_\perp dk_\perp \cdot \delta\tilde{n}_n(\tau_f, k_\perp, k_y) \tilde{F}_n(k_\perp, k_y). \tag{3.65}$$

For a given transverse flow profile at freezeout $\kappa_f(r)$ in Equation 3.60 we can obtain an expression for $\tilde{F}_n(k_\perp, k_y)$ by substituting Equation 3.61 into Equation 3.64 and integrating over variables $(\phi - \psi)$ and $(y - \eta)$ in the definition of the Fourier-Bessel transform Equation 3.26

$$\tilde{F}_n(k_\perp, k_y) = -\frac{e^{\hat{\mu}_\pi}}{\pi^2} \int \hat{m}_\perp^2 d\hat{m}_\perp \int_0^1 \hat{r} d\hat{r}\, J_n(\hat{k}_\perp \hat{r}) \cdot \mathcal{I}_n(\hat{p}_\perp \sinh\kappa_f)\, \mathcal{K}'_{ik_y}(\hat{m}_\perp \cosh\kappa_f), \tag{3.66}$$

where $\mathcal{I}$ is a modified Bessel function, $\mathcal{K}$ is the derivative of a modified Bessel function with respect to its argument and we used convenient dimensionless variables defined in Equation 3.62 as well as

$$\hat{k}_\perp = k_\perp R \quad \text{and} \quad \hat{r} = r/R. \tag{3.67}$$

It is also useful to note that the average value of the total number of charged pions

$$N_{ch} \equiv N_+ + N_- \tag{3.68}$$

per unit rapidity and azimuthal angle given by

$$\left\langle \frac{dN_{ch}}{dyd\phi} \right\rangle = \frac{2\tau_f}{(2\pi)^3} \int m_\perp^2 dm_\perp \int_{-\infty}^{\infty} d\eta \int d^2x_\perp \cdot \cosh(y-\eta) f_0(\vec{x},\vec{p}) \Theta(R-r) \tag{3.69}$$

can be also expressed as

$$\left\langle \frac{dN_{ch}}{dyd\phi} \right\rangle = \tau_f T_{kf}^3 R^2 \tilde{F}_0(0,0)\,. \tag{3.70}$$

3.3.5 Particle Correlations and Balance Function

Finally, to determine the particle correlations, we multiply two fluctuations given by Equation 3.65, average over events and express the correlator $\langle \delta\tilde{n}_n \delta\tilde{n}_m \rangle$ using Equation 3.35, with the self-correlation subtracted. The delta functions in $\hat{\delta}_{mn}$ ensure that the result is only a

function of the rapidity difference $\Delta y \equiv y_2 - y_1$, and angular difference $\Delta\phi = \phi_2 - \phi_1$ and we find

$$\begin{aligned}\left\langle \delta\frac{dN_{net}}{dy_1 d\phi_1}\ \delta\frac{dN_{net}}{dy_2 d\phi_2}\right\rangle &= -\left(\frac{T_{kf}^3}{\chi_{hf}T_{hf}}\right)^2 s_f\tau_f R^2\cdot\int_{-\infty}^{\infty}\frac{dk_y e^{ik_y\Delta y}}{2\pi}\sum_n\frac{e^{in\Delta\phi}}{2\pi}\int_0^{\infty}\hat{k}_\perp d\hat{k}_\perp \\ &\times\ \tilde{A}_f(k_\perp,k_y)\tilde{F}_n(k_\perp,k_y)\tilde{F}_n^*(k_\perp,k_y)\,, \end{aligned} \tag{3.71}$$

where $k_\perp = \hat{k}_\perp/R$ as in Equation 3.67.

When $\langle N_+\rangle = \langle N_-\rangle$, the correlator in Equation 3.71 is related to the balance function defined in (85; 86) by

$$B(\Delta y,\Delta\phi) \equiv -\left\langle \delta\frac{dN_{net}}{dy_1 d\phi_1}\ \delta\frac{dN_{net}}{dy_2 d\phi_2}\right\rangle\left\langle\frac{dN_{ch}}{dyd\phi}\right\rangle^{-1}. \tag{3.72}$$

This relationship is derived in Appendix 3.1. Finally, putting Equation 3.72,Equation 3.71 and Equation 3.70 together, we find the expression for the balance function

$$\begin{aligned} B(\Delta y,\Delta\phi) &= \frac{T_{kf}^3 s_f}{\chi_{hf}^2 T_{hf}^2\tilde{F}_0(0,0)}\cdot\int_{-\infty}^{\infty}\frac{dk_y e^{ik_y\Delta y}}{2\pi}\sum_n\frac{e^{in\Delta\phi}}{2\pi}\int_0^{\infty}\hat{k}_\perp d\hat{k}_\perp \\ &\times\ \tilde{F}_n(k_\perp,k_y)\tilde{F}_n^*(k_\perp,k_y)\tilde{A}_f(k_\perp,k_y)\,. \end{aligned} \tag{3.73}$$

We use Equation 3.73 with $\tilde{A}_f(k_\perp,k_y)$ given by Equation 3.55 to calculate the balance functions in the next section.

We can calculate the rapidity and the azimuthal projections of the balance function

$$\begin{aligned} B(\Delta y) &= \int_{-\pi}^{\pi} d\Delta\phi\, B(\Delta y, \Delta\phi), \\ B(\Delta\phi) &= \int_{-\infty}^{\infty} d\Delta y\, B(\Delta y, \Delta\phi). \end{aligned} \tag{3.74}$$

Integration over $\Delta\phi$ is equivalent to only considering the $n = 0$ moment in the summation of Equation 3.73, while integration over Δy is equivalent to setting $k_y = 0$ instead of performing an integral over k_y.

3.3.6 Results

In order to illustrate the typical shape, width and magnitude of the balance function arising due to the hydrodynamic fluctuations we calculate this function using our semianalytical model of expansion described above. For central collisions at top RHIC energies, we set the time when expansion stops being purely one-dimensional to $\tau_{1D} = 7$ fm and the corresponding temperature to $T_{1D} = 150$ MeV. We set the initial temperature to $T_0 = 350$ MeV. The hydro freezeout temperature (see Section 3.3.1) is taken to be $T_{hf} = 130$ MeV (92) We use the lattice data on entropy density $s(T)$ (90) and electric charge susceptibility $\chi(T)$ (96) as in Figure 5. We set the blast-wave transverse flow profile to be linear $v_r = \frac{3}{2}\langle\beta\rangle r/R$ with $\langle\beta\rangle = 0.6$ and maximum radius $R = 12$ fm at $\tau_f = 12$ fm (97; 92; 98).

In Figure 6, we show the sensitivity of the balance function to the charge diffusion coefficient, taking the dimensionless combination DT to be constant, with other parameters fixed. In particular, we see that, for chosen values of parameters, the data favors small values of the

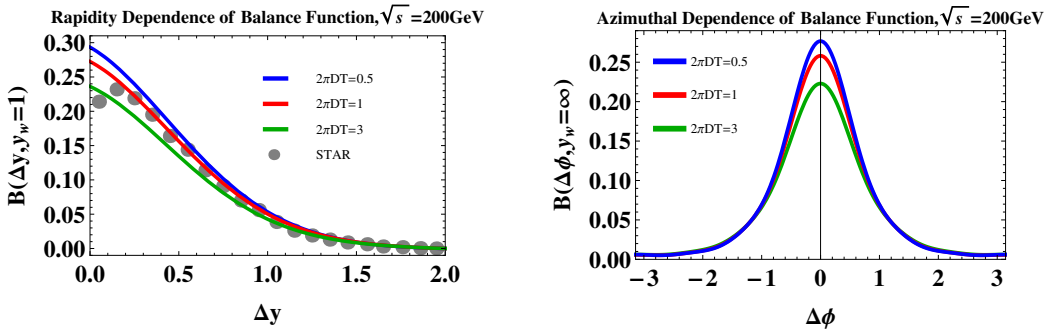

Figure 6. Balance Function at LHC and top energy of RHIC.

diffusion coefficient, $2\pi DT \sim 1$, which is characteristic of a strongly coupled medium (short mean free path). Clearly, our semiquantitative analysis is not sufficient to pin down the value of the diffusion coefficient with adequate precision, due to the balance function's sensitivity to parameters which we fixed by hand (using typical values obtained in numerical hydro simulations). However, our results are indicative of the typical resolution one could achieve if a more realistic numerical hydrodynamic simulation were to be used instead of our simplified analytical model. We leave such quantitative investigations to future work.

3.3.7 Conclusions and discussion

We showed that intrinsic hydrodynamic noise induces correlations of charge fluctuations which are observable and typically quantified in terms of the charge balance functions. We have shown how to calculate the noise contribution to the balance function and applied our method to a semianalytical model of hydrodynamic expansion. The balance functions we obtain are in reasonable agreement with experiments and our results suggest that a more realistic calculation

may allow one to determine or constrain the charge diffusion coefficient D. Our semiquantitative analysis indicates that a small value of D, characteristic of the strongly-coupled medium, is favored by the data.

Two main observations characterize the effect of the hydrodynamic noise and diffusion on the charge balance functions. We find that the magnitude of the balance function receives the most significant contribution from the time interval during the expansion where the charge susceptibility per entropy $\chi T/s$ changes most. The rapidity width of the balance function is determined by the diffusion distance that the (originally local) correlation induced by noise propagates during the time from its origin to the freezeout time. [1]

It is easy to understand that a change of the system's thermodynamic state is necessary to produce a non-local correlation. Indeed, in a static medium the correlations must be *local* (on hydrodynamic scale) despite diffusion. This requires that the contributions from successive time intervals cancel each other in a static medium, leaving eventually only the (local) contribution from the most recent time. We found that such cancellations could also occur in a medium undergoing boost-invariant longitudinal expansion as long as $\chi T\tau$ is constant (which is the same as $\chi T/s$ being constant up to small viscous corrections). In general, however, the expansion leads to nonlocal correlations which carry the memory of the expansion.

---

[1] The azimuthal width of the balance function is also sensitive to diffusion, but is strongly affected by the radial flow.

One can think of this picture as the hydrodynamic description of the mechanism of the suppression of charge fluctuations proposed and analyzed in Refs. (43; 42; 99). Indeed the D-measure, D_m, introduced in Ref.(42) is related to the balance function as (see 3.1)

$$D_m \equiv 4\frac{\langle(\delta N_{net})^2\rangle}{\langle N_{ch}\rangle} = 4\left[1 - \int_{-\infty}^{\infty} B(\Delta y)d\Delta y\right]. \tag{3.75}$$

Therefore a positive balance function corresponds to suppression of net charge fluctuations ($D_m < 4$). The balance function provides differential phase-space information on the distribution of the anti-correlation responsible for the suppression. Moreover, the positivity of the balance function can be seen as a direct consequence of the fact that $\chi T/s$ is smaller in QGP, i.e., $d(\chi T/s)/dT < 0$ (see Equation 3.43), which is the starting point of the argument in (43; 42).

One can also view this hydrodynamic picture as effectively representing the qualitative microscopic mechanism of charge balancing described in (85; 86; 100; 89). The advantage of hydrodynamic description is that it does not need to rely on existence of quasiparticles. This is especially important because both quark and hadron quasiparticle descriptions must break down in the crossover region, and this is the region responsible for the major contribution to the balance function. Our approach allows quantitative description of these phenomena from first principles, i.e., from the (lattice) equation of state and information on kinetic coefficients, within a universal hydrodynamic formalism.

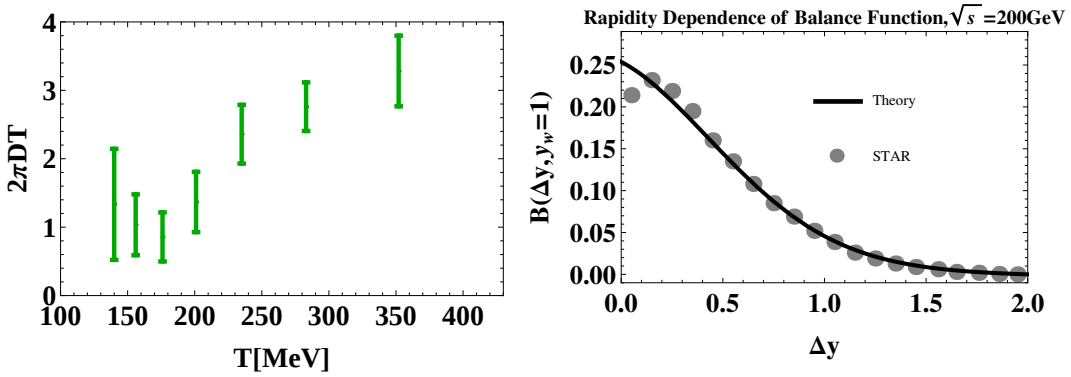

Figure 7. Diffusion constant from lattice QCD and Balance Function

One of the many simplifying assumptions in our semianalytic calculation has been the assumption that dimensionless combination DT is temperature independent. It is, perhaps, the easiest assumption to relax, provided information of the temperature dependence of the diffusion coefficient D was available. Unlike the entropy and charge susceptibility which, being static thermodynamic quantities, can be reliably measured on the lattice, the diffusion coefficient is a property of the real-time low-frequency response, which the Euclidean time lattice calculation has well-known difficulties accessing. With this caveat, it would be still interesting to extract the temperature dependence of the charge diffusion coefficient from the existing lattice data.

As a first exploratory step we attempted to combine recent lattice data on electric conductivity (101) with the electric susceptibility χ data from (96). Using the relation $D = \sigma/\chi$ we can then plot the temperature dependence of the diffusion coefficient, or its dimensionless combination $2\pi DT$ (see Figure 7).

Despite large error bars one can see that lattice results suggest that the diffusion coefficient D is indeed of order $1/2\pi T$ in the crossover region, where we now know most of the contribution to the balance function comes from. This is consistent with the results of our comparison with experimental data in Figure 6.

Taking the lattice data as given (and ignoring the error bars) we can also calculate the balance function using our semianalytic model. The result plotted in Figure 7 shows a reasonable agreement with the data.

3.4 A possible general form of the charge density-density correlations

In 3.2, we study charge density fluctuations induced by stochastic noise in 3+1 system undergoing Bjorken expansion. In 3.3.2, we approximately treat the transverse expansion is extremely fast so that the diffusion process is absent, then at the freezeout, we use add the effect of the transverse flow using blast wave model in 3.3.4. In this section, we are looking for a general solution for charge density density correlations under any flow assuming that we already the type of this flow. Now let's work in a local rest frame in which $u^\mu = (1, 0, 0, 0)$, and that the metric $g^{\mu\nu}$ satisfies $g^{\rho\rho} = 1$ (Here we assume ρ is the time direction like τ for Bjorken flow) and the space projection $h^{\mu\nu} = u^\mu u^\nu - g^{\mu\nu}$ satisfies $h^{\rho\rho} = 0$. Under this coordinates, the charge conservation equation

$$\partial_\mu \left(\sqrt{-g} J^\mu\right) = 0 \tag{3.76}$$

with

$$g \equiv det\left(g^{\mu\nu}\right) \tag{3.77}$$

can be written as

$$\partial_\rho(\frac{\delta n}{s}) + \frac{1}{\sqrt{-g}}\partial_i\left[\sqrt{-g}Dh^{ij}\partial_j(\frac{\delta n}{s}) + \sqrt{-g}(\frac{I^i}{s})\right] = 0 \tag{3.78}$$

where we have use the ideal hydrodynamics

$$\partial_\mu(\sqrt{-g}su^\mu) = \partial_\rho(\sqrt{-g}s) = 0 \tag{3.79}$$

Let's define

$$L(\vec{x},\vec{x'}) = \frac{1}{\sqrt{-g}}\partial_i\left[\sqrt{-g}Dh^{ij}\partial_j\right]\delta(\vec{x}-\vec{x'}), \tag{3.80}$$

then we find the solution is

$$\left(\frac{\delta n}{s}\right)_{\rho_f} = \int d\rho d\vec{x'}^3 e^{-\int_\rho^{\rho_f} d\rho\, L(\vec{x},\vec{x'})} \times \frac{1}{\sqrt{-g}}\partial_i\left[\sqrt{-g}\left(\frac{I^i(\rho,\vec{x'})}{s(\rho,\vec{x'})}\right)\right] \tag{3.81}$$

Let's recall

$$\langle I^i I^j\rangle = 2\sigma T\, h^{ij}\frac{1}{\sqrt{-g}}\delta(\rho-\rho')\delta(\vec{x}-\vec{x}'), \tag{3.82}$$

so we find

$$
\begin{aligned}
&\left\langle \left(\frac{\delta n}{s}\right)(\vec{x}) \left(\frac{\delta n}{s}\right)(\vec{y}) \right\rangle_{\rho_f} \\
= &\int d\rho d\rho' d\vec{x'}^3 d\vec{y'}^3 e^{-\int_\rho^{\rho_f} d\rho\, L(\vec{x},\vec{x'})} \cdot e^{-\int_{\rho'}^{\rho_f} L(\vec{y},\vec{y'})} \cdot \frac{1}{\sqrt{-g(\rho,\vec{x'})}} \frac{1}{\sqrt{-g(\rho',\vec{y'})}} \\
&\frac{\partial}{\partial x'_i}\left(-\frac{\partial}{\partial y'_j}\right)\left[\sqrt{-g(\rho,\vec{x'})}\sqrt{-g(\rho',\vec{y'})}\left(\left(\frac{I^i}{s}\right)(\rho,\vec{x'})\right)\left(\left(\frac{I^j}{s}\right)(\rho',\vec{y'})\right)\right] \\
\\
= &\int d\rho d\rho' d\vec{x'}^3 d\vec{y'}^3 e^{-\int_\rho^{\rho_f} L(\vec{x},\vec{x'})} \cdot e^{-\int_{\rho'}^{\rho_f} d\rho\, L(\vec{y},\vec{y'})} \cdot \frac{1}{s\sqrt{-g(\rho,\vec{x'})}} \frac{1}{s\sqrt{-g(\rho',\vec{y'})}} \cdot \\
&\frac{\partial}{\partial x'_i}\left(-\frac{\partial}{\partial y'_j}\right)\left[2\sigma T\, h^{ij}\sqrt{-g(\rho,\vec{x'})}\sqrt{-g(\rho',\vec{y'})}\,\frac{1}{\sqrt{-g}}\,\delta(\rho-\rho')\delta(\vec{x'}-\vec{y'})\right] \qquad (3.83)
\end{aligned}
$$

where we have consider the conjugate of partial derivative has a minus sign. Now we use the ideal hydrodynamics

$$\partial_\rho\left(s\sqrt{-g(\rho,\vec{x'})}\right) = 0, \qquad (3.84)$$

we find

$$
\begin{aligned}
\left\langle \delta n(\vec{x})\delta n(\vec{y})\right\rangle_{\rho_f} = &\int d\vec{x'}^3 d\vec{y'}^3 \frac{1}{\sqrt{-g(\rho_f,\vec{x'})}\sqrt{-g(\rho_f,\vec{y'})}} \cdot \int d\rho e^{-\int_\rho^{\rho_f} d\rho\, L(\vec{x},\vec{x'})} \cdot \\
&e^{-\int_\rho^{\rho_f} L(\vec{y},\vec{y'})} \cdot \frac{\partial}{\partial x'_i}\left(-\frac{\partial}{\partial y'_j}\right)\left[2\sigma T\, h^{ij}\sqrt{-g(\rho,\vec{x'})}\,\delta(\vec{x'}-\vec{y'})\right] \qquad (3.85)
\end{aligned}
$$

Now, we notice that

$$L(\vec{x},\vec{x'}) = \frac{1}{\sqrt{-g}}\partial_i[\sqrt{-g}Dh^{ij}\partial_j]\delta(\vec{x}-\vec{x'}) \qquad (3.86)$$

is proportional to a identity matrix in coordinate space, so $e^{-\int d\rho L}$ is also proportional to identity matrix $\delta(\vec{x}-\vec{x'})$. Thus Equation 3.48 gives

$$\begin{aligned}\left\langle \delta n(\vec{x})\delta n(\vec{y})\right\rangle_{\rho_f} &= \frac{1}{-g_f}\int d\vec{x'}^3 d\vec{y'}^3 d\rho e^{-\int_\rho^{\rho_f} L_0(\vec{x})}\delta(\vec{x}-\vec{x'})\cdot e^{-\int_\rho^{\rho_f} d\rho\, L_0(\vec{y})}\delta(\vec{y}-\vec{y'})\cdot \\ &\quad \frac{\partial}{\partial x'_i}\frac{\partial}{\partial x'_j}\left[2\sigma T\, h^{ij}\sqrt{-g(\rho,\vec{x'})}\right]\delta(\vec{x'}-\vec{y'}) \qquad (3.87)\end{aligned}$$

where

$$L_0(\vec{x}) = \frac{1}{\sqrt{-g}}\partial_i\left[\sqrt{-g}Dh^{ij}\partial_j\right]. \qquad (3.88)$$

If we find a proper transformation to transform to the momentum space, then the delta function should not bother us at all. If $\partial_i(\sqrt{-g}h^{ij})=0$, then

$$L_0 = \partial_i\partial_j[D\sqrt{-g(\rho,\vec{x'})}h^{ij}]. \qquad (3.89)$$

Therefore, we can perform integration by parts. Finally, we get

$$\begin{aligned}&\left\langle \delta n(\vec{x})\delta n(\vec{y})\right\rangle_{\rho_f} \\ &= \frac{s_f}{\sqrt{-g_f}}\left[\left(\frac{\chi T}{s}\right)_f - \left(\frac{\chi T}{s}\right)_0 - \int d\vec{x'}^3 d\rho \frac{d\left(\frac{\chi T}{s}\right)}{d\rho}e^{-\int_\rho^{\rho_f} d\rho(L_0(\vec{x})+L_0(\vec{y}))}\,\delta(\vec{x}-\vec{x'})\delta(\vec{y}-\vec{x'})\right] \qquad (3.90)\end{aligned}$$

Replace $g_f=-\tau_f^2$, and notice

$$L_0(\vec{x}) = \frac{D}{\tau^2}\partial_\xi^2 \qquad (3.91)$$

we recover the result for Bjorken flow.

CHAPTER 4

SECOND APPLICATION: ACCEPTANCE DEPENDENCE OF PARTICLE CUMULANTS NEAR QCD CRITICAL POINT

In this chapter, we will study the normalized kurtosis measured in beam energy scanning program of the Heavy Ion Collisions. This chapter is following (59).

4.1 Introduction

QCD critical point is a distinct singular feature of the phase diagram, and locate this point in (μ_B, T) plane is an important and well defined task. Even though the exact location of the critical point is not known to us yet, the available theoretical estimates strongly indicate that the point is within the region of the phase diagram probed by the heavy-ion collision experiments(1; 41). The characteristic feature of this critical point is the divergence of the correlation length ξ and the divergence of the magnitude of the fluctuations, thus by scanning on the phase diagram, some non-monotonous behaviors of the magnitude of the thermal fluctuations, such variance of multiplicity and transverse momentum, could be catched by Event-by-Event fluctuations in RHIC experiments (49; 50).

Nevertheless, the magnitude of ξ is limited trivially by the system size, and most stringently by the finite-time effects due to critical slowing down (49; 51), which makes the correlation length may reach at most the value of $2 \sim 3$ fm (51). Compared to its natural value of 1 fm, this relative small divergence may make discovering the critical non-monotonous behavior be

challenging task, if the measures depend on ξ too weakly. Recently, higher, non-Gaussian, moments of the fluctuations which depend much more sensitively on ξ, are suggested for searching QCD critical point (40; 52; 41). The 4-th order cumulant (or kurtosis) of the baryon charge fluctuations are predicted to change the sign when scanning on the phase diagram from crossover region to first order transition region (41). The STAR Collaboration has published the beam energy dependence of higher moments of the net proton (as proxy of net-baryon) multiplicity distributions from RHIC BES $Au + Au$ collision data (102; 103; 53; 54; 104). The protons and anti-protons are identified with ionization energy loss in the Time Projection Chamber (TPC) of the STAR detector within transverse momentum range $0.4 < p_\perp < 0.8$ GeV/c and at mid-rapidity $|y| < 0.5$ (104; 105). They found, for central collisions, within the statistical and systematic errors of the data, the normalized kurtosis values at all energies are consistent with each other, except for $\sqrt{s_{NN}} = 7.7$ GeV where $\mu_B = 420$ MeV and $T_f = 120 \sim 140$ MeV (39). Recently, the STAR Collaboration extends their analysis to $0.4 < p_\perp < 2$ GeV/c and at mid-rapidity $|y| < 0.5$, they find a stronger signal of the sign change of net proton normalized kurtosis at collision energy $\sqrt{s_{NN}} = 11.5$ GeV (102; 103), this encourages people to study the net proton kurtosis with broader $p_\perp$ and larger rapidity acceptance. In this letter, we will study the magnitude of the net proton kurtosis measured by the real detector with finite rapidity and transverse momentum acceptance, related to the one measured by the ideal detector.

4.2 Cumulants, Factorial cumulants and Interactions

4.2.1 Cumulants from particle distribution function

We first review some basics of cumulants, factorial cumulants as well as their relation to the fluctuations induced by the physical interactions. The 2-, 3- and 4- particle correlators can be calculated using the correlation between the fluctuations of particle distribution function $\delta f_{\boldsymbol{s}}(\boldsymbol{x},\boldsymbol{p})$'s at different momenta and spin, where $\delta f_{\boldsymbol{s}}(\boldsymbol{x},\boldsymbol{p}) \equiv f_{\boldsymbol{s}}(\boldsymbol{x},\boldsymbol{p}) - \langle f_{\boldsymbol{s}}(\boldsymbol{x},\boldsymbol{p})\rangle$(Here we choose to reserve $\langle ...\rangle$ for averaging over an ensemble of events). The particle number with momentum and spin $n_{\boldsymbol{s}}(\boldsymbol{p})$ is

$$n_i \equiv n_{\boldsymbol{s}_i}(\boldsymbol{p}_i) \equiv \int_V f_{\boldsymbol{s}_i}(\boldsymbol{x}_i,\boldsymbol{p}_i) \tag{4.1}$$

with the volume integral

$$\int_V \equiv \int d^3\boldsymbol{x}, \tag{4.2}$$

In order to see the non-trivial arising of self correlations by counting the same particle multiple times, we first consider 3-particle correlator

$$\begin{aligned}
& \langle \delta n_1\, \delta n_2\, \delta n_3\rangle \\
= \;& \delta_{1,2}\,\delta_{2,3}\,\bar{n}_1 + \delta_{1,2}\,\langle n_2\,\delta n_3\rangle_{\rm phy} + \delta_{1,3}\,\langle n_1\,\delta n_2\rangle_{\rm phy} + \delta_{2,3}\,\langle \delta n_1\, n_3\rangle_{\rm phy} + \langle \delta n_1\,\delta n_2\,\delta n_3\rangle_{\rm phy} \\
= \;& \delta_{1,2}\,\delta_{2,3}\,\bar{n}_1 + \Big(\delta_{1,2}\;\langle \delta n_2\,\delta n_3\rangle_{\rm phy} + \delta_{1,3}\;\langle \delta n_1\,\delta n_2\rangle_{\rm phy} + \delta_{2,3}\;\langle \delta n_1\,\delta n_3\rangle_{\rm phy}\Big) \\
& + \langle \delta n_1\,\delta n_2\,\delta n_3\rangle_{\rm phy}
\end{aligned} \tag{4.3}$$

Figure 8. Diagrammatic representation of the r.h.s. of Equation 4.8

where we have defined

$$\delta_{ij} \equiv (2\pi)^3 \, \delta(\boldsymbol{p}_i - \boldsymbol{p}_j) \, \delta_{\boldsymbol{s}_i, \boldsymbol{s}_j}, \tag{4.4}$$

$$\bar{n} \equiv \langle n \rangle, \tag{4.5}$$

and the subscript "phy" denote the correlations are due to physical interaction but not trivial statistics. Since the total multiplicity of proton is just

$$\delta N = \sum_{\mathbf{s}} \int_{\boldsymbol{p}} \delta n_{\boldsymbol{s}}(\boldsymbol{p}) \tag{4.6}$$

where the momentum integral is

$$\int_{\boldsymbol{p}} \equiv \frac{1}{(2\pi)^3} \int d^3\boldsymbol{p} \tag{4.7}$$

Thus the 3rd order cumulant is depicted in Figure 8

$$\begin{aligned} \kappa_3 &\equiv \left\langle (\delta N)^3 \right\rangle \\ &= \sum_{\mathbf{s_1}, \mathbf{s_2}, \mathbf{s_3}} \int_{\boldsymbol{p}_1} \int_{\boldsymbol{p}_2} \int_{\boldsymbol{p}_3} \langle \delta n_1 \, \delta n_2 \, \delta n_3 \rangle_c \\ &= \bar{N} + \kappa_{3,\mathrm{phy}} + 3 \, \kappa_{2,\mathrm{phy}} \end{aligned} \tag{4.8}$$

where we have defined

$$\kappa_{3,\mathrm{phy}} \equiv d_{\boldsymbol{s}}^3 \int_{\boldsymbol{p}_1}\int_{\boldsymbol{p}_2}\int_{\boldsymbol{p}_3} \langle \delta n_1\, \delta n_2\, \delta n_3\rangle_{\mathrm{phy}} \tag{4.9}$$

and

$$\kappa_{2,\mathrm{phy}} \equiv d_{\boldsymbol{s}}^2 \int_{\boldsymbol{p}_1}\int_{\boldsymbol{p}_2} \langle \delta n_1 \delta n_2\rangle_{\mathrm{phy}} \tag{4.10}$$

with d_s being the degeneracy of the particle species.

For 4-particle correlator, we find

$$\begin{aligned}
&\langle \delta n_1\, \delta n_2\, \delta n_3\, \delta n_4\rangle \\
=\;& \delta_{1,2}\,\delta_{2,3}\,\delta_{3,4}\bar{n}_1 \\
&+\Big[\;(\delta_{1,2}\,\delta_{3,4}\,\bar{n}_1\,\bar{n}_3 + \delta_{1,3}\,\delta_{2,4}\,\bar{n}_1\,\bar{n}_2 + \delta_{1,4}\,\delta_{2,3}\,\bar{n}_1\,\bar{n}_2) \\
&+\Big(\delta_{1,2}\delta_{3,4}\;\langle \delta n_1 \delta n_3\rangle_{\mathrm{phy}} + \delta_{1,3}\delta_{2,4}\;\langle \delta n_1 \delta n_2\rangle_{\mathrm{phy}} + \delta_{1,4}\delta_{2,3}\;\langle \delta n_1 \delta n_2\rangle_{\mathrm{phy}}\Big)\;\Big] \\
&+\Big[\;\delta_{1,2}\,\bar{n}_1\;\langle \delta n_3\,\delta n_4\rangle_{\mathrm{phy}} + \delta_{1,3}\,\bar{n}_1\;\langle \delta n_2\,\delta n_4\rangle_{\mathrm{phy}} + \delta_{1,4}\,\bar{n}_1\;\langle \delta n_2\,\delta n_3\rangle_{\mathrm{phy}} \\
&+\delta_{2,3}\,\bar{n}_2\;\langle \delta n_1\,\delta n_4\rangle_{\mathrm{phy}} + \delta_{2,4}\,\bar{n}_2\;\langle \delta n_1\,\delta n_3\rangle_{\mathrm{phy}} + \delta_{3,4}\,\bar{n}_3\;\langle \delta n_1\,\delta n_2\rangle_{\mathrm{phy}} \\
&+\Big(\delta_{1,2}\;\langle \delta n_1 \delta n_3\,\delta n_4\rangle_{\mathrm{phy}} + \text{other five combinations}\Big)\;\Big] \\
&+\Big[\delta_{1,2}\delta_{2,3}\;\langle \delta n_1 \delta n_4\rangle_{\mathrm{phy}} + \delta_{1,2}\delta_{2,4}\;\langle \delta n_2 \delta n_3\rangle_{\mathrm{phy}} + \delta_{1,3}\delta_{3,4}\;\langle \delta n_2 \delta n_4\rangle_{\mathrm{phy}} + \delta_{2,3}\delta_{3,4}\;\langle \delta n_1 \delta n_3\rangle_{\mathrm{phy}}\Big] \\
&+\langle \delta n_1\,\delta n_2\,\delta n_3\,\delta n_4\rangle_{\mathrm{phy}}
\end{aligned} \tag{4.11}$$

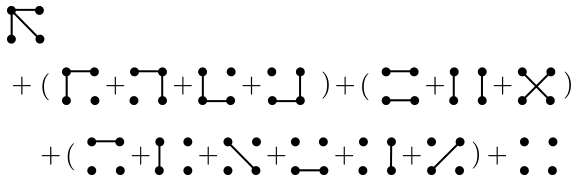

Figure 9. Diagrammatic representation of the r.h.s. of Equation 4.13 and Equation 4.14

Secondly we note

$$
\begin{aligned}
& \left(\langle \delta n_1\, \delta n_2\rangle\ \langle \delta n_3\, \delta n_4\rangle + \langle \delta n_1\, \delta n_3\rangle\ \langle \delta n_2\, \delta n_4\rangle + \langle \delta n_1\, \delta n_4\rangle\ \langle \delta n_2\, \delta n_3\rangle\right) \\
= \quad & \left(\delta_{1,2}\,\delta_{3,4}\,\bar{n}_1\,\bar{n}_3 + \delta_{1,3}\,\delta_{2,4}\,\bar{n}_1\,\bar{n}_2 + \delta_{1,4}\,\delta_{2,3}\,\bar{n}_1\,\bar{n}_2\right) \\
& + \Big[\delta_{1,2}\,\bar{n}_1\ \langle \delta n_3\, \delta n_4\rangle_{\rm phy} + \delta_{1,3}\,\bar{n}_1\ \langle \delta n_2\, \delta n_4\rangle_{\rm phy} + \delta_{1,4}\,\bar{n}_1\ \langle \delta n_2\, \delta n_3\rangle_{\rm phy} \\
& + \delta_{2,3}\,\bar{n}_2\ \langle \delta n_1\, \delta n_4\rangle_{\rm phy} + \delta_{2,4}\,\bar{n}_2\ \langle \delta n_1\, \delta n_3\rangle_{\rm phy} + \delta_{3,4}\,\bar{n}_3\ \langle \delta n_1\, \delta n_2\rangle_{\rm phy}\Big] \\
& + \Big[\langle \delta n_1\, \delta n_2\rangle_{\rm phy}\ \langle \delta n_3\, \delta n_4\rangle_{\rm phy} + \langle \delta n_1\, \delta n_3\rangle_{\rm phy}\ \langle \delta n_2\, \delta n_4\rangle_{\rm phy} + \langle \delta n_1\, \delta n_4\rangle_{\rm phy}\ \langle \delta n_2\, \delta n_3\rangle_{\rm phy}\Big]
\end{aligned}
\tag{4.12}
$$

Then the 4th order cumulant is depicted in Figure 9

$$
\begin{aligned}
& \langle \delta n_1\, \delta n_2\, \delta n_3\, \delta n_4 \rangle_c \\
\equiv\ & \langle \delta n_1\, \delta n_2\, \delta n_3\, \delta n_4 \rangle - (\langle \delta n_1\, \delta n_2 \rangle\ \langle \delta n_3\, \delta n_4 \rangle + \langle \delta n_1\, \delta n_3 \rangle\ \langle \delta n_2\, \delta n_4 \rangle + \langle \delta n_1\, \delta n_4 \rangle\ \langle \delta n_2\, \delta n_3 \rangle) \\
=\ & \delta_{1,2}\, \delta_{2,3}\, \delta_{3,4} \bar{n}_1 + \langle \delta n_1\, \delta n_2\, \delta n_3\, \delta n_4 \rangle_{\rm phy} \\
& - \Big[\langle \delta n_1\, \delta n_2 \rangle_{\rm phy}\ \langle \delta n_3\, \delta n_4 \rangle_{\rm phy} + \langle \delta n_1\, \delta n_3 \rangle_{\rm phy}\ \langle \delta n_2\, \delta n_4 \rangle_{\rm phy} + \langle \delta n_1\, \delta n_4 \rangle_{\rm phy}\ \langle \delta n_2\, \delta n_3 \rangle_{\rm phy} \Big] \\
& + \Big[\delta_{1,2} \delta_{3,4}\ \langle \delta n_1 \delta n_3 \rangle_{\rm phy} + \delta_{1,3} \delta_{2,4}\ \langle \delta n_1 \delta n_2 \rangle_{\rm phy} + \delta_{1,4} \delta_{2,3}\ \langle \delta n_1 \delta n_2 \rangle_{\rm phy} \Big] \\
& + \Big[\delta_{1,2}\ \langle \delta n_1 \delta n_3\, \delta n_4 \rangle_{\rm phy} + \text{other five combinations} \Big] \\
& + \Big[\delta_{1,2} \delta_{2,3}\ \langle \delta n_1 \delta n_4 \rangle_{\rm phy} + \delta_{1,2} \delta_{2,4}\ \langle \delta n_2 \delta n_3 \rangle_{\rm phy} + \delta_{1,3} \delta_{3,4}\ \langle \delta n_2 \delta n_4 \rangle_{\rm phy} + \delta_{2,3} \delta_{3,4}\ \langle \delta n_1 \delta n_3 \rangle_{\rm phy} \Big]
\end{aligned}
\tag{4.13}
$$

Therefore

$$
\begin{aligned}
\kappa_4 \ &\equiv\ \sum_{\boldsymbol{s}_1, \boldsymbol{s}_2, \boldsymbol{s}_3, \boldsymbol{s}_4} \int_{\boldsymbol{p}_1} \int_{\boldsymbol{p}_2} \int_{\boldsymbol{p}_3} \int_{\boldsymbol{p}_4} \langle \delta n_1\, \delta n_2\, \delta n_3\, \delta n_4 \rangle_c \\
&=\ \bar{N} + \kappa_{4,\rm phy} + 6\, \kappa_{3,\rm phy} + 7\, \kappa_{2,\rm phy}
\end{aligned}
\tag{4.14}
$$

where we have defined

$$
\begin{aligned}
\kappa_{4,\rm phy} \ \equiv\ & d_{\boldsymbol{s}}^4 \int_{\boldsymbol{p}_1} \int_{\boldsymbol{p}_2} \int_{\boldsymbol{p}_3} \int_{\boldsymbol{p}_4} \Big[\ \langle \delta n_1\, \delta n_2\, \delta n_3\, \delta n_4 \rangle_{\rm phy} \\
& - \Big(\langle \delta n_1\, \delta n_2 \rangle_{\rm phy}\ \langle \delta n_3\, \delta n_4 \rangle_{\rm phy} + \langle \delta n_1\, \delta n_3 \rangle_{\rm phy}\ \langle \delta n_2\, \delta n_4 \rangle_{\rm phy} + \langle \delta n_1\, \delta n_4 \rangle_{\rm phy}\ \langle \delta n_2\, \delta n_3 \rangle_{\rm phy} \Big)\ \Big]
\end{aligned}
\tag{4.15}
$$

4.2.2 Cumulants and factorial cumulants

For simplicity, we consider the particle number distribution function P(N). The momentum generating function is defined as

$$\mathbb{M}(\tilde{\mu}) \equiv \sum_{N} e^{\tilde{\mu}N}\mathbb{P}(N) \tag{4.16}$$

while the factorial momentum generating function is defined as

$$\mathbb{M}_{fc.}(z) \equiv \sum_{N} z^{N}\mathbb{P}(N) \tag{4.17}$$

Then the cumulant generating function is

$$\mathbb{G}(\tilde{\mu}) \equiv \ln \mathbb{M} \tag{4.18}$$

the factorial cumulant generating function is

$$\mathbb{G}_{fc.}(z) \equiv \ln \mathbb{M}_{fc.} \tag{4.19}$$

The cumulants can be found by

$$\kappa_{n} = \left(\frac{\partial^{n}\mathbb{G}}{\partial\tilde{\mu}}\right)_{\tilde{\mu}=0} \tag{4.20}$$

The factorial cumulants can be found by

$$\kappa_{n,fc.} = \left(\frac{\partial^n \mathbb{G}_{fc.}}{\partial z} \right)_{z=1} \tag{4.21}$$

It is not hard to verify the following relations hold

$$\kappa_{n,fc.} = \sum_{j=1}^{n} s(n,j)\kappa_j \tag{4.22}$$

where $s(n,j)$ are the Stirling numbers of the first kind. Take the first 4 cumulants, we find

$$\kappa_{1,fc.} = \kappa_1 = \bar{N} \tag{4.23}$$

$$\kappa_{2,fc.} = \kappa_2 - \kappa_1 \tag{4.24}$$

$$\kappa_{3,fc.} = \kappa_3 - 3\kappa_2 + 2\kappa_1 \tag{4.25}$$

$$\kappa_{4,fc.} = \kappa_4 - 6\kappa_3 + 11\kappa_2 - 6\kappa_1 \tag{4.26}$$

Thus using Equation 4.8 and Equation 4.14, we find

$$\kappa_{2,fc.} = \kappa_{2,\text{phy}} \tag{4.27}$$

$$\kappa_{3,fc.} = \kappa_{3,\text{phy}} \tag{4.28}$$

$$\kappa_{4,fc.} = \kappa_{4,\text{phy}} \tag{4.29}$$

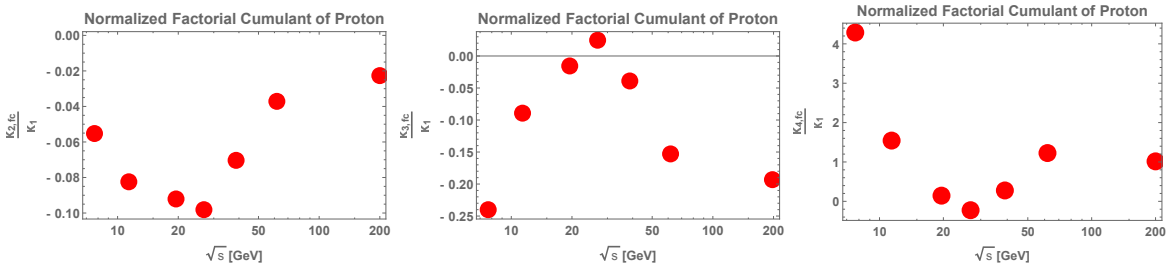

Figure 10. Factorial Cumulants of Proton.

which means factorial cumulants reveal interactions in counting statistics (106; 107). Based on Equation 4.24, Equation 4.25 and Equation 4.26, we could calculate the 2nd, 3rd and 4th order factorial cumulants of protons (not net protons) with transverse momentum $0.4GeV < p_{\perp} < 2GeV$ and the kinetic rapidity $|y| < 0.5$ for most central Au-Au collisions, by using the original data in (102). Their collision energy dependence has been plotted in Figure 10. We find both $\kappa_{2,fc.}$ and $\kappa_{3,fc.}$ are negative, but $\kappa_{4,fc.}$ is positive for most collision energies. In addition, $\kappa_{2,fc.}$, $\kappa_{3,fc.}$ and $\kappa_{4,fc.}$ all show a non-monotonic behavior as a function of collision energy $\sqrt{s}$, and the turning collision energies are all at $\sqrt{s} = 27GeV$ consistently.

4.3 Cumulants in Heavy Ion Collisions

4.3.1 Calculate Cumulants from Classical Chiral Sigma Model

In this section, we will calculate the cumulants induced by fluctuations of critical condensation-σ field. In (52), the authors has shown how to calculate cumulants of critical fluctuations for a homogenous system in equilibrium. Nevertheless, the fireball created in Heavy Ion Collision, is expanding, where the existing longitudinal and transverse flow makes the proton distribu-

tion function be space-time dependent, thus we need more general framework to count non-equilibrium effects. At freeze-out when the proton density is already sufficiently small so that the thermal effects dominate over quantum effects, one can consider coupling between nucleons and σ field to be classical. Thus we are led to consider classical motion of particles with variable mass $m_{_P}(\sigma)$ (108; 40; 45). Then one find the fluctuating proton distribution induced by the fluctuation of σ is

$$\delta f_{\mathbf{s}}(\boldsymbol{p},\boldsymbol{x}) = \frac{\partial f_{\mathbf{s}}}{\partial E_{\boldsymbol{p}}}\,\frac{\partial E_{\boldsymbol{p}}}{\partial \sigma}\,\delta\sigma(\boldsymbol{x}) = -\chi_{\mathbf{p},\mathbf{s}}(\boldsymbol{x})\,\frac{g_{_P}\,m_{_P}}{E_{\boldsymbol{p}}}\,\delta\sigma(\boldsymbol{x}) \tag{4.30}$$

where $g_{_P}$ is the coupling between proton and σ field via the interacting Lagrangian

$$\mathcal{L}_{_{\sigma\,p\,p}} = g_{_P}\,\sigma\,\bar{\Psi}_{_P}\Psi_{_P} \tag{4.31}$$

and

$$\chi_{\mathbf{p},\mathbf{s}} \equiv \frac{\partial f_{\mathbf{s}}}{\partial \mu_{_B}} = -\frac{\partial f_{\mathbf{s}}}{\partial E_{\mathbf{p}}} = \frac{f_{\mathbf{s}}(1-f_{\mathbf{s}})}{T} \tag{4.32}$$

Then one can calculate the three-particle correlator

$$\begin{aligned} & \langle \delta f_s(\boldsymbol{p}_1,\boldsymbol{x}_1)\,\delta f_s(\boldsymbol{p}_2,\boldsymbol{x}_2)\,\delta f_s(\boldsymbol{p}_3,\boldsymbol{x}_3)\rangle_{c,\sigma} \\ = \; & -(g_{_P} m_{_P})^3 \left(\frac{\chi_{\mathbf{p_1},\mathbf{s}}}{E_{\boldsymbol{p}_1}}(\boldsymbol{x}_1)\;\frac{\chi_{\mathbf{p_2},\mathbf{s}}}{E_{\boldsymbol{p}_2}}(\boldsymbol{x}_2)\;\frac{\chi_{\mathbf{p_3},\mathbf{s}}}{E_{\boldsymbol{p}_3}}(\boldsymbol{x}_3)\right) \langle \delta\sigma(\boldsymbol{x}_1)\,\delta\sigma(\boldsymbol{x}_2)\,\delta\sigma(\boldsymbol{x}_3)\rangle_c \end{aligned} \tag{4.33}$$

and the four-particle correlator

$$\begin{aligned} & \langle \delta f_s(\boldsymbol{p}_1, \boldsymbol{x}_1)\, \delta f_s(\boldsymbol{p}_2, \boldsymbol{x}_2)\, \delta f_s(\boldsymbol{p}_3, \boldsymbol{x}_3)\, \delta f_s(\boldsymbol{p}_4, \boldsymbol{x}_4) \rangle_{c,\,\sigma} \\ = \;& (g_{_P} m_{_P})^4 \left(\frac{\chi_{\mathbf{p_1,s}}}{E_{\boldsymbol{p}_1}}(\boldsymbol{x}_1)\; \frac{\chi_{\mathbf{p_2,s}}}{E_{\boldsymbol{p}_2}}(\boldsymbol{x}_2)\; \frac{\chi_{\mathbf{p_3,s}}}{E_{\boldsymbol{p}_3}}(\boldsymbol{x}_3)\; \frac{\chi_{\mathbf{p_4\,s}}}{E_{\boldsymbol{p}_4}}(\boldsymbol{x}_4) \right) \langle \delta\sigma(\boldsymbol{x}_1)\, \delta\sigma(\boldsymbol{x}_2)\, \delta\sigma(\boldsymbol{x}_3)\, \delta\sigma(\boldsymbol{x}_4) \rangle_c \end{aligned} \tag{4.34}$$

where the subscript c means we only consider the connected diagramwe and we have explicitly written $\frac{T\chi_{\mathbf{p_1}}}{E_{\mathbf{p_1}}}(\boldsymbol{x}_1)$ as a function of space coordinate because of the effects of the flow.

Therefore the proton cumulants that are due to critical fluctuations are

$$\begin{aligned} \kappa_{_{2P,\sigma}} &= \left\langle (\delta N_{_P})^2 \right\rangle_{\sigma} \\ &= d_s^2 \int_{\mathbf{p_1}} \int_{\mathbf{p_2}} \int_{\mathbf{V_1}} \int_{\mathbf{V_2}} \langle\, \delta f_s(\boldsymbol{p}_1, \boldsymbol{x}_1)\, \delta f_s(\boldsymbol{p}_2, \boldsymbol{x}_2) \rangle_{\sigma} \;, \end{aligned} \tag{4.35}$$

Then the cubic cumulant due to σ interaction is

$$\begin{aligned} \kappa_{_{3P,\sigma}} &= \left\langle (\delta N_{_P})^2 \right\rangle_{c,\sigma} \\ &= d_s^3 \int_{\mathbf{p_1}} \int_{\mathbf{p_2}} \int_{\mathbf{p_3}} \int_{\mathbf{V_1}} \int_{\mathbf{V_2}} \int_{\mathbf{V_3}} \langle \delta f_s(\boldsymbol{p}_1, \boldsymbol{x}_1)\, \delta f_s(\boldsymbol{p}_2, \boldsymbol{x}_2)\, \delta f_s(\boldsymbol{p}_3, \boldsymbol{x}_3) \rangle_{c,\sigma} \end{aligned} \tag{4.36}$$

and

$$\begin{aligned}\kappa_{4P,\sigma} &= \left\langle (\delta N_{_P})^4 \right\rangle_{c,\,\sigma} \\ &= d_s^4 \int_{\mathbf{V_1}} \int_{\mathbf{V_2}} \int_{\mathbf{V_3}} \int_{\mathbf{V_4}} \int_{\mathbf{p_1}} \int_{\mathbf{p_2}} \int_{\mathbf{p_3}} \int_{\mathbf{p_4}} \langle \delta f_s(\boldsymbol{p}_1, \boldsymbol{x}_1)\, \delta f_s(\boldsymbol{p}_2, \boldsymbol{x}_2)\, \delta f_s(\boldsymbol{p}_3, \boldsymbol{x}_3)\, \delta f_s(\boldsymbol{p}_4, \boldsymbol{x}_4) \rangle_{c,\,\sigma} \ ,\end{aligned} \tag{4.37}$$

In (40), the author finds the probability distribution $P[\delta\sigma]$ can be written as

$$P[\delta\sigma] \sim \exp\left\{-\Omega[\delta\sigma]/T\right\}, \tag{4.38}$$

where Ω is the effective action (free energy) functional for the field $\delta\sigma$, which can be expanded in powers of σ as well as in the gradients:

$$\Omega = \int d^3x \, \left[\frac{1}{2} (\boldsymbol{\nabla}\delta\sigma)^2 + \frac{m_\sigma^2}{2} \delta\sigma^2 + \frac{\lambda_3}{3} \delta\sigma^3 + \frac{\lambda_4}{4} \delta\sigma^4 + \ldots \right] . \tag{4.39}$$

The propagator of the $\delta\sigma$ field in real space is

$$\langle \delta\sigma(\boldsymbol{x}_1)\, \delta\sigma(\boldsymbol{x}_2) \rangle = \frac{T}{m_\sigma^2 - \vec{\nabla}^2} \ \delta(\boldsymbol{x}_1 - \boldsymbol{x}_2) \tag{4.40}$$

and its zero momentum mode is (40)

$$\langle \sigma_0^2 \rangle \equiv \frac{1}{V^2} \int_{\mathbf{V_1}} \int_{\mathbf{V_2}} \langle \delta\sigma(\boldsymbol{x}_1)\, \delta\sigma(\boldsymbol{x}_2) \rangle = \frac{T}{m_\sigma^2\, V} \tag{4.41}$$

The finite size effect and the critical slowing down effect lead the correlation length may reach at most the value of $2-3$ fm (51), while the system transverse size $R \sim 7-10$ fm and the freeze-out time is $\tau_f \sim 10$ fm, then $\xi \ll R,\ \ \xi \ll \tau_f$ approximately. Thus

$$\vec{\nabla} \sim \frac{1}{R} \sim \frac{1}{\tau_f} \ll \frac{1}{\xi} \sim m_\sigma, \tag{4.42}$$

which means, as a first approximation, we can treat the correlation range to be localized, while only the correlation strength does depend on ξ. Then

$$\langle \delta\sigma(\boldsymbol{x}_1)\, \delta\sigma(\boldsymbol{x}_2) \rangle = \frac{T}{m_\sigma^2}\ \delta(\boldsymbol{x}_1 - \boldsymbol{x}_2) = T\, \xi^2\ \delta(\boldsymbol{x}_1 - \boldsymbol{x}_2) \tag{4.43}$$

The three particle correlation of σ field is

$$\begin{aligned} \langle \delta\sigma(\boldsymbol{x}_1)\, \delta\sigma(\boldsymbol{x}_2)\, \delta\sigma(\boldsymbol{x}_3) \rangle_c &= -\frac{\lambda_3}{3T} \int_{\mathbf{V}} \langle \delta\sigma^3(\boldsymbol{x})\, \delta\sigma(\boldsymbol{x}_1)\, \delta\sigma(\boldsymbol{x}_2)\, \delta\sigma(\boldsymbol{x}_3) \rangle_c \\ &= -\frac{2\lambda_3}{T} \int_{\mathbf{V}} \langle \delta\sigma(\boldsymbol{x})\, \delta\sigma(\boldsymbol{x}_1) \rangle \langle \delta\sigma(\boldsymbol{x})\, \delta\sigma(\boldsymbol{x}_2) \rangle \langle \delta\sigma(\boldsymbol{x})\, \delta\sigma(\boldsymbol{x}_3) \rangle \\ &= -2\lambda_3 T^2 \xi^6 \int_{\mathbf{V}} \delta(\boldsymbol{x} - \boldsymbol{x}_1)\, \delta(\boldsymbol{x} - \boldsymbol{x}_2)\, \delta(\boldsymbol{x} - \boldsymbol{x}_3) \end{aligned} \tag{4.44}$$

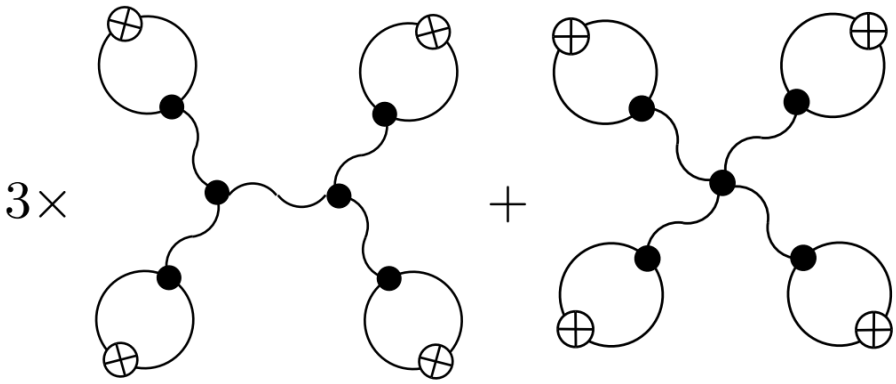

Figure 11. Diagrammatic representation of the four-particle correlator.

Substitute Equation 4.33 and Equation 4.44 into Equation 4.36, we find

$$\begin{aligned}
\kappa_{_{3P,\sigma}} &= 2d_s^3\lambda_3 T^2 \left(g_{_P} m_{_P}\, \xi^2\right)^3 \int_{\mathbf{p_1}}\int_{\mathbf{p_2}}\int_{\mathbf{p_3}}\int_{\mathbf{V}}\int_{\mathbf{V_1}}\int_{\mathbf{V_2}}\int_{\mathbf{V_3}} \\
&\quad \times \frac{\chi_{\mathbf{p_1,s}}}{E_{\mathbf{p_1}}}(\boldsymbol{x}_1)\cdot\frac{\chi_{\mathbf{p_2,s}}}{E_{\mathbf{p_2}}}(\boldsymbol{x}_2)\cdot\frac{\chi_{\mathbf{p_3,s}}}{E_{\mathbf{p_3}}}(\boldsymbol{x}_3)\cdot\delta(\boldsymbol{x}-\boldsymbol{x}_1)\,\delta(\boldsymbol{x}-\boldsymbol{x}_2)\,\delta(\boldsymbol{x}-\boldsymbol{x}_3) \\
&= 2\tilde{\lambda}_3 \left(g_{_P} m_{_P} T^{1/2}\xi^{3/2}\right)^3 \int_{\mathbf{p_1}}\int_{\mathbf{p_2}}\int_{\mathbf{p_3}}\int_{\mathbf{V_1}}\int_{\mathbf{V_2}}\int_{\mathbf{V_3}} \\
&\quad \times \frac{\chi_{\mathbf{p_1,s}}}{E_{\mathbf{p_1}}}(\boldsymbol{x}_1)\cdot\frac{\chi_{\mathbf{p_2,s}}}{E_{\mathbf{p_2}}}(\boldsymbol{x}_2)\cdot\frac{\chi_{\mathbf{p_3,s}}}{E_{\mathbf{p_3}}}(\boldsymbol{x}_3)\cdot\delta(\boldsymbol{x}_1-\boldsymbol{x}_2)\,\delta(\boldsymbol{x}_1-\boldsymbol{x}_3) \qquad (4.45)
\end{aligned}$$

If $\frac{\chi_{\mathbf{p_i\,s}}}{E_{\mathbf{p_i}}}$ has no space time dependence, then Equation 4.45 reduced to the result in (52).

For quartic cumulant, there are two types of diagrams (40)

$$
\begin{aligned}
& \langle \delta\sigma(\boldsymbol{x}_1)\,\delta\sigma(\boldsymbol{x}_2)\,\delta\sigma(\boldsymbol{x}_3)\,\delta\sigma(\boldsymbol{x}_4)\rangle_c \\
= \; & -\frac{\lambda_4}{4T}\int_{\mathbf{V}} \langle \delta\sigma^4(\boldsymbol{x})\,\delta\sigma(\boldsymbol{x}_1)\,\delta\sigma(\boldsymbol{x}_2)\,\delta\sigma(\boldsymbol{x}_3)\,\delta\sigma(\boldsymbol{x}_4)\rangle_c \\
& +\frac{1}{2}\left(\frac{\lambda_3}{3T}\right)^2 \int_{\mathbf{V_a}}\int_{\mathbf{V_b}} \langle \delta\sigma^3(\boldsymbol{x}_a)\,\delta\sigma^3(\boldsymbol{x}_b)\,\delta\sigma(\boldsymbol{x}_1)\,\delta\sigma(\boldsymbol{x}_2)\,\delta\sigma(\boldsymbol{x}_3)\,\delta\sigma(\boldsymbol{x}_4)\rangle_c
\end{aligned}
$$

$$
\begin{aligned}
= \; & -\frac{6\lambda_4}{T}\int_{\mathbf{V}} \langle \delta\sigma(\boldsymbol{x})\,\delta\sigma(\boldsymbol{x}_1)\rangle\,\langle \delta\sigma(\boldsymbol{x})\,\delta\sigma(\boldsymbol{x}_2)\rangle\,\langle \delta\sigma(\boldsymbol{x})\delta\sigma(\boldsymbol{x}_3)\rangle\,\langle \delta\sigma(\boldsymbol{x})\,\delta\sigma(\boldsymbol{x}_4)\rangle \\
& +2\left(\frac{\lambda_3}{T}\right)^2 \int_{\mathbf{V_a}}\int_{\mathbf{V_b}} \langle \delta\sigma(\boldsymbol{x}_a)\,\delta\sigma(\boldsymbol{x}_b)\rangle \;\times \\
& \times \Big[\; \langle \delta\sigma(\boldsymbol{x}_a)\,\delta\sigma(\boldsymbol{x}_1)\rangle\,\langle \delta\sigma(\boldsymbol{x}_a)\,\delta\sigma(\boldsymbol{x}_2)\rangle\,\langle \delta\sigma(\boldsymbol{x}_b)\,\delta\sigma(\boldsymbol{x}_3)\rangle\,\langle \delta\sigma(\boldsymbol{x}_b)\,\delta\sigma(\boldsymbol{x}_4)\rangle \\
& \quad +\langle \delta\sigma(\boldsymbol{x}_a)\,\delta\sigma(\boldsymbol{x}_1)\rangle\,\langle \delta\sigma(\boldsymbol{x}_a)\,\delta\sigma(\boldsymbol{x}_3)\rangle\,\langle \delta\sigma(\boldsymbol{x}_b)\,\delta\sigma(\boldsymbol{x}_2)\rangle\,\langle \delta\sigma(\boldsymbol{x}_b)\,\delta\sigma(\boldsymbol{x}_4)\rangle \\
& \quad +\langle \delta\sigma(\boldsymbol{x}_a)\,\delta\sigma(\boldsymbol{x}_1)\rangle\,\langle \delta\sigma(\boldsymbol{x}_a)\,\delta\sigma(\boldsymbol{x}_4)\rangle\,\langle \delta\sigma(\boldsymbol{x}_b)\,\delta\sigma(\boldsymbol{x}_2)\rangle\,\langle \delta\sigma(\boldsymbol{x}_b)\,\delta\sigma(\boldsymbol{x}_3)\rangle \\
& \quad +\langle \delta\sigma(\boldsymbol{x}_a)\,\delta\sigma(\boldsymbol{x}_2)\rangle\,\langle \delta\sigma(\boldsymbol{x}_a)\,\delta\sigma(\boldsymbol{x}_3)\rangle\,\langle \delta\sigma(\boldsymbol{x}_b)\,\delta\sigma(\boldsymbol{x}_1)\rangle\,\langle \delta\sigma(\boldsymbol{x}_b)\,\delta\sigma(\boldsymbol{x}_4)\rangle, \\
& \quad +\langle \delta\sigma(\boldsymbol{x}_a)\,\delta\sigma(\boldsymbol{x}_2)\rangle\,\langle \delta\sigma(\boldsymbol{x}_a)\,\delta\sigma(\boldsymbol{x}_4)\rangle\,\langle \delta\sigma(\boldsymbol{x}_b)\,\delta\sigma(\boldsymbol{x}_1)\rangle\,\langle \delta\sigma(\boldsymbol{x}_b)\,\delta\sigma(\boldsymbol{x}_3)\rangle \\
& \quad +\langle \delta\sigma(\boldsymbol{x}_a)\,\delta\sigma(\boldsymbol{x}_3)\rangle\,\langle \delta\sigma(\boldsymbol{x}_a)\,\delta\sigma(\boldsymbol{x}_4)\rangle\,\langle \delta\sigma(\boldsymbol{x}_b)\,\delta\sigma(\boldsymbol{x}_1)\rangle\,\langle \delta\sigma(\boldsymbol{x}_b)\,\delta\sigma(\boldsymbol{x}_2)\rangle \;\Big] \qquad (4.46)
\end{aligned}
$$

By the similar procedure, using Equation 4.43, we find

$$
\begin{aligned}
\kappa_{_{4P,\sigma}} &= \langle\langle (\delta N_p)^4\rangle\rangle_{c,\,\sigma} \\
&= 6d_s^4\left(2\tilde{\lambda}_3^2-\tilde{\lambda}_4\right)\left(g_{_P} m_{_P} T^{1/2}\right)^4 \xi^7 \int_{\mathbf{p_1}}\int_{\mathbf{p_2}}\int_{\mathbf{p_3}}\int_{\mathbf{p_4}}\int_{\mathbf{V_1}}\int_{\mathbf{V_2}}\int_{\mathbf{V_3}}\int_{\mathbf{V_4}} \\
&\times \frac{\chi_{\mathbf{p_1},\mathbf{s}}}{E_{\mathbf{p_1}}}(\boldsymbol{x}_1)\cdot\frac{\chi_{\mathbf{p_2},\mathbf{s}}}{E_{\mathbf{p_2}}}(\boldsymbol{x}_2)\cdot\frac{\chi_{\mathbf{p_3},\mathbf{s}}}{E_{\mathbf{p_3}}}(\boldsymbol{x}_3)\cdot\frac{\chi_{\mathbf{p_4},\mathbf{s}}}{E_{\mathbf{p_4}}}(\boldsymbol{x}_4)\cdot\delta(\boldsymbol{x}_1-\boldsymbol{x}_2)\,\delta(\boldsymbol{x}_2-\boldsymbol{x}_3)\,\delta(\boldsymbol{x}_3-\boldsymbol{x}_4) \qquad (4.47)
\end{aligned}
$$

To calculate cumulants of the fireball created in Relativistic Heavy Ion collisions near critical point, it is convenient to work in Bjorken coordinates (61) with blast wave model (94), that is

$$\int_{\mathbf{V}} \to \tau_f R^2 \int_{\eta_{\min}}^{\eta_{\max}} d\eta \int_0^1 x dx \int_0^{2\pi} d\phi \tag{4.48}$$

$$\delta(\boldsymbol{x} - \boldsymbol{x}_1) \to \frac{\delta(x - x_1)\,\delta(\phi - \phi_1)\,\delta(\eta - \eta_1)}{\tau_f R^2 x} \tag{4.49}$$

where $x \equiv \frac{r}{R}$, r is the transverse coordinate, R is the blast wave radius, ϕ is the space azimuthal angle, η is the space rapidity, τ_f is the freeze out time. We shall choose $\eta_{\max} = -\eta_{\min} = 6$ because the beam rapidity in RHIC is $-5.3 < y_{\text{beam}} < 5.3$ which leads the space time rapidity is $-5.3 < \eta < 5.3$ as estimated in (93). Substitute Equation 4.48 and Equation 4.49 into Equation 4.47, we find

$$\begin{aligned} & \kappa_{4P,\sigma} \\ = \;& 6 d_s^4 \left(2\tilde{\lambda}_3^2 - \tilde{\lambda}_4\right) (g_{_P} m_{_P})^4 \xi^7 \left(\tau_f R^2\right) T_f^6 \int_{\eta_{\min}}^{\eta_{\max}} d\eta \int_0^{2\pi} d\phi \int_0^1 x dx \\ & \times F^4 \left[x, \eta, \phi, y_{\min}, y_{\max}, \tilde{p}_{\perp,\min}, \tilde{p}_{\perp,\max}\right] \end{aligned} \tag{4.50}$$

where we have defined

$$\begin{aligned} & F \left[x, \eta, \phi, y_{\min}, y_{\max}, \tilde{p}_{\perp,\min}, \tilde{p}_{\perp,\max}\right] \\ \equiv \;& \frac{1}{(2\pi)^3} \int_{y_{\min}}^{y_{\max}} dy \int_0^{2\pi} d\psi \cdot \int_{\tilde{p}_{\perp,\min}}^{\tilde{p}_{\perp,\max}} \tilde{p}_\perp d\tilde{p}_\perp \cdot \tilde{\chi}_{\mathbf{p},\mathbf{s}}(x, \eta, \phi, \psi, \tilde{p}_\perp, y) \end{aligned} \tag{4.51}$$

with the momentum azimuthal angle to be ψ, the particle kinetic rapidity y, the dimensionless quantity $\tilde{p}_\perp \equiv \frac{p_\perp}{T_f}$ and $\tilde{\chi}_{\mathbf{p},\mathbf{s}} \equiv T\chi_{\mathbf{p},\mathbf{s}}$.

4.3.2 Boltzmann Approximation

For simplicity, we shall only consider the Boltzmann distribution, which turns out to be a very good approximation due to the large proton mass. Then we have

$$\tilde{\chi}_{\mathbf{p},\mathbf{s}} = e^{\mu_B/T - u_\mu \cdot p^\mu/T}. \tag{4.52}$$

Here

$$u_\mu p^\mu = m_{_{P,\perp}} \cosh(y-\eta)\cosh\left[\kappa(x)\right] - p_\perp \cos(\psi-\phi)\,\sinh\left[\kappa(x)\right] \tag{4.53}$$

where we have defined the transverse mass $m_{P,\perp} \equiv \sqrt{m_P^2 + \boldsymbol{p}_\perp^2}$, and the "transverse rapidity" $\kappa(x)$ at freezeout through the relation (98; 57)

$$\tanh\kappa(x) \equiv \frac{u^r}{u^\tau} = \beta_s x^n. \tag{4.54}$$

with $\beta_s = \frac{2+n}{2}\langle\beta\rangle$. Then

$$\begin{aligned} & F\left[x,\eta,\psi,y_{\min},y_{\max},\tilde{p}_{\perp,\min},\tilde{p}_{\perp,\max}\right] \\ \equiv\ & \frac{1}{(2\pi)^3}\int_{y_{\min}}^{y_{\max}} dy \int_0^{2\pi} d\phi \cdot \int_{\tilde{p}_{\perp,\min}}^{\tilde{p}_{\perp,\max}} \tilde{p}_\perp d\tilde{p}_\perp \cdot \\ \times\ & \exp\left[\tilde{\mu}_B - \tilde{m}_{_{P,\perp}}\cosh(y-\eta)\cosh(\kappa(x)) + \tilde{p}_\perp\cos(\psi-\phi)\sinh(\kappa(x))\right] \end{aligned} \tag{4.55}$$

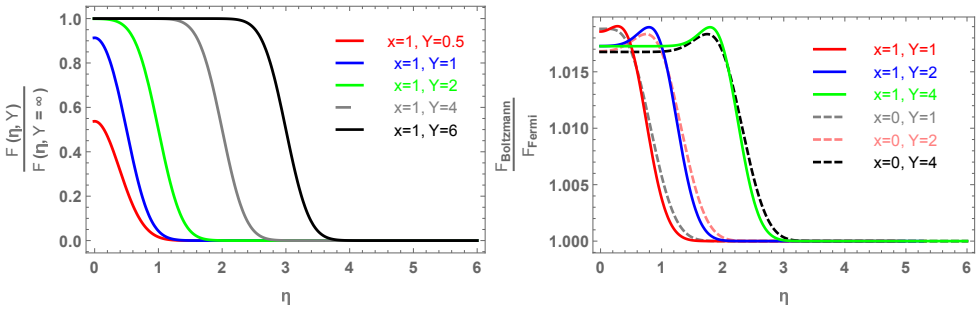

Figure 12. F defined in Equation 4.51 using Boltzmann and Fermi statistics

with

$$\tilde{\mu}_B \equiv \frac{\mu_B}{T_f}, \quad \tilde{m}_{P,\perp} \equiv \frac{m_{P,\perp}}{T_f} \tag{4.56}$$

Use the identity

$$I_0(x) = \frac{1}{2\pi}\int_0^{2\pi} \exp[x\cos(\phi)]d\phi \tag{4.57}$$

One can first integrate out the momentum azimuthal angle dependence ϕ_i, which gives

$$\begin{aligned} & F\left[x, \eta, y_{\min}, y_{\max}, \tilde{p}_{\perp,\min}, \tilde{p}_{\perp,\max}\right] \\ \equiv \quad & \frac{1}{(2\pi)^2}\int_{y_{\min}}^{y_{\max}} dy \cdot \int_{\tilde{p}_{\perp,\min}}^{\tilde{p}_{\perp,\max}} \tilde{p}_\perp d\tilde{p}_\perp \cdot \\ \times \quad & I_0\left[\tilde{p}_\perp \sinh(\kappa(x))\right] \exp\left[\tilde{\mu}_B - \tilde{m}_{P,\perp}\cosh(y-\eta)\cosh(\kappa(x))\right] \end{aligned} \tag{4.58}$$

then integrate out the space azimuthal angle dependence ψ, then we have

$$\begin{aligned}
&\kappa_{4P,\sigma} \\
&= 6d_s^4\left(2\tilde{\lambda}_3^2-\tilde{\lambda}_4\right)\left(g_{_P}m_{_P}\right)^4\xi^7\left(\tau_f R^2\right)T_f^6\int_{\eta_{\min}}^{\eta_{\max}}d\eta\int_0^1 xdx\cdot 2\pi\cdot F^4\left[x,\eta,y_{\min},y_{\max},\tilde{p}_{\perp,\min},\tilde{p}_{\perp,\max}\right]
\end{aligned} \tag{4.59}$$

Similarly, we get

$$\begin{aligned}
\kappa_{3P,\sigma} &= \langle\langle(\delta N_{_P})^3\rangle\rangle_\sigma \\
&= 2d_s^3\tilde{\lambda}_3\left(g_{_P}m_{_P}\right)^3\xi^{9/2}\left(\tau_f R^2\right)T_f^{9/2}\int_{\eta_{\min}}^{\eta_{\max}}d\eta\int_0^1 xdx\cdot 2\pi\cdot F^3\left[x,\eta,y_{\min},y_{\max},\tilde{p}_{\perp,\min},\tilde{p}_{\perp,\max}\right]
\end{aligned} \tag{4.60}$$

and

$$\begin{aligned}
\kappa_{2P,\sigma} &= \langle\langle(\delta N_{_P})^2\rangle\rangle_\sigma \\
&= d_s^2\left(g_{_P}m_{_P}\right)^2\xi^2\left(\tau_f R^2\right)T_f^3\int_{\eta_{\min}}^{\eta_{\max}}d\eta\int_0^1 xdx\cdot 2\pi\cdot F^2\left[x,\eta,y_{\min},y_{\max},\tilde{p}_{\perp,\min},\tilde{p}_{\perp,\max}\right]
\end{aligned} \tag{4.61}$$

One can see that $\kappa_{2p,\sigma}$, $\kappa_{3p,\sigma}$ and $\kappa_{4p,\sigma}$ all have linear volume dependence. In order to make them volume independent, we define *intensive* normalized cumulants (52)

$$\omega_{_{2P,\,\sigma}}(Y) = \frac{\kappa_{_{2P,\sigma}}(Y)}{N(Y)} \tag{4.62}$$

$$\omega_{_{3P,\,\sigma}}(Y) = \frac{\kappa_{_{3P,\sigma}}(Y)}{N(Y)} \tag{4.63}$$

and

$$\omega_{_{4P,\,\sigma}}(Y) = \frac{\kappa_{_{4P,\sigma}}(Y)}{N(Y)} \tag{4.64}$$

where

$$Y = y_{\max} - y_{\min}. \tag{4.65}$$

The *intensive* normalized cumulants is volume independent so that their magnitudes are purely determined by interaction strength and correlation length.

In (57), the authors have found that

$$\begin{aligned} \frac{dN}{p_\perp dp_\perp dy d\phi} &= \frac{d_s\,\tau_f\,R^2\,T_{kf}}{4\pi^2}\int_0^1 x dx \int_{\eta_{\min}}^{\eta_{\max}} d\eta\ \tilde{m}_{_{P,\perp}}\cosh(y-\eta) \\ &\times \exp\left[\tilde{\mu}_{_B} - \tilde{m}_{_{P,\perp}}\cosh(y_i-\eta)\cosh(\kappa(x))\right]\ I_0\left[\tilde{p}_\perp\ \sinh[\kappa(x)]\right. \end{aligned} \tag{4.66}$$

Then

$$N(Y) = \int_{y_{\min}}^{y_{\max}} dy \int_0^{2\pi} d\phi \int p_\perp dp_\perp \frac{dN}{p_\perp dp_\perp dy d\psi} \tag{4.67}$$

where we have used the boost invariance.

If the detector is ideal which can accept all particles with any momentum, we get $N_{\rm tot}$. One can calculate $N_{\rm tot}$ using Equation 4.67

$$\begin{aligned} N_{\rm tot} &= \int_{-\infty}^{\infty} dy \int_0^{2\pi} d\phi \int p_\perp dp_\perp \, \frac{dN}{p_\perp dp_\perp dy d\psi} \\ &= \frac{d_s \, \tau_f \, R^2 \, T_{kf}^3}{\pi} \int_0^1 x dx \int_{\eta_{\rm min}}^{\eta_{\rm max}} d\eta \int \tilde{p}_\perp d\tilde{p}_\perp \, e^{\tilde{\mu}_B} \, \tilde{m}_{_{P,\perp}} \, I_0 \left[\tilde{p}_\perp \, \sinh[\kappa(x)]\right] \, K_1 \left[\tilde{m}_{_{P,\perp}} \, \cosh[\kappa(x)]\right] \end{aligned} \tag{4.68}$$

where K_1 is the modified Bessel function, and we have used

$$K_n(x) = \frac{1}{2} \int_{-\infty}^{\infty} dt \exp[-x \cosh(t)] \, \cosh(n \, t) \tag{4.69}$$

Similarly, we can calculate the total cumulants for particles with all momentum, thus we find

$$\begin{aligned} & \kappa_{_{4P,\sigma}}^{\rm tot} \\ &= 6 d_s^4 \left(2\tilde{\lambda}_3^2 - \tilde{\lambda}_4\right) G^4 \xi^7 \, \left(\tau_f R^2\right) \, T_f^6 \int_{\eta_{\rm min}}^{\eta_{\rm max}} d\eta \int_0^1 \, x dx \, \cdot 2\pi \cdot \, F_{\rm tot}^4 \left[x, \eta\right] \end{aligned} \tag{4.70}$$

where

$$F_{\rm tot} \left[x, \eta\right] = \frac{1}{2\pi^2} \, e^{\tilde{\mu}_B} \, \int_0^\infty \tilde{p}_\perp d\tilde{p}_\perp \cdot I_0 \left[\tilde{p}_\perp \, \sinh(\kappa(x))\right] K_0 \left[\tilde{m}_{_{P,\perp}} \cosh(\kappa(x))\right] \tag{4.71}$$

In Figure 12, we compare F calculated using Boltzmann statistics and Fermi statistics. The left is $\frac{F(\eta,Y,x=1)}{F(\eta,Y=\infty,x=1)}$ where F is defined in Equation 4.51, and the right is the ratio between F calculated with Boltzmann statistics and the one calculated with Fermi statistics. We have set $p_{\perp,\min} = 0$ GeV, $p_{\perp,\max} = 2$ GeV, and integrate out the space and particle azimuthal angle ψ and ϕ. One can see that, the Boltzmann statistics is a very good approximation when calculating the kurtosis of proton because of its large mass. In next, we will present our results calculated from Boltzmann statiscs only.

4.3.3 Results and Interpretation

In order to illustrate the typical shape and magnitude of the dependence of the cumulants on the rapidity and transverse momentum acceptance due to critical mode σ, we use our results for Boltzmann distribution. For simplicity, we fix the transverse flow to be $\langle\beta\rangle = 0.40$, $n = 1$, which is consistent with the freeze-out parameters found through matching the single particle spectrum for central collisions near critical region (39). The baryon chemical potential and temperature at chemical freeze-out for different collision energy near the critical region can be found using the model suggested in (109)

$$T(\mu_{_B}) = a - b\,\mu_{_B}^2 - c\,\mu_{_B}^4 \tag{4.72}$$

and

$$\mu_{_B}(\sqrt{s}) = \frac{d}{1 + e\,\sqrt{s}} \tag{4.73}$$

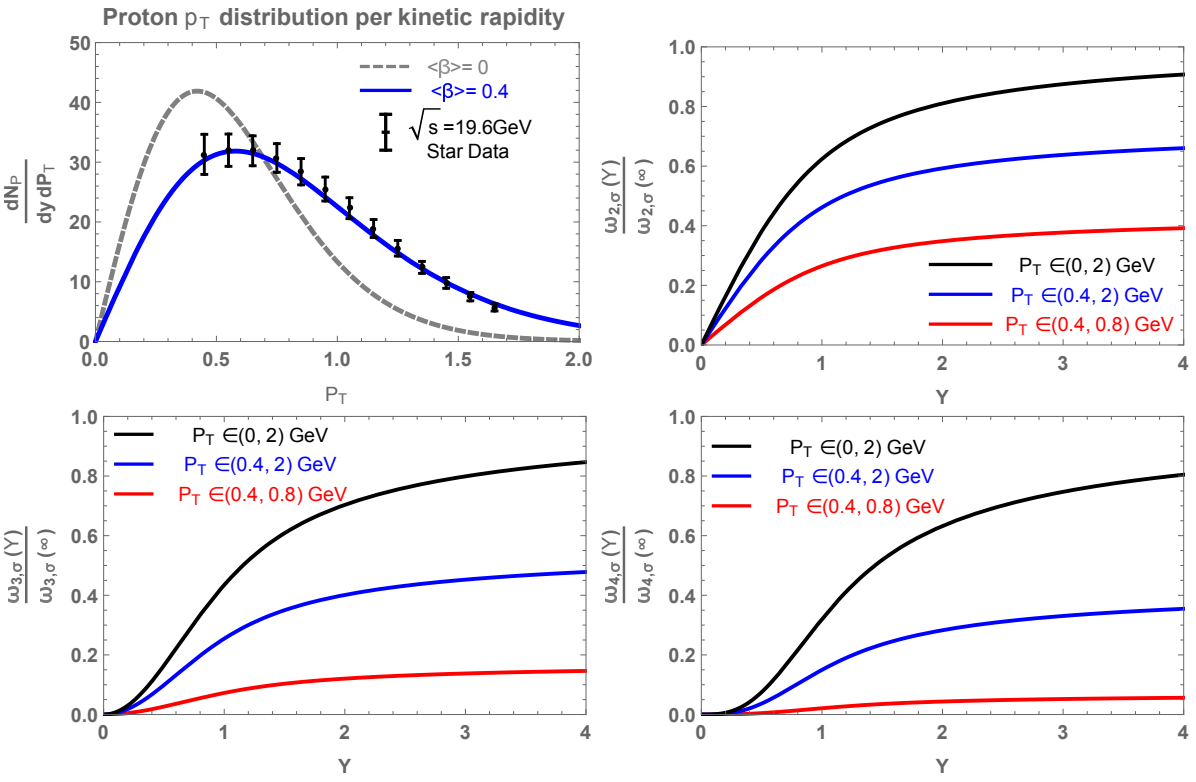

Figure 13. The rapidity acceptance dependence of the magnitude of kurtosis.

where $a = 0.166$ GeV, $b = 0.139\,GeV^{-1}$, $c = 0.053\,GeV^{-3}$, $d = 1.308$ GeV, $e = 0.273\,GeV^{-1}$. Then one find μ_B =0.42, 0.315, 0.205 GeV and $T_f = 0.14$, 0.15, 0.16 GeV for collision energies $\sqrt{s_{NN}} = 7.7$, 11.5, 19.6 GeV respectively (109; 103). The space rapidity cut $\eta_{\max} = -\eta_{\min} = 6$ are estimated in (93). The volume per space rapidity

$$V_\eta \equiv \pi\,\tau_f\,R^2 \tag{4.74}$$

is useful to fit the proton $p_\perp$ spectrum, but is not important for us to calculate the *intensive* normalized cumulants. Here we set $V_\eta = 1960$, 2322, $2432\,fm^3$ for $\sqrt{s} = 7.7$ GeV, $\sqrt{s} = 11.5$ GeV and $\sqrt{s} = 19.6$ GeV respectively. In Figure 14, we plot the rapidity acceptance dependence of *intensive* normalized cumulants normalized by the ones measured by the ideal detectors which could measure particles with any transverse momentum ($p_\perp = 0$ GeV to $p_\perp = \infty$ GeV) and any kinetic rapidity ($Y = y_{\max} - y_{\min} = \infty$). We find, enlarging the transverse momentum cutoff from $0.4\,GeV < p_\perp < 0.8\,GeV$ to $0.4\,GeV < p_\perp < 2\,GeV$ or enlarging the rapidity acceptance as big as $Y = 1$, makes the critical signal much stronger, which is consistent with the findings in (102; 103). Meanwhile, we see that the *intensive* normalized cumulants have a very strong dependence on the kinetic rapidity acceptance Y only when $Y < 2$, and it saturates at some constant value when the acceptance Y becomes larger.

The crucial issue for the dependence of a fluctuation signal on the width Y of rapidity acceptance window is the range of the correlations $\Delta y_{\rm corr}$. The argument below generalizes the discussion in Ref.(1) from quadratic to higher-order cumulants. If $Y \ll \Delta y_{\rm corr}$, the critical point

contribution to the n-th order factorial cumulant $\kappa_{n,fc.}$ of the fluctuations grows as Y^n. This is because the n-th cumulant measures the strength of an n-particle correlation and, therefore, if all particles in the acceptance are correlated, the signal is proportional to the number of possible n-plets, which is roughly $N^n \sim Y^n$. When $Y \gg \Delta y_{\rm corr}$, all factorial cumulants strop growing with Y, as uncorrelated contributions are additive in a cumulant. It is convenient to define the *intensive* normalized factorial cumulants

$$\omega_{nP,fc.} \equiv \frac{\kappa_{nP,fc.}}{N} \tag{4.75}$$

which only counts the fluctuations that are due to interaction, then

$$\omega_{nP,.fc.} = \omega_{nP,\sigma} + \omega_{nP,\,\rm background} \tag{4.76}$$

Then the critical contribution $\omega_{nP,\sigma}(Y)$ grows as Y^{n-1} for $Y \ll \Delta y_{\rm corr}$ and then saturates at a constant value.

The value of $\Delta y_{\rm corr}$ can be estimated within the boost invariant assumption, and it is closely related to the freeze-out smearing and the space correlation width $\Delta\eta_{\rm corr}$ due to the critical modes σ. The range of the correlations due to freeze-out smearing is approximately 2. While $\Delta\eta_{\rm corr} \sim \frac{\xi}{\tau_f} \sim 0.1 - 0.3$ if all the particles emit from the same transverse position of the fireball, but more generally $\Delta\eta_{\rm corr}$ is even smaller. Thus $\Delta y_{\rm corr} \gg \Delta\eta_{\rm corr}$ and our assumption $\Delta\eta_{\rm corr} = 0$ in Equation 4.43 is not bad.

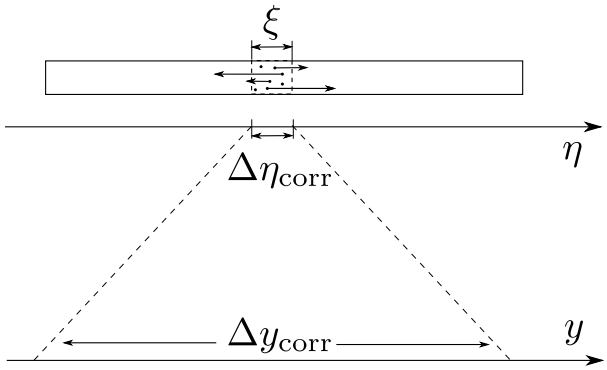

Figure 14. Spatial (Bjorkens) vs kinematic rapidity.

4.4 Conclusions and Future Work

We showed that the magnitude of the observed cumulants has strong dependence on both transverse momentum cutoff and kinetic rapidity acceptance. The protons with low transverse momentum $0 < p_\perp < 0.4\,GeV$ almost contribute one half to the total fourth order cumulants for all kinetic rapidity acceptance. Moreover, the dependence of the kinetic rapidity acceptance at fixed momentum cutoff is also very strong when $Y < 2$, however, it saturates at some constant value for the larger rapidity acceptance. Our results tell that, in order to obtain stronger critical signal, one can at least do two things: capture more protons with small transverse momentum $p_\perp = 0.4$ or capture protons with larger kinetic rapidity.

Our method has neglected the following effects and could be improved by carefully dealing with these as well:

- The most obvious approximation we made above is Equation 4.43, thus the simplest improvement one could made is to use the more realistic 2-particle correlator of σ field

$$\langle \sigma(\vec{r}_1)\, \sigma(\vec{r}_2) \rangle = \frac{T}{4\pi\ |\vec{r}_1 - \vec{r}_2|}\ \exp\left[-\frac{|\vec{r}_1 - \vec{r}_2|}{\xi} \right]. \tag{4.77}$$

  to get n-particle correlators.

- We only calculate the cumulants at chemical freeze-out since when the proton yield does not change. Even though the chemical freeze-out may be in deep of the critical region for the collision energies we are interested in, the evolution of the n-particle correlations of proton from chemical freeze-out to kinetic freeze-out may not be negligible. We are considering the process from chemical freeze-out to kinetic freeze-out, and the net proton density is assumed to be already sufficiently small, so that their motion can be considered classically, using Boltzmann equation. The evolution of 2-particle correlations from chemical freeze-out to kinetic freeze-out has been discussed in (45), and one may generate the arguments there to higher order cumulants as well.

- The n-particle correlators of σ field found in Equation 4.43, Equation 4.44 and Equation 4.46 are calculated, through the distribution function defined in Equation 4.38 and (Equation 4.39), by assuming the system contacts with an external heat bath with equilibrium temperature T. For fireball created in Relativistic Heavy Ion Collisions, this external heat bath is not static but expanding and cooling. Thus the n-particle correlators at chemical freeze-out may not be as simple as the ones we gave, because of the memorial effects

(58) and the critical slowing down (51). One has to use full relativistic hydrodynamics to calculate the time evolution of these correlators with initial conditions determined by the collision conditions, and this requires people have a great understanding of relativistic hydrodynamics near critical point.

CHAPTER 5

SUMMARY AND OUTLOOK

To summarize, we have showed that, the charged particle fluctuations have a great importance on studying QCD phase structure, near both crossover region and critical region. In particular, we have developed stochastic hydrodynamics to study the charge-charge fluctuations as well as its relation to the "Balance Function" of the fireball created in LHC and top energy of RHIC. We found that the time evolution of the charge susceptibility per entropy $\frac{\chi T}{s}$ is essential to determine "Balance Function", and the narrowness of "Balance Function" reflects the strongly coupled nature of QGP matter created in Heavy Ion Collisions. We have also studied the acceptance dependence of the magnitude of kurtosis–the most important quantity for searching QCD critical point. We found the additional *intensive* normalized kurtosis that is due to the critical fluctuations has a strong dependence on transverse momentum cutoff and on the kinematic rapidity acceptance; More quantitatively speaking, this additional *intensive* normalized kurtosis follows a certain power law when the rapidity acceptance window Y is much less than the thermal width of the freeze-out $y_{\rm thermal}$, and it saturates at larger value of Y.

There are a lot of further theoretical efforts that could be made based on our current findings. For example, one could use stochastic hydrodynamics as well as its general solutions developed in Chapter.2 to study "Balance Function" of the fireball created by lower collision energy, where energy momentum and charge fluctuations strongly mixed with each other(56); Or study the other conserved charges such as baryon charge, strangeness as well as the mixing between

different charges (89; 110), or even for the heavy flavors(111). One could also study, the baryon charge diffusion(112; 106), the memorial effects of the chiral condensate fluctuations (45; 58), the resonance decay(113; 114), from chemical freeze-out to kinetic freeze-out, and their impacts on final observed cumulants. Using universality (115) to find out the non-Gaussian couplings $\tilde{\lambda}_3$ and $\tilde{\lambda}_4$ is also useful for us to estimate the magnitude of the correlation length ξ at different freeze-out chemical potential. This might be helpful for us to estimate the bulk viscosity–the most divergent transport coefficients near critical point.(116; 117).

APPENDICES

Appendix A

SOME NOTATIONS

$\mathbb{Z}$ – Partition function defined in Equation 1.1.

$\mu_{_B}$ – Baryon chemical potential.

β, δ, γ – Critical exponents.

$\rho(p,q)$ – Phase density defined in Equation 1.3.

D_m – D-measure defined in Equation 1.5

$K(p,p')$, $\boldsymbol{\zeta_F}$ – Collision kernel and random force defined in Equation 2.1.

$\lambda_i(x)$, $\Phi_i(p)$ – Eigen-values and Eigen-modes of Collision kernel defined in Equation 2.14.

$h^{\mu\nu}$ – Projection tensor norma to u^μ.

η_{shear}, ζ – Shear and Bulk viscosity.

η, y – Space and kinetic rapidity.

ω – Fluctuation of the longitudinal flow

$w \equiv \varepsilon + p$ – Enthalpy.

$\rho \equiv \frac{\delta s}{s}$, $\delta q \equiv \delta\left(\frac{n}{s}\right)$ – Entropy and charge fluctuations.

$v_q^2 \equiv \left(\frac{\partial p}{\partial \varepsilon}\right)_{\frac{n}{s}}$ – Speed of sound squared.

ν, h – Viscous coefficients in Equation 2.95, Equation 2.96 and Equation 2.97.

$\tilde{\boldsymbol{\Psi}}$, $\boldsymbol{D}$, $\tilde{\boldsymbol{f}}$ – Defined in Equation 2.100, Equation 2.101 and Equation 2.102.

CITED LITERATURE

1. Stephanov, M. A.: QCD phase diagram and the critical point. Prog. Theor. Phys. Suppl., 153:139–156, 2004.

2. Gross, D. J. and Wilczek, F.: Ultraviolet behavior of non-abelian gauge theories. Phys. Rev. Lett., 30:1343–1346, Jun 1973.

3. Politzer, H. D.: Reliable perturbative results for strong interactions? Phys. Rev. Lett., 30:1346–1349, Jun 1973.

4. Stephanov, M.: QCD phase diagram: An Overview. PoS, LAT2006:024, 2006.

5. Kogut, J. and Stephanov, M.: The phases of quantum chromodynamics: From confinement to extreme environments. Camb.Monogr.Part.Phys.Nucl.Phys.Cosmol., 21:1–364, 2004.

6. Cahill, K.: Example of color screening. Phys. Rev. Lett., 41:599–601, Aug 1978.

7. Klevansky, S. P.: The nambu¯jona-lasinio model of quantum chromodynamics. Rev. Mod. Phys., 64:649–708, Jul 1992.

8. Cheng, M., Christ, N., Datta, S., van der Heide, J., Jung, C., et al.: The QCD equation of state with almost physical quark masses. Phys.Rev., D77:014511, 2008.

9. Cheng, M., Hendge, P., Jung, C., Karsch, F., Kaczmarek, O., et al.: Baryon Number, Strangeness and Electric Charge Fluctuations in QCD at High Temperature. Phys.Rev., D79:074505, 2009.

10. Bazavov, A., Bhattacharya, T., Cheng, M., Christ, N., DeTar, C., et al.: Equation of state and QCD transition at finite temperature. Phys.Rev., D80:014504, 2009.

11. Bazavov, A. et al.: Fluctuations and Correlations of net baryon number, electric charge, and strangeness: A comparison of lattice QCD results with the hadron resonance gas model. Phys.Rev., D86:034509, 2012.

CITED LITERATURE (Continued)

12. Troyer, M. and Wiese, U.-J.: Computational complexity and fundamental limitations to fermionic quantum monte carlo simulations. Phys. Rev. Lett., 94:170201, May 2005.

13. Schmidt, C.: Lattice QCD at finite density. PoS, LAT2006:021, 2006.

14. Scavenius, O., Mócsy, A., Mishustin, I. N., and Rischke, D. H.: Chiral phase transition within effective models with constituent quarks. Phys. Rev. C, 64:045202, Aug 2001.

15. Schaefer, B.-J. and Wambach, J.: The Phase diagram of the quark meson model. Nucl.Phys., A757:479–492, 2005.

16. Ratti, C., Thaler, M. A., and Weise, W.: Phases of QCD: Lattice thermodynamics and a field theoretical model. Phys.Rev., D73:014019, 2006.

17. Schaefer, B.-J., Pawlowski, J. M., and Wambach, J.: The Phase Structure of the Polyakov–Quark-Meson Model. Phys.Rev., D76:074023, 2007.

18. Skokov, V., Friman, B., and Redlich, K.: Quark number fluctuations in the polyakov loop-extended quark-meson model at finite baryon density. Phys. Rev. C, 83:054904, May 2011.

19. Landau, L. D. and Lifshitz, E. M.: Statistical physics Part 1. Course of theoretical physics Volume 5, Oxford: Pergamon Press, 1980.

20. Bjorken, J. D.: Highly relativistic nucleus-nucleus collisions: The central rapidity region. Phys. Rev. D, 27:140–151, Jan 1983.

21. Baier, R., Mueller, A. H., Schiff, D., and Son, D. T.: 'Bottom up' thermalization in heavy ion collisions. Phys. Lett., B502:51–58, 2001.

22. Gyulassy, M. and McLerran, L.: New forms of QCD matter discovered at RHIC. Nucl. Phys., A750:30–63, 2005.

23. Balasubramanian, V., Bernamonti, A., de Boer, J., Copland, N., Craps, B., Keski-Vakkuri, E., Muller, B., Schafer, A., Shigemori, M., and Staessens, W.: Thermalization of Strongly Coupled Field Theories. Phys. Rev. Lett., 106:191601, 2011.

CITED LITERATURE (Continued)

24. Kurkela, A. and Moore, G. D.: Thermalization in Weakly Coupled Nonabelian Plasmas. JHEP, 12:044, 2011.

25. Blaizot, J.-P., Gelis, F., Liao, J.-F., McLerran, L., and Venugopalan, R.: Bose–Einstein Condensation and Thermalization of the Quark Gluon Plasma. Nucl. Phys., A873:68–80, 2012.

26. Casalderrey-Solana, J., Liu, H., Mateos, D., Rajagopal, K., and Wiedemann, U. A.: Gauge/String Duality, Hot QCD and Heavy Ion Collisions. 2011.

27. Berges, J., Boguslavski, K., Schlichting, S., and Venugopalan, R.: Turbulent thermalization process in heavy-ion collisions at ultrarelativistic energies. Phys. Rev., D89(7):074011, 2014.

28. Brambilla, N. et al.: QCD and Strongly Coupled Gauge Theories: Challenges and Perspectives. Eur. Phys. J., C74(10):2981, 2014.

29. Wang, H.: Study of particle ratio fluctuations and charge balance functions at RHIC. Doctoral dissertation, Michigan State U., 2012.

30. Novak, J. F.: Energy dependence of fluctuation and correlation observables of transverse momentum in heavy-ion collisions. Doctoral dissertation, Michigan State U., 2013.

31. Teaney, D.: The Effects of viscosity on spectra, elliptic flow, and HBT radii. Phys. Rev., C68:034913, 2003.

32. Kovtun, P. K., Son, D. T., and Starinets, A. O.: Viscosity in strongly interacting quantum field theories from black hole physics. Phys. Rev. Lett., 94:111601, Mar 2005.

33. Dusling, K. and Teaney, D.: Simulating elliptic flow with viscous hydrodynamics. Phys. Rev., C77:034905, 2008.

34. Webber, B. R.: Fragmentation and hadronization. Int. J. Mod. Phys., A15S1:577–606, 2000. [,577(1999)].

35. Braun-Munzinger, P., Stachel, J., and Wetterich, C.: Chemical freezeout and the QCD phase transition temperature. Phys. Lett., B596:61–69, 2004.

36. Teaney, D., Lauret, J., and Shuryak, E. V.: A Hydrodynamic description of heavy ion collisions at the SPS and RHIC. 2001.

CITED LITERATURE (Continued)

37. Song, H. and Heinz, U. W.: Suppression of elliptic flow in a minimally viscous quark-gluon plasma. Phys.Lett., B658:279–283, 2008.

38. Song, H. and Heinz, U. W.: Causal viscous hydrodynamics in 2+1 dimensions for relativistic heavy-ion collisions. Phys.Rev., C77:064901, 2008.

39. Kumar, L.: Systematics of Kinetic Freeze-out Properties in High Energy Collisions from STAR. Nucl. Phys., A931:1114–1119, 2014.

40. Stephanov, M.: Non-Gaussian fluctuations near the QCD critical point. Phys.Rev.Lett., 102:032301, 2009.

41. Stephanov, M.: On the sign of kurtosis near the QCD critical point. Phys.Rev.Lett., 107:052301, 2011.

42. Jeon, S. and Koch, V.: Charged particle ratio fluctuation as a signal for QGP. Phys.Rev.Lett., 85:2076–2079, 2000.

43. Asakawa, M., Heinz, U. W., and Muller, B.: Fluctuation probes of quark deconfinement. Phys.Rev.Lett., 85:2072–2075, 2000.

44. Bass, S. A.: QGP theory: Status and perspectives. Pramana, 60:593–612, 2003.

45. Stephanov, M.: Evolution of fluctuations near QCD critical point. Phys.Rev., D81:054012, 2010.

46. Abelev, B. et al.: Beam-Energy and System-Size Dependence of Dynamical Net Charge Fluctuations. Phys.Rev., C79:024906, 2009.

47. Abelev, B. et al.: Net-Charge Fluctuations in Pb-Pb collisions at $\sqrt{s_{NN}} = 2.76$ TeV. Phys.Rev.Lett., 110:252301, 2012.

48. Jena, S. and Collaboration, A.: Recent results on event-by-event fluctuations in alice at the lhc. Journal of Physics: Conference Series, 612(1):012047, 2015.

49. Stephanov, M. A., Rajagopal, K., and Shuryak, E. V.: Event-by-event fluctuations in heavy ion collisions and the QCD critical point. Phys. Rev., D60:114028, 1999.

50. Stephanov, M. A., Rajagopal, K., and Shuryak, E. V.: Signatures of the tricritical point in QCD. Phys. Rev. Lett., 81:4816–4819, 1998.

CITED LITERATURE (Continued)

51. Berdnikov, B. and Rajagopal, K.: Slowing out of equilibrium near the QCD critical point. Phys. Rev., D61:105017, 2000.

52. Athanasiou, C., Rajagopal, K., and Stephanov, M.: Using Higher Moments of Fluctuations and their Ratios in the Search for the QCD Critical Point. Phys.Rev., D82:074008, 2010.

53. Adamczyk, L. et al.: Energy Dependence of Moments of Net-proton Multiplicity Distributions at RHIC. Phys.Rev.Lett., 112(3):032302, 2014.

54. Adamczyk, L. et al.: Beam energy dependence of moments of the net-charge multiplicity distributions in Au+Au collisions at RHIC. Phys.Rev.Lett., 113:092301, 2014.

55. Kapusta, J., Muller, B., and Stephanov, M.: Relativistic Theory of Hydrodynamic Fluctuations with Applications to Heavy Ion Collisions. Phys.Rev., C85:054906, 2012.

56. Kapusta, J. I. and Torres-Rincon, J. M.: Thermal Conductivity and Chiral Critical Point in Heavy Ion Collisions. Phys.Rev., C86:054911, 2012.

57. Ling, B., Springer, T., and Stephanov, M.: Hydrodynamics of charge fluctuations and balance functions. 2013.

58. Mukherjee, S., Venugopalan, R., and Yin, Y.: Real time evolution of non-Gaussian cumulants in the QCD critical regime. 2015.

59. Ling, B. and Stephanov, M. A.: Acceptance dependence of fluctuation measures near the QCD critical point. 2015.

60. Denicol, G. S.: Kinetic foundations of relativistic dissipative fluid dynamics. Journal of Physics G: Nuclear and Particle Physics, 41(12):124004, 2014.

61. Bjorken, J.: Highly Relativistic Nucleus-Nucleus Collisions: The Central Rapidity Region. Phys.Rev., D27:140–151, 1983.

62. Bearden, I. G. et al.: Charged meson rapidity distributions in central Au+Au collisions at s(NN)**(1/2) = 200-GeV. Phys. Rev. Lett., 94:162301, 2005.

63. Back, B., Baker, M., Ballintijn, M., Barton, D., Becker, B., et al.: The PHOBOS perspective on discoveries at RHIC. Nucl.Phys., A757:28–101, 2005.

CITED LITERATURE (Continued)

64. Abbas, E. et al.: Centrality dependence of the pseudorapidity density distribution for charged particles in Pb-Pb collisions at $\sqrt{s_{NN}} = 2.76$ TeV. Phys. Lett., B726:610–622, 2013.

65. Adams, J. et al.: Azimuthal anisotropy at RHIC: The First and fourth harmonics. Phys. Rev. Lett., 92:062301, 2004.

66. Romatschke, P. and Romatschke, U.: Viscosity Information from Relativistic Nuclear Collisions: How Perfect is the Fluid Observed at RHIC? Phys. Rev. Lett., 99:172301, 2007.

67. Adare, A. et al.: Elliptic and hexadecapole flow of charged hadrons in Au+Au collisions at $\sqrt{s_{NN}} = 200$ GeV. Phys. Rev. Lett., 105:062301, 2010.

68. Aad, G. et al.: Measurement of the azimuthal anisotropy for charged particle production in $\sqrt{s_{NN}} = 2.76$ TeV lead-lead collisions with the ATLAS detector. Phys. Rev., C86:014907, 2012.

69. Staig, P. and Shuryak, E.: The Fate of the Initial State Fluctuations in Heavy Ion Collisions. II The Fluctuations and Sounds. Phys. Rev., C84:034908, 2011.

70. Staig, P. and Shuryak, E.: The Fate of the Initial State Fluctuations in Heavy Ion Collisions. III The Second Act of Hydrodynamics. Phys. Rev., C84:044912, 2011.

71. Kovtun, P., Moore, G. D., and Romatschke, P.: Towards an effective action for relativistic dissipative hydrodynamics. 2014.

72. Grad, H.: On the kinetic theory of rarefied gases. Comm. Pure Appl. Math., 1949.

73. Sydney Chapman, University of Alaska, F. G. C.: The Mathematical Theory of Non-uniform Gases. Cambridge University Press, 1970.

74. Stewart, J. M.: Non-equilibrium relativistic kinetic theory. Lecture Notes in Physics, vol. 10, p.1-113, 1971.

75. S. R. de Groot, W. A. v. L. and van Weert, C. G.: S. R. de Groot, W. A. van Leeuwen and Ch. G. van Weert. Amsterdam: North-Holland Pub. Co., 1980.

76. Brandt, F. T., Frenkel, J., and Taylor, J. C.: High temperature QCD and the classical Boltzmann equation in curved space-time. Nucl. Phys., B437:433–446, 1995.

CITED LITERATURE (Continued)

77. Baier, R., Romatschke, P., and Wiedemann, U. A.: Dissipative hydrodynamics and heavy ion collisions. Phys. Rev., C73:064903, 2006.

78. Baier, R., Romatschke, P., Son, D. T., Starinets, A. O., and Stephanov, M. A.: Relativistic viscous hydrodynamics, conformal invariance, and holography. JHEP, 0804:100, 2008.

79. Fox, R. F. and Uhlenbeck, G. E.: Contributions to nonequilibrium thermodynamics. i. theory of hydrodynamical fluctuations. Physics of Fluids, 13(8):1893–1902, 1970.

80. Fox, Ronald Forrest; Uhlenbeck, G. E.: Contributions to Nonequilibrium Thermodynamics. II. Fluctuation Theory for the Boltzmann Equation. Physics of Fluids, Vol. 13, p.2881-2890, 12/1970.

81. Bixon, M. and Zwanzig, R.: Boltzmann-langevin equation and hydrodynamic fluctuations. Phys. Rev., 187:267–272, Nov 1969.

82. Landau, L. D. and Lifshitz, E. M.: Statistical physics Part 2. Course of theoretical physics Volume 9, Oxford: Pergamon Press, 1980.

83. Lifshitz, E. M. and Pitaevskii, L. P.: Physical kinetics. Course of theoretical physics, Oxford: Pergamon Press, 1981.

84. Kovtun, P.: Lectures on hydrodynamic fluctuations in relativistic theories. J.Phys., A45:473001, 2012.

85. Bass, S. A., Danielewicz, P., and Pratt, S.: Clocking hadronization in relativistic heavy ion collisions with balance functions. Phys.Rev.Lett., 85:2689–2692, 2000.

86. Jeon, S. and Pratt, S.: Balance functions, correlations, charge fluctuations and interferometry. Phys.Rev., C65:044902, 2002.

87. Gardiner, C.: Stochastic Methods. Springer; 4th ed., 2009.

88. Fox, R. F.: Gaussian stochastic processes in physics. Phys. Rep., 48:179–283, 1978.

89. Pratt, S.: Identifying the Charge Carriers of the Quark-Gluon Plasma. Phys.Rev.Lett., 108:212301, 2012.

CITED LITERATURE (Continued)

90. Borsanyi, S., Endrodi, G., Fodor, Z., Jakovac, A., Katz, S. D., et al.: The QCD equation of state with dynamical quarks. JHEP, 1011:077, 2010.

91. Huovinen, P. and Petreczky, P.: QCD Equation of State and Hadron Resonance Gas. Nucl.Phys., A837:26–53, 2010.

92. Teaney, D.: Chemical freezeout in heavy ion collisions. 2002.

93. Teaney, D. A.: Viscous Hydrodynamics and the Quark Gluon Plasma. 2009.

94. Schnedermann, E., Sollfrank, J., and Heinz, U. W.: Thermal phenomenology of hadrons from 200-A/GeV S+S collisions. Phys.Rev., C48:2462–2475, 1993.

95. Teaney, D.: Viscous corrections to spectra, elliptic flow, and HBT radii. Nucl.Phys., A715:817–820, 2003.

96. Borsanyi, S., Fodor, Z., Katz, S. D., Krieg, S., Ratti, C., et al.: Fluctuations of conserved charges at finite temperature from lattice QCD. JHEP, 1201:138, 2012.

97. Shen, C. and Heinz, U.: Collision Energy Dependence of Viscous Hydrodynamic Flow in Relativistic Heavy-Ion Collisions. Phys.Rev., C85:054902, 2012.

98. Abelev, B. et al.: Systematic Measurements of Identified Particle Spectra in pp, d^+ Au and Au+Au Collisions from STAR. Phys.Rev., C79:034909, 2009.

99. Shuryak, E. V. and Stephanov, M. A.: When can long range charge fluctuations serve as a QGP signal? Phys.Rev., C63:064903, 2001.

100. Pratt, S.: General Charge Balance Functions, A Tool for Studying the Chemical Evolution of the Quark-Gluon Plasma. Phys.Rev., C85:014904, 2012.

101. Amato, A., Aarts, G., Allton, C., Giudice, P., Hands, S., et al.: Electrical conductivity of the quark-gluon plasma across the deconfinement transition. 2013.

102. Luo, X.: Energy Dependence of Moments of Net-Proton and Net-Charge Multiplicity Distributions at STAR. PoS, CPOD2014:019, 2014.

103. Luo, X.: Exploring the qcd phase structure with beam energy scan in heavy-ion collisions. PoS, Quark Matter 2015, 2015.

CITED LITERATURE (Continued)

104. Luo, X., Mohanty, B., and Xu, N.: Baseline for the cumulants of net-proton distributions at STAR. Nucl. Phys., A931:808–813, 2014.

105. Luo, X.: Fluctuations of Conserved Quantities in High Energy Nuclear Collisions at RHIC. J. Phys. Conf. Ser., 599(1):012023, 2015.

106. Sakaida, M., Asakawa, M., and Kitazawa, M.: Effects of global charge conservation on time evolution of cumulants of conserved charges in relativistic heavy ion collisions. Phys. Rev., C90(6):064911, 2014.

107. Kambly, D., Flindt, C., and Büttiker, M.: Factorial cumulants reveal interactions in counting statistics. Phys. Rev. B, 83:075432, Feb 2011.

108. Stephanov, M. A.: Thermal fluctuations in the interacting pion gas. Phys. Rev., D65:096008, 2002.

109. Cleymans, J., Oeschler, H., Redlich, K., and Wheaton, S.: Comparison of chemical freeze-out criteria in heavy-ion collisions. Phys. Rev., C73:034905, 2006.

110. Ang'ong'a, J. and Springer, T.: Conserved Charge Susceptibilities in a Chemically Frozen Hadronic Gas. 2015.

111. Cao, S., Qin, G.-Y., and Bass, S. A.: Modeling of heavy-flavor pair correlations in Au-Au collisions at 200A GeV at the BNL Relativistic Heavy Ion Collider. Phys. Rev., C92(5):054909, 2015.

112. Kitazawa, M., Asakawa, M., and Ono, H.: Non-equilibrium time evolution of higher order cumulants of conserved charges and event-by-event analysis. Phys. Lett., B728:386–392, 2014.

113. Kitazawa, M. and Asakawa, M.: Revealing baryon number fluctuations from proton number fluctuations in relativistic heavy ion collisions. Phys. Rev., C85:021901, 2012.

114. Kitazawa, M. and Asakawa, M.: Relation between baryon number fluctuations and experimentally observed proton number fluctuations in relativistic heavy ion collisions. Phys. Rev., C86:024904, 2012. [Erratum: Phys. Rev.C86,069902(2012)].

115. Tsypin, M. M.: Universal effective potential for scalar field theory in three dimensions by monte carlo computation. Phys. Rev. Lett., 73:2015–2018, Oct 1994.

CITED LITERATURE (Continued)

116. Rajagopal, K. and Tripuraneni, N.: Bulk Viscosity and Cavitation in Boost-Invariant Hydrodynamic Expansion. JHEP, 1003:018, 2010.

117. Habich, M. and Romatschke, P.: Onset of cavitation in the quark-gluon plasma. 2014.

118. Aamodt, K. et al.: Charged-particle multiplicity density at mid-rapidity in central Pb-Pb collisions at $\sqrt{s_{NN}} = 2.76$ TeV. Phys.Rev.Lett., 105:252301, 2010.

119. Abelev, B. et al.: Three-particle coincidence of the long range pseudorapidity correlation in high energy nucleus-nucleus collisions. Phys.Rev.Lett., 105:022301, 2010.

120. Abelev, B. et al.: Pion, Kaon, and Proton Production in Central Pb–Pb Collisions at $\sqrt{s_{NN}} = 2.76$ TeV. Phys.Rev.Lett., 109:252301, 2012.

121. Abelev, B. et al.: Centrality dependence of π, K, p production in Pb-Pb collisions at $\sqrt{s_{NN}} = 2.76$ TeV. 2013.

122. Aggarwal, M. et al.: Balance Functions from Au+Au, d+Au, and $p + p$ Collisions at $\sqrt{s_{NN}} = 200$ GeV. Phys.Rev., C82:024905, 2010.

123. Arnold, P. B., Moore, G. D., and Yaffe, L. G.: Transport coefficients in high temperature gauge theories. 2. Beyond leading log. JHEP, 0305:051, 2003.

124. Bozek, P. and Broniowski, W.: Charge conservation and the shape of the ridge of two-particle correlations in relativistic heavy-ion collisions. Phys.Rev.Lett., 109:062301, 2012.

125. Dinh, P. M., Borghini, N., and Ollitrault, J.-Y.: Effects of HBT correlations on flow measurements. Phys.Lett., B477:51–58, 2000.

126. Gubser, S. S., Pufu, S. S., and Yarom, A.: Entropy production in collisions of gravitational shock waves and of heavy ions. Phys.Rev., D78:066014, 2008.

127. Gubser, S. S.: Symmetry constraints on generalizations of Bjorken flow. Phys.Rev., D82:085027, 2010.

128. Gubser, S. S. and Yarom, A.: Conformal hydrodynamics in Minkowski and de Sitter spacetimes. Nucl.Phys., B846:469–511, 2011.

129. Kaczmarek, O.: Recent Developments in Lattice Studies for Quarkonia. 2012.

CITED LITERATURE (Continued)

130. Landau, L. D. and Lifshitz, E. M.: Fluid mechanics. Course of theoretical physics, Oxford: Pergamon Press, 1959.

131. Muller, B. and Rajagopal, K.: From entropy and jet quenching to deconfinement? Eur.Phys.J., C43:15–21, 2005.

132. Pruneau, C., Gavin, S., and Voloshin, S.: Methods for the study of particle production fluctuations. Phys.Rev., C66:044904, 2002.

133. Wang, H.: Reaction plane and beam energy dependence of the balance function at RHIC. J.Phys.Conf.Ser., 316:012021, 2011.

134. Timmins, A. R.: Untriggered di-hadron correlations in Pb-Pb collisions at $\sqrt{s_{NN}} = 2.76$ TeV from ALICE. 2011.

135. Abelev, B. et al.: Charge correlations using the balance function in Pb-Pb collisions at $\sqrt{s_{NN}} = 2.76$ TeV. Phys.Lett., B723:267–279, 2013.

136. Weinberg, S.: Gravitation and Cosmology: Principles and Applications of the General Theory of Relativity. John Wiley & Sons, 1972.

137. Teaney, D. and Venugopalan, R.: Classical computation of elliptic flow at large transverse momentum. Phys.Lett., B539:53–58, 2002.

138. Hatta, Y. and Stephanov, M. A.: Proton number fluctuation as a signal of the QCD critical end-point. Phys. Rev. Lett., 91:102003, 2003.

139. James L. Anderson, E. N.: Stochastic forces and fluctuation-dissipation theorems in a relativistic one-component gas. Physica A: Statistical Mechanics and its Applications, 02/1990.

140. Jeon, S. and Koch, V.: Event by event fluctuations. 2003.

141. Pratt, S. and Paech, K.: Viscosity at RHIC. 2006.

142. Denicol, G. S., Kodama, T., Koide, T., and Mota, P.: Effect of bulk viscosity on elliptic flow near the qcd phase transition. Phys. Rev. C, 80:064901, Dec 2009.

143. Karsch, F., Kharzeev, D., and Tuchin, K.: Universal properties of bulk viscosity near the QCD phase transition. Phys.Lett., B663:217–221, 2008.

CITED LITERATURE (Continued)

144. Denicol, G., Kodama, T., Koide, T., and Mota, P.: Effect of bulk viscosity on Elliptic Flow near QCD phase transition. Phys.Rev., C80:064901, 2009.

145. Noronha-Hostler, J., Noronha, J., and Greiner, C.: Transport Coefficients of Hadronic Matter near T(c). Phys.Rev.Lett., 103:172302, 2009.

146. Dobado, A. and Torres-Rincon, J. M.: Bulk viscosity and the phase transition of the linear sigma model. Phys.Rev., D86:074021, 2012.

147. Asakawa, M., Majumder, A., and Muller, B.: Electric Charge Separation in Strong Transient Magnetic Fields. Phys.Rev., C81:064912, 2010.

148. Cooper, F. and Frye, G.: Comment on the Single Particle Distribution in the Hydrodynamic and Statistical Thermodynamic Models of Multiparticle Production. Phys.Rev., D10:186, 1974.

149. Cremonini, S., Gursoy, U., and Szepietowski, P.: On the Temperature Dependence of the Shear Viscosity and Holography. JHEP, 1208:167, 2012.

150. Lacey, R. A., Ajitanand, N., Alexander, J., Chung, P., Holzmann, W., et al.: Has the QCD Critical Point been Signaled by Observations at RHIC? Phys.Rev.Lett., 98:092301, 2007.

151. Meyer, H. B.: A Calculation of the bulk viscosity in SU(3) gluodynamics. Phys.Rev.Lett., 100:162001, 2008.

152. Kharzeev, D. and Tuchin, K.: Bulk viscosity of QCD matter near the critical temperature. JHEP, 0809:093, 2008.

153. Paech, K. and Pratt, S.: Origins of bulk viscosity in relativistic heavy ion collisions. Phys.Rev., C74:014901, 2006.

154. Kovtun, P., Son, D. T., and Starinets, A. O.: Viscosity in strongly interacting quantum field theories from black hole physics. Phys.Rev.Lett., 94:111601, 2005.

155. Song, H., Bass, S. A., and Heinz, U.: Elliptic flow in 200 A GeV Au+Au collisions and 2.76 A TeV Pb+Pb collisions: insights from viscous hydrodynamics + hadron cascade hybrid model. Phys.Rev., C83:054912, 2011.

CITED LITERATURE (Continued)

156. Pal, S.: Shear viscosity to entropy density ratio of a relativistic Hagedorn resonance gas. Phys.Lett., B684:211–215, 2010.

157. Fries, R. J., Muller, B., and Schafer, A.: Stress Tensor and Bulk Viscosity in Relativistic Nuclear Collisions. Phys.Rev., C78:034913, 2008.

158. Song, H., Bass, S. A., Heinz, U., Hirano, T., and Shen, C.: 200 A GeV Au+Au collisions serve a nearly perfect quark-gluon liquid. Phys.Rev.Lett., 106:192301, 2011.

159. Stephanov, M. and Yin, Y.: Reversing a heavy-ion collision. 2014.

160. Adams et al.: Distributions of charged hadrons associated with high transverse momentum particles in pp and au+au collisions at snn=200 gev.

161. Abelev, B. et al.: Long range rapidity correlations and jet production in high energy nuclear collisions. Phys.Rev., C80:064912, 2009.

162. Majumder, A., Müller, B., and Bass, S. A.: Longitudinal broadening of quenched jets in turbulent color fields. Phys. Rev. Lett., 99:042301, Jul 2007.

163. Chiu, C. B. and Hwa, R. C.: Pedestal and peak structure in jet correlation. Phys. Rev. C, 72:034903, Sep 2005.

164. Wong, C.-Y.: Momentum kick model description of the near-side ridge and jet quenching. Phys. Rev. C, 78:064905, Dec 2008.

165. De Dominicis, C. and Peliti, L.: Field-theory renormalization and critical dynamics above tc: Helium, antiferromagnets, and liquid-gas systems. Phys. Rev. B, 18:353–376, Jul 1978.

166. Endlich, S., Nicolis, A., Porto, R. A., and Wang, J.: Dissipation in the effective field theory for hydrodynamics: First order effects. Phys.Rev., D88:105001, 2013.

167. Dubovsky, S., Hui, L., Nicolis, A., and Son, D. T.: Effective field theory for hydrodynamics: thermodynamics, and the derivative expansion. Phys.Rev., D85:085029, 2012.

168. Kovtun, P., Moore, G. D., and Romatschke, P.: The stickiness of sound: An absolute lower limit on viscosity and the breakdown of second order relativistic hydrodynamics. Phys.Rev., D84:025006, 2011.

CITED LITERATURE (Continued)

169. Hohenberg, P. C. and Halperin, B. I.: Theory of dynamic critical phenomena. Rev. Mod. Phys., 49:435–479, Jul 1977.

170. Tuber, U. C.: 7 field-theory approaches to nonequilibrium dynamics.

171. Springer, T. and Stephanov, M.: Hydrodynamic fluctuations and two-point correlations. Nucl.Phys., A904-905:1027c–1030c, 2013.

172. Nickel, D. and Son, D. T.: Deconstructing holographic liquids. New J.Phys., 13:075010, 2011.

173. Borsanyi, S., Fodor, Z., Katz, S., Krieg, S., Ratti, C., et al.: Freeze-out parameters from electric charge and baryon number fluctuations: is there consistency? Phys.Rev.Lett., 113:052301, 2014.

174. Alba, P., Alberico, W., Bellwied, R., Bluhm, M., Mantovani Sarti, V., et al.: Freeze-out conditions from net-proton and net-charge fluctuations at RHIC. Phys.Lett., B738:305–310, 2014.

175. Caron-Huot, S., Chesler, P. M., and Teaney, D.: Fluctuation, dissipation, and thermalization in non-equilibrium AdS5 black hole geometries. Phys.Rev., D84:026012, 2011.

176. Chesler, P. M. and Teaney, D.: Dynamical Hawking Radiation and Holographic Thermalization. 2011.

177. Siggia, E. D., Halperin, B. I., and Hohenberg, P. C.: Renormalization-group treatment of the critical dynamics of the binary-fluid and gas-liquid transitions. Phys. Rev. B, 13:2110–2123, Mar 1976.

178. Onuki, A.: Dynamic equations and bulk viscosity near the gas-liquid critical point. Phys. Rev. E, 55:403–420, Jan 1997.

179. Minami, Y.: Dynamics near QCD critical point by dynamic renormalization group. Phys.Rev., D83:094019, 2011.

180. Son, D. and Stephanov, M.: Dynamic universality class of the QCD critical point. Phys.Rev., D70:056001, 2004.

CITED LITERATURE (Continued)

181. Romatschke, P.: Relativistic (Lattice) Boltzmann Equation with Non-Ideal Equation of State. Phys.Rev., D85:065012, 2012.

182. Rehr, J. J. and Mermin, N. D.: Revised scaling equation of state at the liquid-vapor critical point. Phys. Rev. A, 8:472–480, Jul 1973.

183. Mermin, N. D.: Solvable model of a vapor-liquid transition with a singular coexistence-curve diameter. Phys. Rev. Lett., 26:169–172, Jan 1971.

184. Mermin, N. D.: Lattice gas with short-range pair interactions and a singular coexistence-curve diameter. Phys. Rev. Lett., 26:957–959, Apr 1971.

185. Vovchenko, V., Anchishkin, D. V., and Gorenstein, M. I.: Particle number fluctuations for the van der Waals equation of state. J. Phys., A48(30):305001, 2015.

186. Bertrand, C. E., Nicoll, J. F., and Anisimov, M. A.: Comparison of complete scaling and a field-theoretic treatment of asymmetric fluid criticality. Phys. Rev. E, 85:031131, Mar 2012.

187. Fisher, M. E. and Orkoulas, G.: The yang-yang anomaly in fluid criticality: Experiment and scaling theory. Phys. Rev. Lett., 85:696–699, Jul 2000.

188. Wang, J. and Anisimov, M. A.: Nature of vapor-liquid asymmetry in fluid criticality. Phys. Rev. E, 75:051107, May 2007.

189. Kim, Y. C., Fisher, M. E., and Orkoulas, G.: Asymmetric fluid criticality. i. scaling with pressure mixing. Phys. Rev. E, 67:061506, Jun 2003.

190. Nicoll, J. F.: Critical phenomena of fluids: Asymmetric landau-ginzburg-wilson model. Phys. Rev. A, 24:2203–2220, Oct 1981.

191. Wegner, F. J.: Corrections to scaling laws. Phys. Rev. B, 5:4529–4536, Jun 1972.

192. Nonaka, C. and Asakawa, M.: Hydrodynamical evolution near the QCD critical end point. Phys. Rev., C71:044904, 2005.

193. Widom, B. and Rowlinson, J. S.: New model for the study of liquidvapor phase transitions. The Journal of Chemical Physics, 52(4), 1970.

CITED LITERATURE (Continued)

194. Widom, B.: Equation of state in the neighborhood of the critical point. The Journal of Chemical Physics, 43(11), 1965.

195. Wang, J., Cerdeiriña, C. A., Anisimov, M. A., and Sengers, J. V.: Principle of isomorphism and complete scaling for binary-fluid criticality. Phys. Rev. E, 77:031127, Mar 2008.

196. Weiner, J., Langley, K. H., and Ford, N. C.: Experimental evidence for a departure from the law of the rectilinear diameter. Phys. Rev. Lett., 32:879–881, Apr 1974.

197. Yang, C. N. and Yang, C. P.: Critical point in liquid-gas transitions. Phys. Rev. Lett., 13:303–305, Aug 1964.

198. Barducci, A., Casalbuoni, R., De Curtis, S., Gatto, R., and Pettini, G.: Chiral phase transitions in qcd for finite temperature and density. Phys. Rev. D, 41:1610–1619, Mar 1990.

199. Barducci, A., Casalbuoni, R., Pettini, G., and Gatto, R.: Chiral phases of qcd at finite density and temperature. Phys. Rev. D, 49:426–436, Jan 1994.

200. Halasz, A. M., Jackson, A. D., Shrock, R. E., Stephanov, M. A., and Verbaarschot, J. J. M.: On the phase diagram of QCD. Phys. Rev., D58:096007, 1998.

201. Scavenius, O., Mocsy, A., Mishustin, I. N., and Rischke, D. H.: Chiral phase transition within effective models with constituent quarks. Phys. Rev., C64:045202, 2001.

202. Antoniou, N. G. and Kapoyannis, A. S.: Bootstraping the QCD critical point. Phys. Lett., B563:165–172, 2003.

203. Hatta, Y. and Ikeda, T.: Universality, the QCD critical / tricritical point and the quark number susceptibility. Phys. Rev., D67:014028, 2003.

204. Stephanov, M.: The phase diagram of QCD and the critical point. Acta Phys. Polon., B35:2939–2962, 2004.

205. Zinn-Justin, J.: Precise determination of critical exponents and equation of state by field theory methods. Phys. Rept., 344:159–178, 2001.

206. Zinn-Justin, J.: .

CITED LITERATURE (Continued)

207. Fisher, M. E. and yong Zinn, S.: The shape of the van der waals loop and universal critical amplitude ratios. Journal of Physics A: Mathematical and General, 31(37):L629, 1998.

208. Akira Onuki : Phase Transition Dynamics. Cambridge University Press; 1 edition, 2002.

209. Karsch, F. and Redlich, K.: Probing freeze-out conditions in heavy ion collisions with moments of charge fluctuations. Phys. Lett., B695:136–142, 2011.

210. Garg, P., Mishra, D. K., Netrakanti, P. K., Mohanty, B., Mohanty, A. K., Singh, B. K., and Xu, N.: Conserved number fluctuations in a hadron resonance gas model. Phys. Lett., B726:691–696, 2013.

211. Jeon, S. and Koch, V.: Charged particle ratio fluctuation as a signal for quark-gluon plasma. Phys. Rev. Lett., 85:2076–2079, Sep 2000.

212. McConnell, L.: Using a Classical Gluon Cascade to study the Equilibration of a Gluon-Plasma. J. Phys. Conf. Ser., 645(1):012013, 2015.

VITA

Education

- Ph.D. in Physics, University of Illinois, Chicago, IL 2009-2016.

  Advisor: Mikhail Stephanov.

  Thesis: Applications of Fluctuations on Heavy-Ion Collisions.

- M.S. in Statistics, University of Illinois, Chicago, IL 2011-2013.

- B.S. in Physics, Nanjing University, Nanjing, Jiangsu, China 2005-2009.

Courses

- **Physics(GPA 4.0)**: All Physics Courses.
- **Computer Science(GPA 4.0)**: Computer Algorithms I, Objective-Oriented Languages and Environments, Data Mining and Text Mining.
- **Finance(GPA 4.0)**: Computational Finance, Portfolio Analysis, Options and Futures Markets.
- **Statistics(GPA 4.0)**: Statistical Theory, Probability Theory I, Computational Statistics, Linear Statistical Inference, Applied Statistical Methods II.

Publications

- Hydrodynamics of charge fluctuations and balance functions, Phys. Rev. C 89, 064901.

Academic Honors

- Paul M. Raccah Award for Doctoral Studies in Physics. Awarded for best Ph.D. qualifying exam, 2010

Skills

- C++, Python, R, SQL, Mathematica, Latex.